AFCRL 67-0122

15 JANUARY 1967

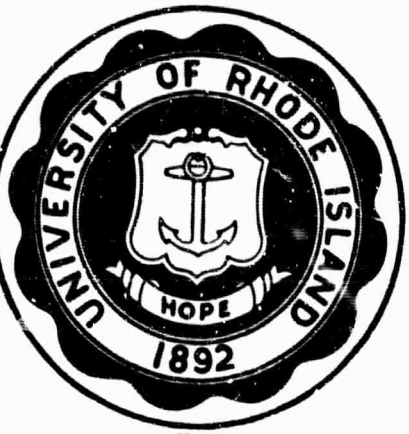


DIVISION OF ENGINEERING RESEARCH AND DEVELOPMENT

DEPARTMENT OF ELECTRICAL ENGINEERING





# Seismic Diffraction By Crustal Discontinuities

BY

JULIUS KANE

Contract No. AF19 (628) - 319
Project No. 8652
Task No. 865206



FINAL REPORT

Period Covered: 1 Jan. '62 to 30 Sept. '66

Prepared for:

AIR FORCE CAMBRIDGE RESEARCH LABORATORIES
OFFICE OF AEROSPACE RESEARCH
UNITED STATES AIR FORCE
BEDFORD, MASSACHUSETTS

WORK SPONSORED BY ADVANCED RESEARCH PROJECTS AGENCY
PROJECT VELA-UNIFORM
ARPA Order No. 180-62 and 292-12

Project Code No. 4810

UNIVERSITY OF RHODE ISLAND
KINGSTON, RHODE ISLAND

# DISCLAIMER NOTICE

THIS DOCUMENT IS THE BEST QUALITY AVAILABLE.

COPY FURNISHED CONTAINED A SIGNIFICANT NUMBER OF PAGES WHICH DO NOT REPRODUCE LEGIBLY.

A F C R L 67-0122

# SEISMIC DIFFRACTION BY CRUSTAL DISCONTINUITIES

by

JULIUS KANE

University of Rhode Island

Kingston, Rhode Island

Contract No. AF19(628)-319

Project No. 8652

Task No. 865206

FINAL REPORT

Period Covered: 1 Jan.'62 to 30 Sept.'66

Report Date: 15 January 1967

Prepared for:

AIR FORCE CAMBRIDGE RESEARCH LABORATORIES
OFFICE OF AEROSPACE RESEARCH
UNITED STATES AIR FORCE
BEDFORD, MASSACHUSETTS

WORK SPONSORED BY ADVANCED RESEARCH PROJECTS AGENCY
PROJECT VELA-UNIFORM
ARPA Order No. 180-62 and 292-12

Project Code No. 4810

TABLE OF CONTENTS

# SEISMIC DIFFRACTION BY NON-UNIFORM CRUSTAL STRUCTURES

by Julius Kane

## abstract

The final report on contract AF 19(628) - 319 describes the research contributions of a group studying theoretical problems of seismology at the University of Rhode Island. These are described in simplified terms and formulations which are mathematically tractable and still relevent to realistic crustal structures. Reprints of papers describing the methods are included as appendices in the report.

## SUMMARY OF WORK DONE UNDER SUBJECT CONTRACT

The mathematical problems of theoretical seismology are especially acute for two distinct wave equations need be satisfied. Furthermore, at refracting interfaces, the continuity relations usually demand that complex transcendental relationships be satisfied. For these reasons, the geometric configurations for which seismic problems are tractable are quite few. Separable geometries include parallel stacks of plane layers, and concentric spherical shells of differing elastic media. The separability of the wave equations in the latter case is particularly fortunate because it describes a spherical geometry which duplicates the actual situation quite faithfully. However, geophysical waveguides encountered in practice contain many irregularities whose variation does not fall within the scope of separable analysis. Such configurations include transition regions at the continental margins, and tapering crustal layers. In addition, unexplained, and possibly important diffraction effects arise from wall irregularities; that is, the interfaces bounding geophysical waveguides are not smooth, but rough in nature. In the past, such effects could have been neglected, but with the desire of the seismologist to continually resolve finer details of the earth's crustal structure, such effects can no longer be ignored. High resolution means that we need analyze and understand the high frequency portions of seismic records. Interpreting such data in terms of abstract idealizations can be misleading and deceive the geologist in his understanding of the subterranean characteristics of the world. Questions of this nature have prompted our investigations under the

of the above problem in that we studied a layered elastic surface which is bent through an angle. In this geometry, the layering means that an infinite number of modes contribute to the field. Of course, for any given frequency, only a finite number of these are propagating modes. To make the problem a little more interesting, we considered the case when two modes can propagate. The methods we used for this problem were not complex variable techniques, but rather tools from the theory of functional analysis. That is, we matched fields on two sides of some conveniently chosen "aperture plane." In terms of a suitable metric, a least squares fitting is automatically satisfied. Mathematically speaking, this is an interesting method because it is applicable to a wide variety of otherwise intractable problems. Included within the material of Appendix B are various graphs showing the reflection, transmission, and conversion coefficients as functions of wedge angle and frequency. One conclusion not previously established is that seismic energy has a great tendency to continue propagating in the same direction, preferring to be converted into a different forward mode rather than a reflected one of the same type.

During the course of our studies, it became increasingly evident that solution of generalized problems depended upon the solution of the second order linear differential equation with coefficients that might be substantially different from the standard cases treated in the literature. For this reason we considered the relevent mathematical problem from a computational point of view, one which would furnish

numbers and graphs in a straight-forward manner without being hindered by questions of turning points and transition regions. The results of this study are presented in Appendix C, Integrals of the Second-order Linear Differential Equation which was published in the Journal of Mathematical Physics.

An immediate application of the results mentioned in the paragraph above was a way of estimating the corruption of time/phase data by random inhomogeneities along the propagation path. Assuming only that the mean square variation of the velocity profile is known, we were able to find a correction formula for dispersion characteristics of waves propagating along inhomogeneous paths. The formula given is a very simple one and is given explicity as equation (27) of Appendix D.

In Appendix E we found a method to use dispersion relations between interacting waveguides as a novel type of strain guage. In this case, dispersion of optical surface waves is used to measure lengths or strains to high accuracy, of the order of one part in $10^8$.

In Appendix F, we present a new way of solving diffraction problems. Customarily, the technique has been to distort the geometry of crustal configurations and consider them to be of idealized, but highly distorted types: step function changes in elevation and other abrupt transitions. In actual crustal configurations, staircase elevations are not encountered, waveguides are joined smoothly by some transition region. Rather than pose a boundary value problem, it seemed reasonable to ask the question: In what ways can seismic energy be converted from the modes of one structure to another? We

expected that the answer would not be unique. After all, there are a nondenumerable infinity of ways by which the transition can be effected. On the other hand, we did expect that the low order effects would remain stable; that is, relatively insensitive to the type of transition chosen. This, of course, is the principle behind assuming step function changes. However, in our analysis, we were not confined to step function changes, and the type transition we discussed could easily be extended to cover the case of more involved geometries. The future of this method seems particularly promising, especially in light of the ease by which the results in Appendix F were found. Nothing more than the solution of five algebraic equations in five unknowns was required, and even that required no matrix algebra because a simple substitution allowed the equations to be solved by inspection. After the termination of the present contract, subsequent studies have been initiated. Based upon our preliminary results, we can mention that it now seems as though diffraction by arbitrary transitions between geophysical waveguides are easily handled.

Finally, in Appendix G we describe the results of a computer study of the array problem. Considering the large investment embodied in such projects as the LASA array, it seemed reasonable to ask the following question: How severe might the effects of irregular crustal layering be on its discrimination characteristics? Already, some field estimates have been given that indicate the theoretical signal to noise ratio falls below expectations. In view of this, we

considered the perturbation effects of a stack of skew layers on a seismic pulse. This is one problem wherein the harmonic problem did not seem as though it would yield readily useful information. For that reason we worked directly in the time domain, thus sparing ourselves of the burden of taking extensive Fourier transforms. In Appendix G, we summarize the distortion of a plane pulse as it propagates through a uniform dipping crust. The results show that distortion across the elements of the array is to be expected, and, owing to reverberation effects, this distortion increases with time. However, there are simple equlization techniques which can restore the signals to a standard reference. The "rubber sheet equalization" is fully discussed in Appendix G.

Appendices H and I summarize some of the last work done on the contract. In the last months, we followed up the work done in Appendix G to allow for stacks of arbitrary skew layers. In addition, we initiated some work on zero-frequency seismology -- the static problem. In Appendix I we summarize a novel approach to the elastostatic problem. Reprints of these papers will be forwarded to the contracting officers once they are available.

Appendix J is an abstract of a master's thesis [illegible] under this contract, but not published. Mr. David Defanti's results extend and elaborate upon some of the published results discussed in the previous abstracts.

## references

1. Kane, J., The Propagation of Rayleigh Waves Past a Fluid-Loaded Boundary, J. Math and Physics, Vol XLI, No. 3, Sept. 1962.

2. Hudson, J. A., and Knopoff, L., Contributions 1177 and 1178, Division of Geological Sciences, California Institute of Technology

## RECOMMENDATIONS FOR FUTURE STUDY

Based upon our experience and published results, we feel that the techniques of analytic continuation can contribute a great deal to solving the problems of theoretical seismology, particularly those dealing with diffraction by realistic crustal structures. The chief advantage of this method is that, unlike separation of variables, it is not confined to standard geometries. We hope to be able to develop these methods further at a future date.

Much work still needs to be done in time-dependent diffraction. While Fourier analysis has often been proposed as a means to translate harmonic information into time domain information, this is in practice seldom done. The reason, of course, is the large amount of computer time to take the required Fourier transforms. Furthermore, there are theoretical difficulties: For example, the spectrum of actual pulses is not time-invariant.

In the same fashion, the operation of seismic arrays in the time domain needs to be fully explored. While array theory has been extensively developed for electromagnetic antennas, the seismic problem is quite different: Transients play a bigger role, and the propagation medium is anything but homogeneous. Also, in electromagnetic problems reverberations can be ignored, but this is not the situation in the seismic case.

Any inverse problem is highly unstable, and approaches such as those in Appendix I should be followed up. In effect, what we did was to admit that the complete characteristics of the source could not be recovered with perfect fidelity. But even granting this, there is still the question: Can we say anything about the source with

with reasonable assurance? The answer is in the affirmative, and things can be said about the source region provided the right questions are asked. The right questions and techniques of answering them should be the subject of a highly rewarding study.

## STUDENT AND FACULTY CONTRIBUTORS

Perhaps even more important than the written reports and research performed under contract sponsorship are the contributions that will be made by student and faculty contributors whose further research participation training has been made possible in part by the contract's financial support. Personnel, in addition to the principal investigator Dr. Julius Kane, include:

Faculty

Dr. John Spence, Assistant Professor of Electrical Engineering at U.R.I.

Dr. E. Suryanarayan, Associate Professor of Mathematics at U.R.I.

Dr. A. Mal, Assistant Research Geophysicist at U.C.LA.

Dr. D. Sadeh, Assistant Research Geophysicist at U.C.L.A.

Students

Mr. David Dence, graduate student at U.R.I.

Mr. Stewart Davis, graduate student at U.R.I.

Mr. J. Massore, graduate student at U.R.I.

Mr. Jose Chirivella, graduate student at Caltech.

Mr. John Rouse, student at Caltech.

Mr. Richard Vogel, graduate student at Caltech.

Mr. Carl Henreich, graduate student at Caltech.

Mr. M. Young, student at U.C.L.A.

APPENDIX A

# RAYLEIGH WAVE TRANSMISSION ON ELASTIC WEDGES*

J. KANE† AND J. SPENCE†

A method is introduced by which transmission or conversion coefficients can readily be calculated for surface-wave diffraction at crustal discontinuities which can be idealized as wedge-shaped obstacles. The method, an iteration procedure, is illustrated by an application to Rayleigh-wave propagation on elastic wedges with free boundaries. It is shown that the leading term of the iteration procedure yields an expression for the transmission coefficient which matches the experimental data for a range of wedge angles which includes the crustal wedges commonly found in seismic practice. Numerical data are presented which illustrate the transmission coefficient's variation in terms of Poisson's ratio and the wedge angle.

## INTRODUCTION

The diffraction of Rayleigh waves by wedges is a topic of practical importance because it is related to the generation of seismic noise and to other geophysical and acoustical applications. In addition, it has considerable inherent theoretical interest because the associated boundary value problem has not yet yielded to any available mathematical techniques. In this report, we introduce a procedure which is useful for estimating the propagation effects on seismic waves propagating past wedge-shaped obstacles. Our method is basically an iteration procedure by which the boundary conditions on either face of the wedge are alternately satisfied. The convergence of the associated series and the higher-order iterations will be discussed in a subsequent paper. It is the purpose of this report to demonstrate that the first iteration yields the principal information desired by the seismologist, namely the field that propagates past the discontinuity. This data is obtained readily by our analysis because the faces of wedges associated with crustal discontinuities are nearly parallel, and our procedure yields the transmission coefficients by rather elementary operations. We shall illustrate the treatment by calculating the transmission coefficient of a Rayleigh wave which is incident upon a free elastic wedge.

In some respects our first iteration is related to the Kirchoff-Huygen method which finds an approximate field by integrating a suitable Green's function over an aperture with a weight function proportional to an assumed illumination. Our method differs in several respects: we neither need obtain a Green's function, nor integrate it, and our calculations can be systematically improved.

## FORMULATION

We consider an isolated wedge with free boundaries (Figure 1). It is very convenient to introduce two coordinate systems: first, the $x$, $y$ system simplifies the discussion of the left face, and second, the $\xi$, $\eta$ system is appropriate for the right one. The two coordinate systems differ by a rotation through an angle $\theta$ which we shall call the *wedge angle*; thus, we have

$$\begin{aligned} x &= \xi \cos\theta - \eta \sin\theta, \\ y &= \xi \sin\theta + \eta \cos\theta, \end{aligned} \tag{1}$$

and the inverse transformation

$$\begin{aligned} \xi &= x \cos\theta + y \sin\theta, \\ \eta &= -x \sin\theta + y \cos\theta. \end{aligned} \tag{2}$$

The angle $\theta$ is positive when measured counterclockwise from $\theta = 0$, the $x$ axis, so that negative values of $\theta$ correspond to elastic wedges whose

* The research described in this report has been sponsored by the Advanced Research Projects Agency, Project Vela-Uniform, under contract AF 19(628)-319 of the Geophysics Research Directorate, Air Force Cambridge Research Laboratories, Office of Aerospace Research, United States Air Force, Bedford, Massachusetts. Manuscript received by the Editor January 25, 1963.

† University of Rhode Island, Kingston, R. I.

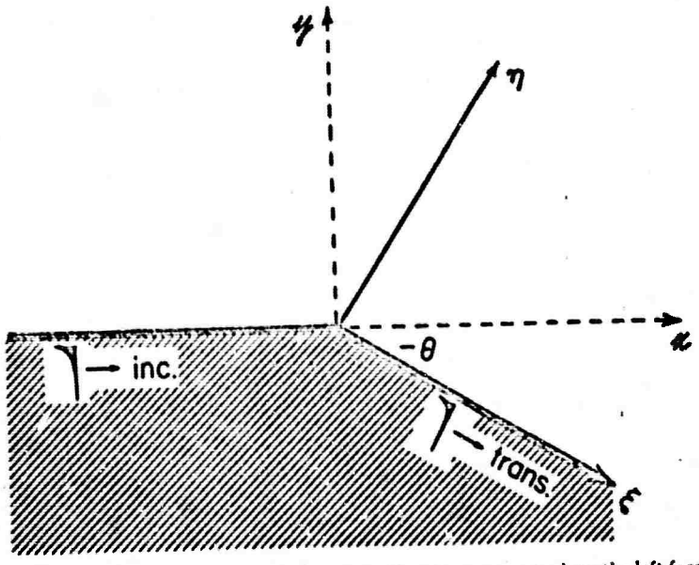


FIG. 1. The geometry of our problem: A Rayleigh wave is incident from $x=-\infty$ along the left face of a free elastic wedge. In this illustration, the wedge angle $\theta$ is negative.

interior angles are less than $\pi$ radians and positive values to wedges whose interior angles are greater than $\pi$ radians. If $\theta=0$, then the wedge degenerates into a half-space with no discontinuity at the origin.

In the absence of body forces, small displacements $s(u, v, w)$ of an elastic solid characterized by the Lamé parameters $\lambda$, $\mu$, and density $\rho$, can be derived from a scalar potential $\phi$, and a vector potential $\Psi(\psi_1, \psi_2, \psi_3)$, namely,

$$s(u, v, w) = \text{grad}\ \phi + \text{curl}\Psi(\psi_1, \psi_2, \psi_3).$$

For two-dimensional motions, $\phi=\phi(x, y)$, $\psi_3 = \psi_3(x, y)$, and we can neglect pure distortions by setting $\psi_1=\psi_2=0$, so that without introducing any confusion we can drop the subscript on $\psi_3(x, y)$. For monochromatic vibrations, we can suppress a time factor $e^{-i\omega t}$, and it can be shown that $\phi$ and $\psi$ satisfy the reduced wave equations:

$$(\nabla^2 + k_c^2)\phi = 0, \qquad k_c^2 = \omega^2\rho/(\lambda+\mu), \tag{3}$$
$$(\nabla^2 + k_s^2)\psi = 0, \qquad k_s^2 = \omega^2\rho/\mu,$$

in the interior of the wedge. Let $(\xi, \eta)$ be dummy variables which represent either the $(\xi, \eta)$ or $(x, y)$ coordinate systems; then the tangential stress,

$$p_{t\eta}(\phi, \psi) = \mu\left(2\frac{\partial^2\phi}{\partial l\partial n} - \frac{\partial^2\psi}{\partial l^2} + \frac{\partial^2\psi}{\partial n^2}\right), \tag{4}$$

and the normal stress,

$$p_{nn}(\phi, \psi) = \lambda\nabla^2\phi + 2\mu\left(\frac{\partial^2\phi}{\partial n^2} - \frac{\partial^2\psi}{\partial l\partial n}\right), \tag{5}$$

must vanish on either face of the wedge. As our excitation, we shall choose a Rayleigh wave of unit amplitude,

$$R(\phi_r, \psi_r) = \phi_r + \psi_r,$$

in the elastic wedge which is incident from $x=-\infty$, so that

$$R(\phi_r, \psi_r) = \begin{cases} \phi_r = 1e^{ik_r x + iy\sqrt{k_r^2 - k_c^2}} \\ \psi_r = Ze^{ik_r x + iy\sqrt{k_r^2 - k_s^2}}. \end{cases} \tag{6}$$

We shall speak of the coefficient, in this case unity, of the compressional potential $\phi_r$ as the amplitude of the Rayleigh wave. The parameters $k_r$ and $Z$ are so chosen that the Rayleigh wave exerts neither normal nor tangential stress at the free elastic surface at $y=0$. In general, $|k_r| > |k_s| > |k_c|$, so that both $\phi_r$ and $\psi_r$ are exponentially attenuated with increasing depth. We seek diffracted fields $(\phi_d, \psi_d)$ which we can add to the Rayleigh wave so that the total field $u_T$, where

$$u_T = (\phi_r + \phi_d) + (\psi_r + \psi_d$$

exerts neither normal nor tangential stress on either wedge face.

## THE ITERATED SOLUTION

### *Preliminary remarks*

Let $u_{inc}^0$ denote the incident field, or zeroth-order iteration, which in our case would be the Rayleigh wave

$$u_{inc}^0 = \phi_r + \psi_r.$$

Each term in this expression is a wave function, and the combination $\phi_r+\psi_r$ satisfies the boundary conditions on the left face of the wedge, but not those on the right face. There is no known[1] way by which one can add wave functions $(\phi_d, \psi_d)$ to $u_{inc}^0$ so that *all* boundary conditions are satisfied. However, it is possible to introduce wave functions $(\phi^1, \psi^1)$ so that

$$u^1 = u_{inc}^0 + (\phi^1, \psi^1) = (\phi_r + \phi^1, \psi_r + \psi^1)$$

satisfies the boundary conditions on the right face. One can think of $\phi^1$ and $\psi^1$ as elastic waves generated by the response of the second face to the incident Rayleigh wave. Of course $u^1$ will not satisfy the boundary condition on the left face because the terms $(\phi^1, \psi^1)$ have been introduced without consideration of the left-hand boundary conditions. However, on heuristic principles, we would imagine that if the wedge angle $\theta$ were small, then very little of the secondary energy associated with $(\phi^1, \psi^1)$ would be returned to the left face. Thus, although we could introduce another term in the iteration procedure, namely

$$u^2 = u^1 + (\phi^2, \psi^2),$$

so that $u^2$ satisfies the left boundary condition, we shall not do so in the present paper, because we shall show that $u^1$ yields a transmission coefficient which agrees very well with experimental data for a rather wide variation of $\theta$.

### *Integral representations*

The incident Rayleigh wave $u_{inc}$ does not satisfy the boundary conditions on the second wedge face for it applies nonvanishing stresses:

$$p_{t\eta}(\phi_r, \psi_r) = f(\xi), \tag{7}$$

$$p_{\eta\eta}(\phi_r, \psi_r) = g(\xi), \tag{8}$$

to that half-plane $\eta=0$, $\xi \gtrless 0$. In our context, the expressions $p_{t\eta}$ and $p_{\eta\eta}$ are linear differential operators on $\phi$ and $\psi$ which involve exponential functions of algebraic argument. Since differentiation of such exponentials is equivalent to multiplication by algebraic expressions, it is very convenient to introduce the following functions of $k$ defined over the complex wave number plane:

$$P(k) = 2k\mu\sqrt{k_s^2 - k^2}, \tag{9}$$

$$Q(k) = \mu(2k^2 - k_s^2), \tag{10}$$

$$R(k) = -\lambda k_s^2 - 2\mu(k_s^2 - k^2), \tag{11}$$

$$S(k) = -2k\mu\sqrt{k_s^2 - k^2}, \tag{12}$$

and a useful determinant

$$\text{Det}\,(k) = \begin{vmatrix} P(k) & Q(k) \\ R(k) & S(k) \end{vmatrix}. \tag{13}$$

It is important to note that since the Rayleigh wave $R(\phi_r, \psi_r)$ exerts neither normal nor tangential stress at $y=0$, we have

$$P(k_r) + Q(k_r)Z = 0, \tag{14}$$

$$R(k_r) + S(k_r)Z = 0, \tag{15}$$

so that the columns of $\text{Det}(k_r)$ are proportional, or the period equation

$$\text{Det}\,(k) = 0 \tag{16}$$

has a root at $k=k_r$.

With these definitions, the Rayleigh wave stresses $f(\xi)$ and $g(\xi)$ on the right face, $\eta=0$, $\xi=0$, are explicitly

$$f(\xi) = P(\alpha)e^{i\alpha\xi} + Q(\beta)Ze^{i\beta\xi} \tag{17}$$

and

$$g(\xi) = R(\alpha)e^{i\alpha\xi} + S(\beta)Ze^{i\beta\xi}, \tag{18}$$

where $\alpha(\theta)$ and $\beta(\theta)$ lie on ellipses (see Figure 2) in the complex $k$ plane:

$$\alpha(\theta) = k_r\cos\theta - i\sqrt{k_r^2 - k_s^2}\sin\theta, \tag{19}$$

$$\beta(\theta) = k_r\cos\theta - i\sqrt{k_r^2 - k_s^2}\sin\theta. \tag{20}$$

Note that for small values of $\theta$, both $\alpha$ and $\beta$ are approximately equal to $k_r$. For $\xi>0$, we can rewrite the stresses (17) and (18) in integral form

[1] Indeed, because of the geometric singularity at the sharp edge, there may well be no solution if the boundary conditions are used uniformly at all distances from the vertex. The only well-posed boundary value problem of this type may be one where the wedge has a rounded tip.

by the Cauchy integral theorem as

$$f(\xi) = \frac{1}{2\pi i}\int_C \left(\frac{P(\alpha)}{k-\alpha} + Z\frac{Q(\beta)}{k-\beta}\right) e^{ikx} dk \quad (21)$$

and

$$g(\xi) = \frac{1}{2\pi i}\int_C \left(\frac{R(\alpha)}{k-\alpha} + Z\frac{S(\beta)}{k-\beta}\right) e^{ikx} dk, \quad (22)$$

where the contour $C$ is sketched in Figure 3. Expressions (21) and (22) display the stresses on $\eta = 0$ as Fourier transforms. Let us note that if the boundary values $u(\xi, 0)$ of a function $u(\xi, \eta)$ are given in the form

$$u(\xi, 0) = \frac{1}{2\pi i}\int_C U(k) e^{ikx} dk, \qquad \xi > 0,$$

then it is a trivial matter to analytically continue $u(\xi, 0)$ as a solution of the wave equation

$$(\nabla^2 + \kappa^2) u(\xi, \eta) = 0$$

into the half-space $\eta < 0$ by inserting a factor $e^{-i\sqrt{\kappa^2 - k^2}\,\eta}$ under the integral sign

$$u(\xi, \eta) = \frac{1}{2\pi i}\int_C U(k) e^{ikx - i\sqrt{\kappa^2 - k^2}\,\eta} dk,$$

and suitably indenting the contour $C$ about the branch points $\pm\kappa$ in the complex $k$ plane. Vertical branch cuts have been chosen so that the cut $k$ plane (see Figure 3) represents that sheet of the Riemann surface for which the radicals $\sqrt{k_c^2 - k^2}$ and $\sqrt{k_s^2 - k^2}$ are respectively $+k_c$ and $+k_s$ at the origin $k = 0$; by analytic continuation, this fixes the values of the radicals throughout the entire cut $k$ plane.

With these preliminaries, we seek the first unknown wave functions $(\phi^1, \psi^1)$ in the form:

$$\phi^1 = \frac{1}{2\pi i}\int_C X(k) e^{ikx - i\sqrt{k_c^2 - k^2}\,\eta} dk, \quad (23)$$

$$\psi^1 = \frac{1}{2\pi i}\int_C Y(k) e^{ikx - i\sqrt{k_s^2 - k^2}\,\eta} dk, \quad (24)$$

where the kernels $X(k)$ and $Y(k)$ are to be chosen

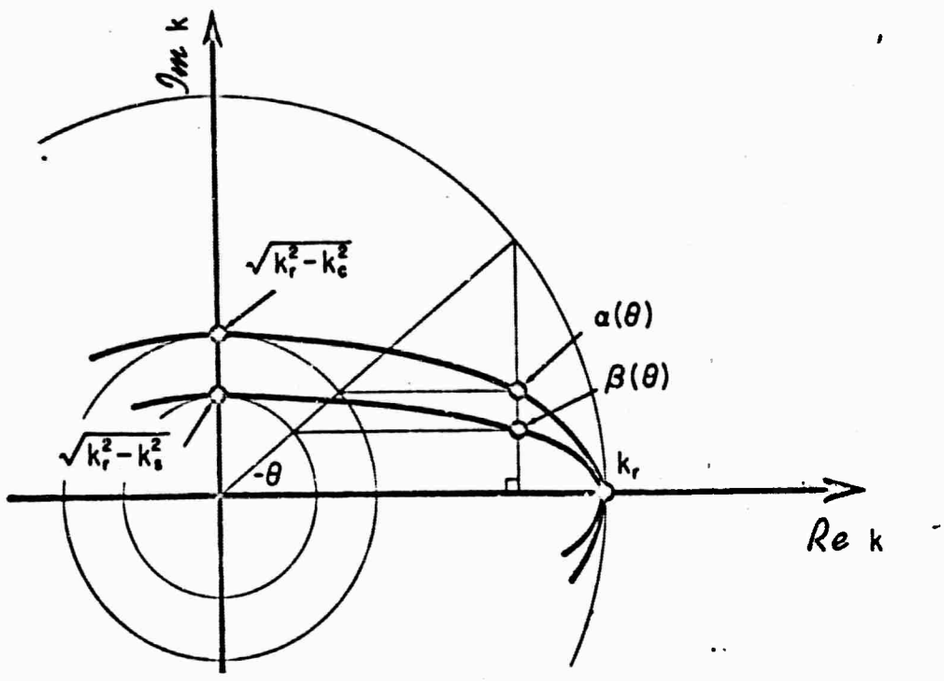


FIG. 2. The location of the poles $k = \alpha, \beta$ in the complex $k$ plane as a function of the wedge angle $\theta$. Because of the minus signs in equations (19) and (20), the poles $\alpha$ and $\beta$ lie in the upper half-plane when $\theta$ is negative.

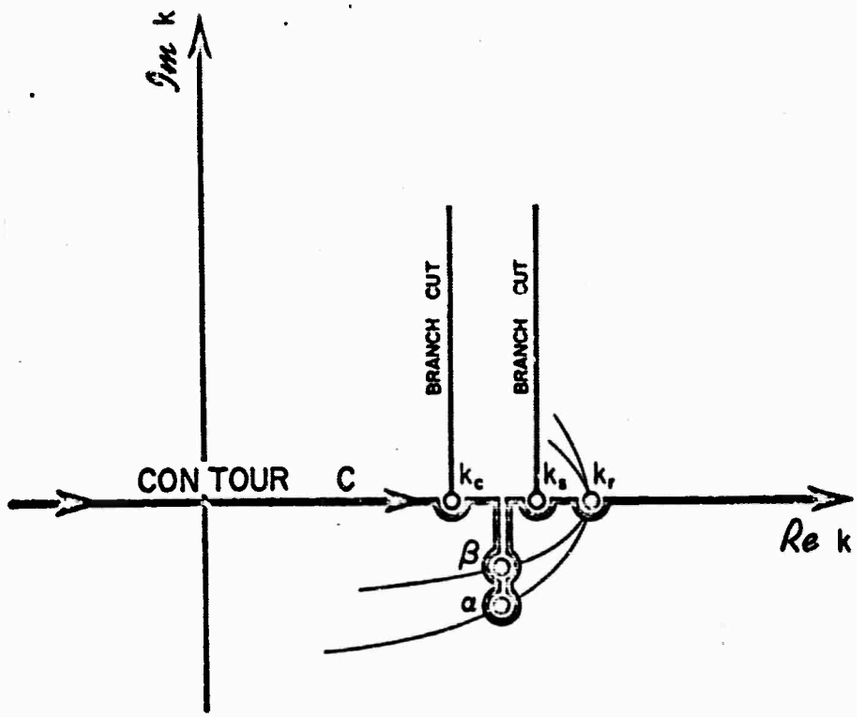


FIG. 3. The contour $C$ is chosen to lie along the real $k$ axis except for indentations *below* any singularities if $\mathrm{Re}\, k>0$ and *above* any singularities if $\mathrm{Re}\, k<0$. In the diagram, $\alpha$, $\beta$ have been drawn for a positive wedge angle.

so that the combination $(\phi_r+\phi^1, \psi_r+\psi^1)$ exerts neither tangential stress

$$p_{t\eta}(\phi_r + \phi^1, \psi_r + \psi^1) = 0, \qquad (25)$$

nor normal stress

$$p_{\eta\eta}(\phi_r + \phi^1, \psi_r + \psi^1) = 0 \qquad (26)$$

on the wedge face $\eta=0$, $\xi>0$. Assuming that we can differentiate freely under the integral signs, we find that (25) and (26) require that $X(k)$ and $Y(k)$ be solutions of the pair of algebraic equations:

$$\begin{aligned} &P(k)X(k) + Q(k)Y(k) \\ &\quad = -\left[\frac{P(\alpha)}{k-\alpha} + Z\frac{Q(\beta)}{k-\beta}\right], \\ &R(k)X(k) + S(k)Y(k) \\ &\quad = -\left[\frac{R(\alpha)}{k-\alpha} + Z\frac{S(\beta)}{k-\beta}\right], \end{aligned} \qquad (27)$$

which can be solved by inspection as

$$X(k;\theta) = \frac{A(k,\theta)S(k) - B(k,\theta)Q(k)}{\mathrm{Det}\,(k)}, \qquad (28)$$

$$Y(k;\theta) = \frac{B(k,\theta)P(k) - A(k,\theta)R(k)}{\mathrm{Det}\,(k)}, \qquad (29)$$

where the $\theta$ variation is contained in the expressions

$$A(k,\theta) = \frac{P(\alpha)}{k-\alpha} + Z\frac{Q(\beta)}{k-\beta}, \qquad (30)$$

and

$$B(k,\theta) = \frac{R(\alpha)}{k-\alpha} + Z\frac{S(\beta)}{k-\beta}. \qquad (31)$$

Hence, the field up to the first iteration would be

*(Please turn the page for equation 32.)*

$$u^1(\phi^1, \psi^1) = \begin{cases} \phi_r + \dfrac{1}{2\pi i}\displaystyle\int_C \dfrac{A(k,\theta)S(k) - B(k,\theta)Q(k)}{\text{Det}\,(k)}\, e^{ik[-t\sqrt{k_r^2-k^2}-\cdots]}\,dk \\ \psi_r + \dfrac{1}{2\pi i}\displaystyle\int_C \dfrac{B(k,\theta)P(k) - A(k,\theta)R(k)}{\text{Det}\,(k)}\, e^{ik[-t\sqrt{k_r^2-k^2}\cdots]}\,dk. \end{cases} \tag{32}$$

## THE RAYLEIGH TRANSMISSION COEFFICIENT

### *Comparison with experiment*

The integrals in (32) represent the first-order reaction of the right wedge face to the incident Rayleigh wave, and include both body waves and surface waves as contributions to the net field. The cylindrical body waves can be evaluated by a standard appeal to the method of saddle points and will not be discussed. The surface waves emerge as residue fields of the various poles of (32). By construction, the poles at $k=\alpha$ and $k=\beta$ give rise to a field which just cancels the *incident* Rayleigh wave on the right face of the wedge. We have observed in equation (16) that DET($k$) has a zero at $k=k_r$, so that both integrals in (32) have another pole at $k=k_r$. Clearly, the residue field associated with this pole:

$$\begin{aligned} \phi_t^1 &= T(\theta,\sigma)e^{ik_r[\cdots+\sqrt{k_r^2-k_s^2}\cdots]}, \\ \psi_t^1 &= T(\theta,\sigma)Ze^{ik_r[\cdots+\sqrt{k_r^2-k_s^2}\cdots]}, \end{aligned} \tag{33}$$

represents the leading contribution to the transmitted Rayleigh wave. The amplitude coefficient $T(\theta,\sigma)$ of this transmitted field can be readily calculated from (32) as

$$T(\theta,\sigma) = \frac{A(k_r,\theta)S(k_r) - B(k_r,\theta)Q(k_r)}{\dfrac{d}{dk}\,\text{Det}\,(k)\Big|_{k=k_r}}, \tag{34}$$

which is a function of the wedge angle $\theta$ and Poisson's ratio $\sigma$. When there is no discontinuity, it can easily be shown that

$$\lim_{\theta\to 0} T(\theta,\sigma) = 1, \tag{35}$$

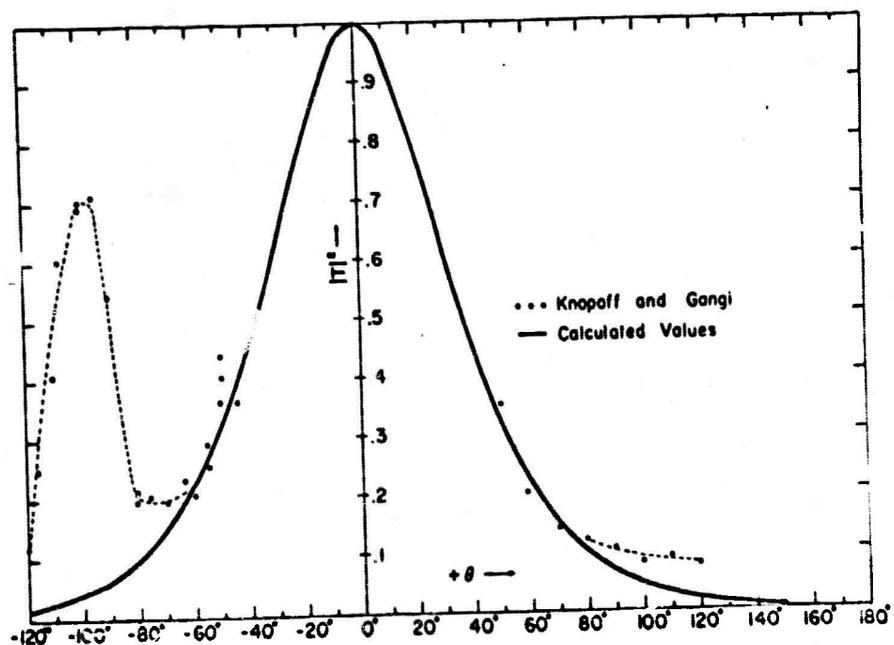


FIG. 4. A comparison of the leading term in an iteration of $|T(\theta,\sigma)|^2$ with the measured data of Knopoff and Gangi for Poisson's ratio $\sigma=.266$.

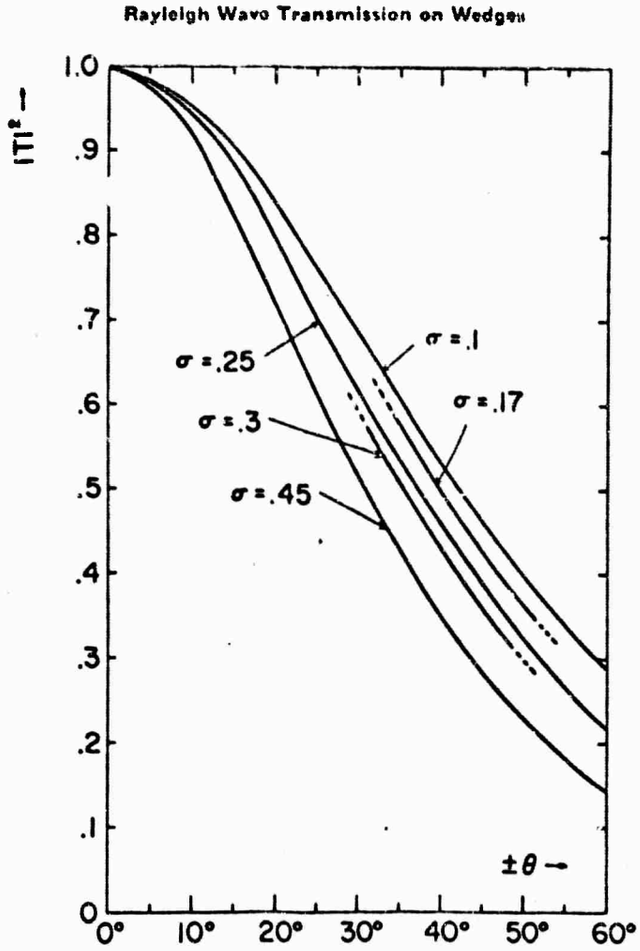


FIG. 5. The absolute square of the transmission coefficient $T$, which is an even function of the wedge angle $\theta$.

as it should. Furthermore, since both the numerator and denominator of (34) are homogeneous functions of the same order of the parameter $k_r$, there is no frequency dependence in the leading term of the transmission coefficient.

The range of utility of (34) can be gauged by an appeal to *carefully measured* experimental evidence: in Figure 4, we plot $|T|^2$ as a function of $\theta$ for Poisson's ratio $\sigma = 0.266$, and compare it to the data of Knopoff and Gangi (1960). We note that the experimental points straddle the calculated values for $-60° < \theta < +70°$. Of course, this range includes practically all crustal wedges commonly found in seismic practice.

However, there are theoretical reasons why extreme values of $\theta$ are of interest, and it may be useful to comment upon Figure 4 in more detail. For $\theta > +70°$, some of the discrepancy should be removed by including the contribution of higher iterations, but experimental sources of error which increase the transmission coefficient should not be ruled out: these might include a slight rounding of the vertex, or multiple scattering from minor inhomogeneities in the model. A much more interesting item in the experimental data is the secondary peak in the transmission coefficient at about $\theta = -100°$ which is not reproduced by (34), the first-order transmission coefficient. Similar humps appear even in less refined measurements (deBremaecker, 1958; Viktorov, 1958), which implies that this secondary maximum is a characteristic feature of Rayleigh-wave diffraction by wedges. Although this peak does not appear in our first-order analysis, a qualitative inspection of

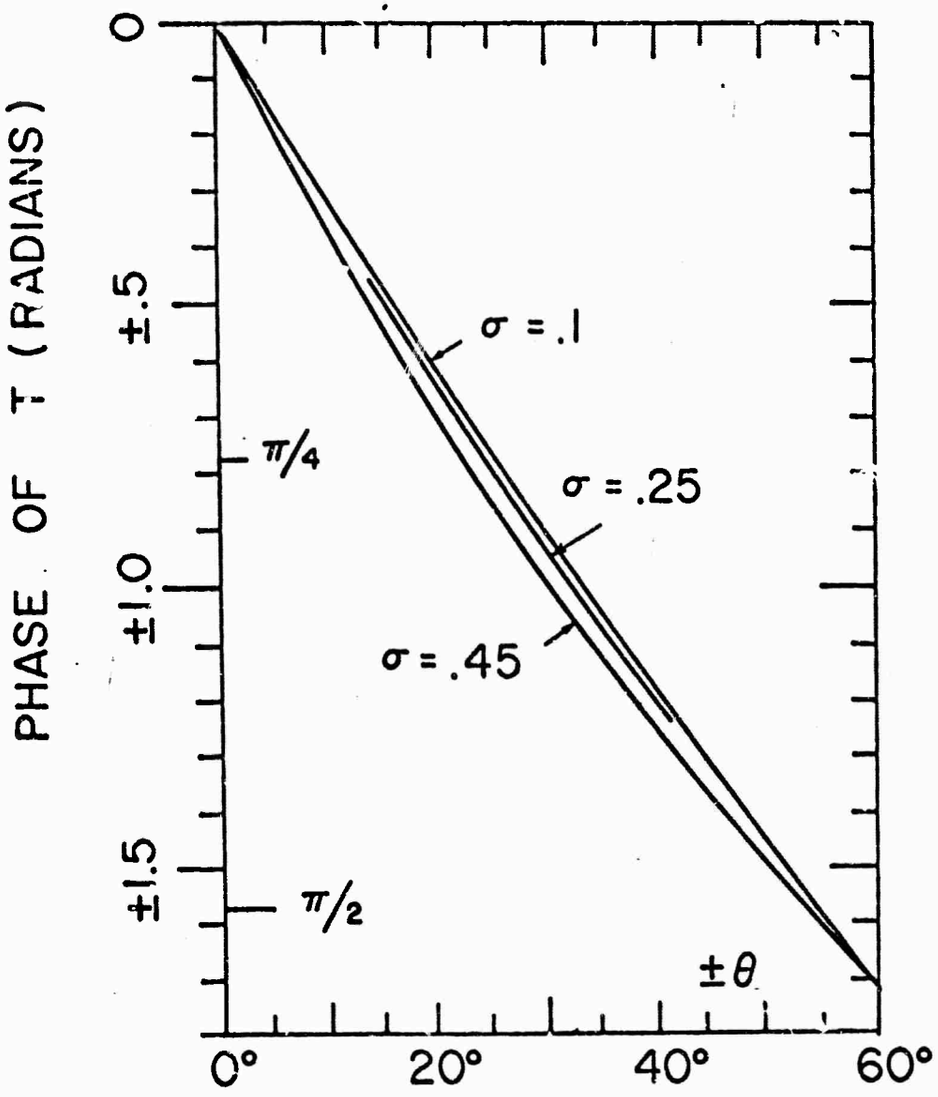


FIG. 6 The phase of $T(\theta, \sigma)$ which is an odd function of the wedge angle $\theta$. Positive values of phase correspond to positive values of $\theta$.

the higher-order iterations indicates a theoretical basis for this phenomenon in terms of the sensitive dependence of the transmission coefficient upon the location of the reflected Rayleigh-wave pole when $-110° < \theta < -80°$. This invites an interpretation in terms of a resonance between the reflected and transmitted fields within this range of $\theta$.

*Presentation of numerical data*

The agreement between theory and experiment for the range $-60° < \theta < +70°$ prompts a detailed display of the behavior of the transmission coefficient $T(\theta, \sigma)$ in this band. In Figure 5, we illustrate the dependence of $|T(\theta, \sigma)|^2$, which is an even function of $\theta$, upon Poisson's ratio $\sigma$. For fixed $\theta$, the magnitude of the transmission

coefficient varies inversely as Poisson's ratio. However, we note that this variation is not pronounced. In general, the transmission coefficient is a complex number, and in Figure 6 we plot the phase of $T(\theta, \sigma)$, which is an odd function of $\theta$ for the same range of $\theta$ as in Figure 5. This phase variation is almost linear and is practically insensitive to changes in Poisson's ratio.

## CONCLUSIONS

The method we have used to discuss Rayleigh-wave transmission can be readily adapted to estimate transmission or conversion coefficients for surface-wave diffraction at other crustal discontinuities which can be idealized as wedge-shaped obstacles. The principal advantage of the technique is that these coefficients can be obtained with an economy of effort, particularly if the wedge angle is small. Although contour integration has been introduced in describing the method, an examination of the analysis will reveal that the residue coefficients could have been calculated directly from the boundary conditions, and by an explicit representation of the incident field.

## REFERENCES

deHremaecker, J. Cl., 1958, Transmission and reflection of Rayleigh waves at corners: Geophysics, v. 23, pp. 253–266.

Knopoff, L., and Gangi, A. F., 1960, Transmission and reflection of Rayleigh waves by wedges: Geophysics, v. 25, pp. 1203–1214.

Viktorov, I. A., 1958, The effects of surface defects on the propagation of Rayleigh waves: Soviet Physics—Doklady, v. 3, pp. 304–306.

APPENDIX B

# The Theory of Surface Wave Diffraction by Symmetric Crustal Discontinuities

Julius Kane and John Spence

(Received 1964 May 4)*

*Summary*

The techniques of functional analysis are used to find approximate solutions to the problem of surface wave diffraction by symmetric wedge-shaped obstacles. The complex amplitudes of the scattered surface waves are found by a variational procedure which requires but the solution of a small number of linear algebraic equations: the Gauss normal equations. The analysis is illustrated by a discussion of the vector problem of Rayleigh wave diffraction by elastic wedges, and the scalar problem of Love wave diffraction in a layered wedge which supports *two* propagating modes.

## Introduction

A major barrier in comparing seismic theory with observed wave trains, stems from the fact that elastic wave characteristics are influenced by discontinuities along the propagation path, and any understanding of such signal corruption would require a knowledge of the diffracted fields at the appropriate obstacles. However, even a relatively simple crustal feature such as a discontinuous change in terrain presents major difficulties if the relevant problem of diffraction in a wedge-shaped region is considered. Although some first-order calculations have been made by Lapwood (1961), Kane & Spence (1963), and Hudson & Knopoff (1963), the theoretical discussion of the diffraction effects are hampered by the intractability of the associated boundary value problems. In this report, we show how one can take advantage of symmetry considerations and variational techniques to estimate rapidly reflection, transmission, and conversion coefficients for elastic wave diffraction at symmetric wedge-shaped obstacles. In Part 1, we illustrate the ideas by a discussion of the vector problem of Rayleigh wave propagation along the faces of an elastic wedge with free boundaries. In Part 2, we analyse the scalar problem of *multi-mode Love wave* diffraction in a symmetric layered wedge.

## Part 1. Rayleigh waves on an elastic wedge

### 1. Fundamental equations

The tremors $\mathbf{s}(u, v, w)$ of an elastic solid characterized by the Lamé parameters $\lambda$, $\mu$, and density $\rho$, can be derived from a scalar potential $\phi(x, y, z)$, and a vector potential $\Psi[\psi_x(x, y, z), \psi_y(x, y, z), \psi_z(x, y, z)]$ by the relation

$$\mathbf{s}(u, v, w) = \nabla.\phi + \nabla \times \Psi. \tag{1.1}$$

* Received in original form 1963 November 8.

For two-dimensional motions which are independent of the $z$-coordinate, both $\phi$ and $\Psi$ are but functions of $x$ and $y$, or $\phi = \phi(x, y)$, and $\Psi = \Psi(x, y)$. Furthermore, we can neglect pure distortions by setting $\psi_x = \psi_y = 0$, so that the vector potential $\Psi = \Psi[0, 0, \psi_z(x, y)]$ is characterized by one scalar component and the subscript on $\psi_z$ can be dropped without confusion. If we assume that the vibrations are harmonic, we can suppress a time factor $e^{-i\omega t}$, and it can be shown that $\phi$ and $\psi$, the $z$-component of the vector potential, satisfy the reduced wave equations

$$(\nabla^2 + k_c^2)\phi = 0, \qquad k_c^2 = \omega^2\rho/(\lambda+\mu), \tag{1.2}$$

$$(\nabla^2 + k_s^2)\psi = 0, \qquad k_s^2 = \omega^2\rho/\mu. \tag{1.3}$$

Once the potentials $\phi$ and $\psi$ are known, the displacement vector $\mathbf{s}$ is given by (1.1), and the normal and tangential stresses $\sigma_{rr}$, $\sigma_{r\vartheta}$ can be obtained from the stress dyadic $\mathfrak{S}(\phi, \psi)$ given in symbolic notation as

$$\mathfrak{S}(\phi, \psi) = \lambda\mathfrak{I}\nabla\cdot\mathbf{s} + \mu(\nabla\mathbf{s} + \mathbf{s}\nabla) \tag{1.4}$$

where $\mathfrak{I}$ is the unity dyadic, the idemfactor.

## 2. The Rayleigh wave potentials

A time harmonic Rayleigh wave, or $\mathscr{R}$-wave for brevity, is comprised of a pair of exponential solutions of (1.2) and (1.3), $\mathscr{R} = \mathscr{R}(\phi_R, \psi_R)$. If the elastic solid lies within the half-space $y \leq 0$ (see Figure 1(*a*)), then these solutions, in polar coordinates $x = r\cos\vartheta$, $y = r\sin\vartheta$, assume the form

$$\mathscr{R}(\phi_R, \psi_R) = \begin{cases} \phi_R = e^{\alpha(\vartheta)\Xi} & (1.5) \\ \psi_R = -i\Gamma e^{\beta(\vartheta)\Xi} & (1.6) \end{cases}$$

wherein the exponential variation is given by

$$\alpha(\vartheta) = \sqrt{[1-(v_R/v_c)^2]}\sin\vartheta + i\cos\vartheta, \qquad v_c^2 = \frac{\lambda+\mu}{\rho} \tag{1.7}$$

$$\beta(\vartheta) = \sqrt{[1-(v_R/v_s)^2]}\sin\vartheta + i\cos\vartheta, \qquad v_s^2 = \frac{\mu}{\rho} \tag{1.8}$$

and $\Gamma$, the magnitude of the ratio of the shear potential coefficient of $\psi_R$ to the compressional one $\phi_R$ is

$$\Gamma = \frac{\sqrt{[1-(v_R/v_c)^2]}}{1-\frac{1}{2}(v_R/v_s)^2}, \tag{1.9}$$

and $\Xi$ is a dimensionless distance parameter

$$\Xi = k_R r = \frac{\omega}{v_R} r. \tag{1.10}$$

The parameters $v_c$ and $v_s$ represent the velocities of the compressional and shear body waves respectively. For a given Poisson's ratio $\sigma$

$$\sigma = \frac{\lambda}{2(\lambda+\mu)} \tag{1.11}$$

one needs solve for the Rayleigh wave velocity $v_R$, which is less than $v_s$, so that the

stresses induced by $\phi_R$ and $\psi_R$ vanish at the surface $y = 0$

$$\sigma_{rr}(\phi_R, \psi_R) = \sigma_{r\theta}(\phi_R, \psi_R) = 0, \qquad y = 0. \tag{1.12}$$

With this choice of $c_R$, the $\phi_R$ and $\psi_R$ given by (1.5) and (1.6) are the vector and scalar potentials characterizing a Rayleigh wave travelling to the right with unit amplitude. (We shall speak of the coefficient of the compressional potential as the amplitude.) It is very convenient to note that *we can reverse the direction of any harmonic wave by the operation of complex conjugation.* Thus

$$R\mathscr{R}(\phi_R^*, \psi_R^*) = \begin{cases} R\phi_R^* = Re^{+i\Gamma(\theta)\Sigma} & (1.13) \\ \\ R\psi_R^* = +iR\Gamma e^{+i\Gamma(\theta)\Sigma} & (1.14) \end{cases}$$

represents a Rayleigh wave travelling in the opposite direction with amplitude $R$.

## 2 Formulation of the boundary value problems

### (a) *The major problem*

The conundrum posed by Rayleigh wave diffraction in a wedge-shaped region is to find additional solutions $\phi_d$ and $\psi_d$ of (1.2) and (1.3) which represent diffracted fields in the interior of the wedge such that the stresses $\sigma_{rr}$ and $\sigma_{r\theta}$ vanish on both faces of the wedge for $\mathscr{R}$-wave excitation along one face. In our geometry, (see Figure 1(*a*)), the $\mathscr{R}$-wave is incident from infinity along the negative $x$-axis. We shall be principally concerned with calculating the complex amplitudes of the reflected and transmitted $\mathscr{R}$-waves as a function of the wedge angle $\Theta$ and Poisson's ratio $\sigma$. This task can be substantially eased by reducing the major problem to a pair of minor problems involving even and odd symmetries. Consider the incident $\mathscr{R}$-wave along the left wedge face to be the sum of two waves, each of half amplitude. Likewise, the absence of any excitation along the right wedge face is equivalent to a pair of incident $\mathscr{R}$-waves along it, each of half amplitude, *but opposed in sign,*

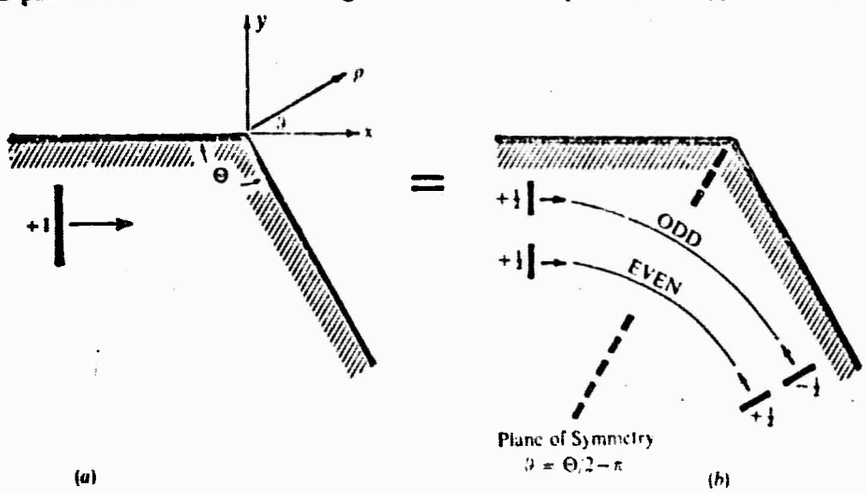


FIG. 1.—A unit Rayleigh Wave incident along one face of an elastic wedge is equivalent to four partial waves. The partial waves of like parity comprise the excitation for the even problem, and the partial waves of unlike parity furnish the initial disturbance for the odd problem.

(see, Figure 1(*b*)). The four partial $\mathscr{H}$-waves can be separated into two groups. First, a pair of $\mathscr{H}$-waves on either face of like parity which serves as the excitation of what we call the *even minor problem*. Second, another pair of $\mathscr{H}$-waves whose amplitudes are of unlike parity which constitutes the excitation of the *odd minor problem*. If we designate the diffracted fields of the even and odd problems by the subscripts e and o respectively, then since we are dealing with linear equations, the desired major potentials $\phi_d$ and $\psi_d$ can be expressed as a superposition of the minor potentials

$$\phi_d = \phi_e + \phi_o, \tag{1.15}$$

$$\psi_d = \psi_e + \psi_o, \tag{1.16}$$

and likewise the displacement vector $\mathbf{s} = \mathbf{s}_e + \mathbf{s}_o$ can be decomposed into even and odd components.

(*b*) *The even minor problem*

In the even problem, the wedge will suffer only *even displacements** $\mathbf{s}_e$ about the plane of symmetry, and as a result, there can be no component of normal displacement along the plane of symmetry at $\vartheta = \Theta/2 - \pi$. It follows that the even problem is equivalent to finding the potentials in a *bisected wedge* with one face free of stresses which supports the incident Rayleigh wave, and the other face so constrained that the *normal* displacement vanishes there. That is, we seek solutions $\phi_e$ and $\psi_e$ of (1.2) and (1.3) in a wedge of half-angle $\Theta/2$

$$\text{EVEN} \begin{cases} \sigma_{rr}(\phi_R + \phi_e, \psi_R + \psi_e) = \sigma_{r\vartheta}(\phi_R + \phi_e, \psi_R + \psi_e) = 0, & \vartheta = \pi \qquad (1.17) \\ \dfrac{1}{r}\dfrac{\partial}{\partial \vartheta}(\phi_R + \phi_e) + \dfrac{\partial}{\partial r}(\psi_R + \psi_e) = 0, & \vartheta = \Theta/2 - \pi \qquad (1.18) \end{cases}$$

(*c*) *The odd minor problem*

By similar arguments, the odd problem which involves $\phi_o$, $\psi_o$ is a complementary version in the bisected wedge, wherein the *tangential* displacements must vanish identically along the plane of symmetry, i.e.,

$$\text{ODD} \begin{cases} \sigma_{rr}(\phi_R + \phi_o, \psi_R + \psi_o) = \sigma_{r\vartheta}(\phi_R + \phi_o, \psi_R + \psi_o) = 0, & \vartheta = \pi \qquad (1.19) \\ \dfrac{\partial}{\partial r}(\phi_R + \phi_o) + \dfrac{1}{r}\dfrac{\partial}{\partial \vartheta}(\psi_R + \psi_o) = 0, & \vartheta = \Theta/2 - \pi \qquad (1.20) \end{cases}$$

(*d*) *The reflection coefficients*

For either the even or the odd problem, the solution will contain a reflected Rayleigh wave. Let $\rho_e(\Theta/2, \sigma)$ and $\rho_o(\Theta/2, \sigma)$ be the complex ratios of the reflected to the incident Rayleigh wave amplitude for the even and odd minor problems in the bisected wedge. The reflection coefficient $R(\Theta, \sigma)$ for the original major problem will be

$$R(\Theta, \sigma) = \tfrac{1}{2}[\rho_e(\Theta/2, \sigma) + \rho_o(\Theta/2, \sigma)], \tag{1.21}$$

and likewise the overall transmission coefficient $T(\Theta, \sigma)$ will be

$$T(\Theta, \sigma) = \tfrac{1}{2}[\rho_e(\Theta/2, \sigma) - \rho_o(\Theta/2, \sigma)]. \tag{1.22}$$

* The displacements and the compressional potential will be even about the plane of symmetry, but the shear potential will be an odd function, and *vice versa* for the odd problem.

Formulas (1.21) and (1.22) can be verified by a glance at figure 1(*b*) which indicates that the overall reflection coefficient $R$ results from a superposition of the partial reflection coefficients $\frac{1}{2}(\rho_e + \rho_o)$, and the transmission coefficient $T$ from their interference $\frac{1}{2}(\rho_e - \rho_o)$.

## 4. The variational principle

### (*a*) *Discussion*

Variational procedures consist of assuming a suitable trial function containing unspecified coefficients, and then choosing these parameters to minimize certain quantities. One major advantage of the variational method is that first-order accuracy in the trial function usually gives results which are accurate to second-order, because of the stationary character of the approximation.

A natural aperture in the present problem is the plane of symmetry and we can assume it to be illuminated by an incident $\mathscr{R}$-wave, and a reflected one with an adjustable amplitude. In the even problem, the net angular displacement must vanish along the plane of symmetry. A unit $\mathscr{R}$-wave travelling to the right gives rise to the angular component of the displacement

$$s_\vartheta^{\text{inc}} = k_R\left[\frac{\partial \alpha}{\partial \vartheta} e^{\alpha \Xi} + \beta e^{\beta \Xi}\right], \tag{1.23}$$

and likewise an $\mathscr{R}$-wave of amplitude $\rho_e$ moving to the left generates the disturbance

$$\rho_e s_\vartheta^{\text{ref}} = \rho_e (s_\vartheta^{\text{inc}})^* \tag{1.24}$$

which apart from an amplitude factor is the complex conjugate of (1.23). Only if there is no discontinuity, or if $\Theta = \pi$ can we make the angular displacement of the trial function

$$s_\vartheta^T = s_\vartheta^{\text{inc}} + \rho_e (s_\vartheta^{\text{inc}})^* \tag{1.25}$$

vanish for all $r$ along the plane of symmetry by properly choosing $\rho_e$. Otherwise $\alpha$ and $\beta$ are complex $\alpha \neq \alpha^*$, $\beta \neq \beta^*$, and no choice of $\rho_e$ can make $s_\vartheta^T$ vanish at more than an isolated set of points. There are at least two ways by which we can improve matters. We could use a more complex trial function which acknowledges body-wave contributions to the diffracted field, or, since the residual displacement $s_\vartheta^T$ is explicitly known, we can use it as the aperture illumination of a Green's theorem type calculation to correct the variational estimate.

However, the practical seismic interest is in the realm of small discontinuities, and for this case we shall see that the elementary trial function yields satisfactory results.

### (*b*) *Definition of the scalar product*

While there are many gauges by which $s_\vartheta^T$ can be minimized, we shall choose a $\rho_e$ which minimizes $s_\vartheta^T$ in the mean square sense. For this purpose, let us define the complex scalar product of two functions $u(r, \vartheta)$ and $v(r, \vartheta)$ to be

$$(u, v) \equiv \int_0^\infty u(r, \vartheta) v^*(r, \vartheta)\, dr, \tag{1.26}$$

where the integration is to be carried out along the plane of symmetry. $\vartheta = \Theta/2 - \pi$. To each complex function $u(r, \vartheta)$ we can attach a positive definite number, the

norm of $u$ or $\|u\|$ which is defined to be $\sqrt{(u,u)}$. The norm $\|u\|^2$ pends on the wedge angle, and is to be distinguished from $u^2 = (u, u^*)$ which is in general complex.

(c) *The even subsidiary reflection coefficient*

With this notation, the mean square value of the angular displacement of the trial function $s_3^T$ is

$$\|s_3^T\|^2 = (s_3^{inc} + \rho_e(s_3^{inc})^*, s_3^{inc} + \rho_e(s_3^{inc})^*), \tag{1.27}$$

and this will be a minimum if, and only if, $\rho_e$ is chosen as

$$\rho_e(\Theta/2, \sigma) = \frac{(s_3^{inc})^2}{\|s_3^{inc}\|^2}, \tag{1.28}$$

or explicitly in terms of $\alpha(\vartheta)$, $\beta(\vartheta)$ and $\Gamma$,

$$\rho_e(\Theta/2, \sigma) = \frac{-\frac{1}{2\alpha}\left(\frac{\partial\alpha}{\partial\vartheta}\right)^2 + \frac{\Gamma^2\beta}{2} - \frac{2i\Gamma\beta}{\alpha+\cdots}\left(\frac{\partial\alpha}{\partial\vartheta}\right)}{\frac{1}{\alpha+\alpha^*}\left|\frac{\partial\alpha}{\partial\vartheta}\right|^2 + \frac{\Gamma^2|\beta|^2}{\beta+\beta^*} + i\Gamma\left[\frac{\beta}{\alpha^*+\beta}\frac{\partial\alpha^*}{\partial\vartheta} - \frac{\beta^*}{\alpha+\beta^*}\left(\frac{\partial\alpha}{\partial\vartheta}\right)\right]}. \tag{1.29}$$

(d) *The odd subsidiary reflection coefficient*

If we use an analogous trial function, and similar reasoning, we find that if $\rho_o$ is to be an optimal choice we need make the selection

$$\rho_o(\Theta/2, \sigma) = \frac{(s_r^{inc})^2}{\|s_r^{inc}\|^2}, \tag{1.30}$$

or

$$\rho_o(\Theta/2, \sigma) = \frac{-\frac{\alpha^2}{2\alpha} + \frac{\Gamma^2}{2\beta}\left(\frac{\partial\beta}{\partial\vartheta}\right)^2 + \frac{2i\alpha\Gamma}{\alpha+\beta}\left(\frac{\partial\beta}{\partial\vartheta}\right)}{\frac{|\alpha|^2}{\alpha+\alpha^*} + \frac{\Gamma^2}{\beta+\beta^*}\left|\frac{\partial\beta}{\partial\vartheta}\right|^2 - i\Gamma\left[\frac{\alpha^*}{\alpha^*+\beta}\left(\frac{\partial\beta}{\partial\vartheta}\right) - \frac{\alpha}{\alpha+\beta^*}\left(\frac{\partial\beta^*}{\partial\vartheta}\right)\right]}. \tag{1.31}$$

## 5. Discussion of the overall reflection and transmission coefficients

With an explicit $\rho_e$ and $\rho_o$ at our disposal, we can evaluate the $R(\Theta, \sigma)$ and $T(\Theta, \sigma)$ germane to our elementary trial function. For reference, their complex variation is plotted as a function of the discontinuity angle $\Theta - \pi$, in Figure 2 for Poisson's ratio $\sigma = \frac{1}{4}$. The present magnitudes $|T|$ are somewhat smaller than that given by earlier first-order calculations (Kane and Spence 1963), which do not simultaneously yield $R$ and $T$. Since we evaluate both $R$ and $T$ together, we must, in effect, withdraw some energy from the transmitted field to allow for the reflected wave. Furthermore, it is the nature of the variational technique to underestimate the subsidiary diffraction coefficients $\rho_e$ and $\rho_o$ since it only yields their projection in the sub-space spanned by the trial function.

Although the analysis is certainly valid for a small enough discontinuity in wedge angle, the utility of the procedure cannot be established until there is some estimate of the errors committed. A feature of the present procedure is that it suggests a natural gauge of the accuracy. While $\rho_e$ and $\rho_o$ are so chosen that $\|s_3^T\|$ and $\|s_r^T\|$ are minimized, both $s_3^T$ and $s_r^T$ are non-zero along the aperature plane.

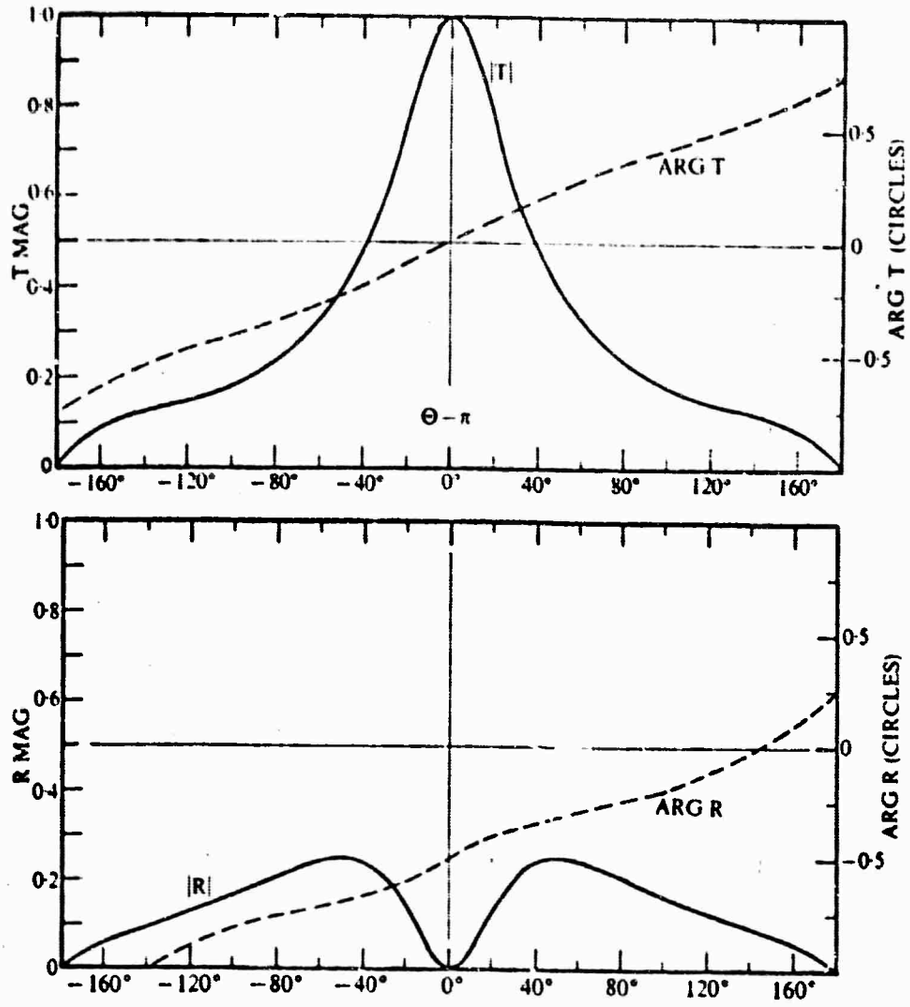


FIG. 2.—The diffraction coefficients $R$ and $T$ for a trial function consisting of but an incident and reflected wave. In this case, Poisson's ratio $\sigma = \frac{1}{4}$.

These residuals, which are explicitly known, cannot be farther reduced without introducing new features such as body wave contributions into the analysis. Since $(1 - |R|^2 - |T|^2)$ represents that fraction of energy unaccounted for, we can estimate the need for improving the calculations by examining this quantity.

*This error estimate is a very generous one* because only part of it implies higher-order corrections to $R$ and $T$, the remainder representing energy which is accounted for by $\mathscr{R}$-wave to body wave conversion. The data of Figure 2 show that if

$$|\Theta - \pi| < 10°,$$

the present analysis accounts for at least 92 per cent of the energy, and therefore the theory should not require further improvement within this range. We can also compare the present theory with experiment, but we must be very careful if we do so, because there are fundamental distinctions between analysis in the harmonic domain and pulse measurements (see Appendix).

### 6. Comment on the formulation

In our formulation, we have used as boundary conditions the demand that either the normal or tangential displacement vanish along the bisector plane depending upon the parity of the problem under consideration. Actually, the rigorous boundary conditions along the plane of symmetry are somewhat stronger demands. For example in the symmetric problem the correct formulation would be the pair of conditions that the compressional potential be an even function about the plane of symmetry and the shear potential an odd function about the plane of symmetry, and *vice versa* for the asymmetric problem. Then, since only continuous potentials are acceptable as solutions within the wedge, this would guarantee that there would be no discontinuity in the stresses across the plane of symmetry. For an approximate solution however, using pairs of boundary conditions for the even and odd problems is unduly complicated. For example, consider the even problem; any trial function under consideration would have shear and compressional potentials which vary at different rates along the bisector plane. The boundary condition (1.18) is the sum of two terms. If the first term vanishes then $(\phi_R + \phi_e)$ is an *even* function, and the vanishing of the second term implies that $(\psi_R + \psi_e)$ is an *odd* function. As a result, since we minimize (1.18) in the mean square sense, and the shear and compressional components of the trial function vary at different rates, it follows that minimizing the sum is equivalent to minimizing both terms in the sum simultaneously.

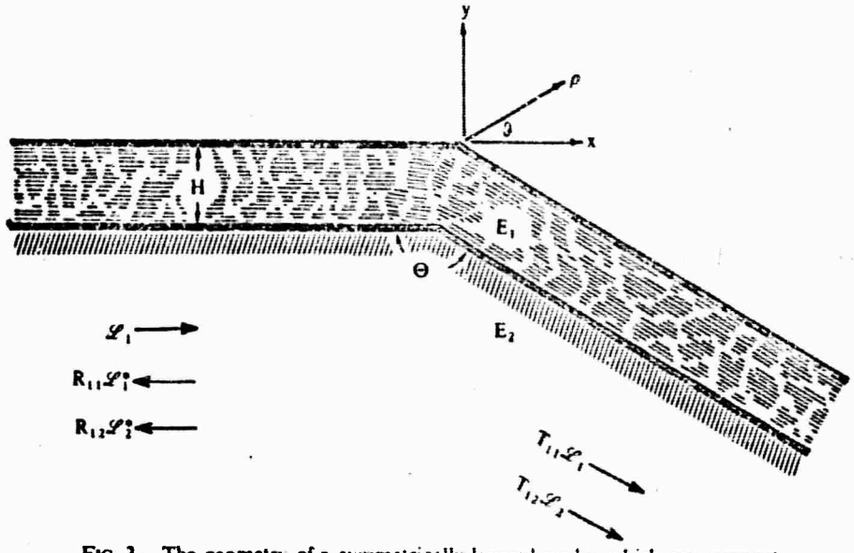


FIG. 3.—The geometry of a symmetrically layered wedge which can support Love waves. In the figure, it is assumed that the height $H$ is such that only two modes propagate.

## Part 2. Love waves on an elastic wedge

### 1. Introduction

A layered solid can support surface waves which are horizontally polarized shear waves trapped in the superficial layer. Since these Love waves, as they are known, have no compressional component, it is not necessary to introduce potentials, and it is possible to work directly with one scalar function $w(x, y)$, the $z$-component of the displacement vector

$$\mathbf{s} = [0, 0, w(x, y)]. \tag{2.1}$$

Within the $E_1$ layer, $w$ satisfies the wave equation

$$(\nabla^2 + k_1^2)w(x, y) = 0, \qquad k_1^2 = \omega^2\rho_1/\mu_1, \tag{2.2}$$

and within the $E_2$ substrate, $w$ obeys

$$(\nabla^2 + k_2^2)w(x, y) = 0, \qquad k_2^2 = \omega^2\rho_2/\mu_2. \tag{2.3}$$

At the free surface of $E_1$, the normal stress must vanish and this will be true provided that the normal derivative

$$\frac{\partial w}{\partial n} = 0 \tag{2.4}$$

vanishes there.

We assume the $E_1$-$E_2$ interface to be welded so that the displacement and normal stress must be continuous across this boundary. Along the horizontal wedge face, these conditions will be satisfied provided that the Love waves, or $\mathscr{L}_i$-waves of amplitude $A_i$ have the form

$$A_i\mathscr{L}_i = \begin{cases} A_i \cos\sqrt{(k_1^2 - \lambda_i^2)}y\, e^{i\lambda_i x}, & 0 \geq y \geq -H \qquad (2.5) \\ A_i \cos\sqrt{(k_1^2 - \lambda_i^2 H)} \exp\sqrt{(\lambda_i^2 - k_2^2)}y\, e^{i\lambda_i x}, & y \leq -H, \qquad (2.6) \end{cases}$$

and the propagation constants $\lambda_i$ are chosen as the real roots of the period equation

$$\tan\sqrt{(k_1^2 - \lambda_i^2 H)} = \frac{\mu_2}{\mu_1}\sqrt{\left(\frac{\lambda_i^2 - k_2^2}{k_1^2 - \lambda_i^2}\right)}. \tag{2.7}$$

If the shear wave is to be trapped in the layer, or if the Love wave is to propagate, we need $|k_2| \leq |\lambda_i| \leq |k_1|$. For any thickness, however small, there is at least one root $\lambda_1$ corresponding to an acceptable solution—the fundamental $\mathscr{L}_1$-wave. As the acoustic thickness $k_1 H$ increases, other modes can propagate. In our discussion, we shall assume that the thickness is such that only two modes propagate, the fundamental, and one harmonic, the $\mathscr{L}_2$-wave with a propagation constant $\lambda_2$. The analysis proceeds in a similar fashion if an arbitrary number of modes can propagate.

## 2. Formulation of the boundary value problem

We assume that an $\mathscr{L}_1$-wave is incident along one face of a symmetrically layered wedge. At the discontinuity, four propagating surface waves will be excited: a reflected and transmitted $\mathscr{L}_1$-wave with amplitude coefficients $R_{11}$ and $T_{11}$ respectively, and reflected and transmitted $\mathscr{L}_2$ waves whose amplitudes are the conversion coefficients $R_{12}$ and $T_{12}$ respectively. Our task will be to determine these diffraction coefficients as functions of the wedge angle $\Theta$, the layer thickness $H$ and the elastic constants $\rho_1, \rho_2, \mu_1, \mu_2$.

By the same argument as in Part 1, we can add and subtract a symmetric $\mathscr{L}_1$-excitation on the right wedge face which leads us to consider a pair of even and odd problems in a bisected wedge. Since Love wave diffraction is a scalar problem, the subsidiary boundary conditions along the aperture or plane of symmetry are simply

$$\text{EVEN} \quad \frac{1}{r}\frac{\partial w}{\partial \vartheta} = 0, \qquad \vartheta = \Theta/2 - \pi \tag{2.8}$$

$$\text{ODD} \quad w = 0, \qquad \vartheta = \Theta/2 - \pi \tag{2.9}$$

for the even and odd problems. The trial function will consist of an incident $\mathscr{L}_1$-wave, and reflected $\mathscr{L}_1^*$- and $\mathscr{L}_2^*$-waves, with unknown amplitudes. If we denote the subsidiary reflection and conversion coefficient for the even problem in the bisected wedge as $r_{11}^e$ and $r_{12}^e$, and similarly $r_{11}^o$ and $r_{12}^o$ for the odd problem, then the desired major coefficients are

$$R_{11} = \tfrac{1}{2}(r_{11}^e + r_{11}^o), \tag{2.10}$$

$$R_{12} = \tfrac{1}{2}(r_{12}^e + r_{12}^o), \tag{2.11}$$

$$T_{11} = \tfrac{1}{2}(r_{11}^e - r_{11}^o), \tag{2.12}$$

$$T_{12} = \tfrac{1}{2}(r_{12}^e - r_{12}^o). \tag{2.13}$$

As in Part 1, we shall determine these coefficients by a variational procedure which ignores body wave contributions.

## 3. Solution

In the odd problem we shall choose $r_{11}^o$ and $r_{12}^o$ so that the residual variation $\varepsilon(r)$ along the aperture plane

$$\varepsilon(r) = \mathscr{L}_1 + r_{11}^o \mathscr{L}_1^* + r_{12}^o \mathscr{L}_1^*, \qquad \vartheta = \Theta/2 - \pi \tag{2.14}$$

is as small as possible in the mean square sense. Using the same definition of scalar product as in Part 1, we have

$$\|\varepsilon(r)\|^2 = (\mathscr{L}_1 + r_{11}^o \mathscr{L}_1^* + r_{12}^o \mathscr{L}_2^*, \mathscr{L}_1 + r_{11}^o \mathscr{L}_1^* + r_{12}^o \mathscr{L}_2^*), \tag{2.15}$$

and this expression will be a minimum if, and only if, $r_{11}^o$ and $r_{12}^o$ satisfy the normal equations

$$(\mathscr{L}_1, \mathscr{L}_1) + r_{11}^o (\mathscr{L}_1^*, \mathscr{L}_1) + r_{12}^o (\mathscr{L}_2^*, \mathscr{L}_1) = 0, \tag{2.16}$$

$$(\mathscr{L}_1, \mathscr{L}_2) + r_{11}^o (\mathscr{L}_1^*, \mathscr{L}_2) + r_{12}^o (\mathscr{L}_2^*, \mathscr{L}_2) = 0. \tag{2.17}$$

Equations (2.16) and (2.17) can immediately be solved for $r_{11}^o$ and $r_{11}^o$

$$r_{11}^o = -\frac{1}{DET^o} \begin{vmatrix} (\mathscr{L}_1, \mathscr{L}_1) & (\mathscr{L}_2^*, \mathscr{L}_1) \\ (\mathscr{L}_1, \mathscr{L}_2) & (\mathscr{L}_2^*, \mathscr{L}_2) \end{vmatrix}, \tag{2.18}$$

and

$$r_{12}^o = -\frac{1}{DET^o} \begin{vmatrix} (\mathscr{L}_1^*, \mathscr{L}_1) & (\mathscr{L}_1, \mathscr{L}_1) \\ (\mathscr{L}_1^*, \mathscr{L}_2) & (\mathscr{L}_2, \mathscr{L}_2) \end{vmatrix}, \tag{2.19}$$

where

$$DET^o = \begin{vmatrix} (\mathscr{L}_1^*, \mathscr{L}_1) & (\mathscr{L}_2^*, \mathscr{L}_1) \\ (\mathscr{L}_1^*, \mathscr{L}_2) & (\mathscr{L}_2^*, \mathscr{L}_2) \end{vmatrix}. \tag{2.20}$$

In the same fashion, for the even problem we need choose $r_{11}^e$ and $r_{12}^e$ as

$$r_{11}^e = -\frac{1}{DET^e} \begin{vmatrix} \left(\frac{1}{r}\frac{\partial \mathscr{L}_1}{\partial \vartheta}, \frac{1}{r}\frac{\partial \mathscr{L}_1}{\partial \vartheta}\right) & \left(\frac{1}{r}\frac{\partial \mathscr{L}_2^*}{\partial \vartheta}, \frac{1}{r}\frac{\partial \mathscr{L}_1}{\partial \vartheta}\right) \\ \left(\frac{1}{r}\frac{\partial \mathscr{L}_1}{\partial \vartheta}, \frac{1}{r}\frac{\partial \mathscr{L}_2}{\partial \vartheta}\right) & \left(\frac{1}{r}\frac{\partial \mathscr{L}_2^*}{\partial \vartheta}, \frac{1}{r}\frac{\partial \mathscr{L}_2}{\partial \vartheta}\right) \end{vmatrix}, \tag{2.21}$$

and

$$r_{12}^{*} = -\frac{1}{\mathrm{DET}^{*}}\begin{vmatrix} \left(\frac{1}{r}\frac{\partial \mathscr{L}_1^{*}}{\partial \vartheta}, \frac{1}{r}\frac{\partial \mathscr{L}_1}{\partial \vartheta}\right) & \left(\frac{1}{r}\frac{\partial \mathscr{L}_1}{\partial \vartheta}, \frac{1}{r}\frac{\partial \mathscr{L}_1}{\partial \vartheta}\right) \\ \left(\frac{1}{r}\frac{\partial \mathscr{L}_1^{*}}{\partial \vartheta}, \frac{1}{r}\frac{\partial \mathscr{L}_2}{\partial \vartheta}\right) & \left(\frac{1}{r}\frac{\partial \mathscr{L}_1}{\partial \vartheta}, \frac{1}{r}\frac{\partial \mathscr{L}_2}{\partial \vartheta}\right) \end{vmatrix}, \tag{2.22}$$

where

$$\mathrm{DET}^{*} = \begin{vmatrix} \left(\frac{1}{r}\frac{\partial \mathscr{L}_1^{*}}{\partial \vartheta}, \frac{1}{r}\frac{\partial \mathscr{L}_1}{\partial \vartheta}\right) & \left(\frac{1}{r}\frac{\partial \mathscr{L}_2^{*}}{\partial \vartheta}, \frac{1}{r}\frac{\partial \mathscr{L}_1}{\partial \vartheta}\right) \\ \left(\frac{1}{r}\frac{\partial \mathscr{L}_1^{*}}{\partial \vartheta}, \frac{1}{r}\frac{\partial \mathscr{L}_2}{\partial \vartheta}\right) & \left(\frac{1}{r}\frac{\partial \mathscr{L}_2^{*}}{\partial \vartheta}, \frac{1}{r}\frac{\partial \mathscr{L}_2}{\partial \vartheta}\right) \end{vmatrix}. \tag{2.23}$$

With this knowledge, the reflection, transmission and conversion coefficients are given by (2.10) to (2.13).

## 4. Discussion of the results

### (a) *Numerical data*

We have used the preceeding formulas to calculate the diffraction coefficients for an $E_1$-layer and $E_2$-substrate for which $k_1/k_2 = 1{\cdot}297$ and $\mu_2/\mu_1 = 2{\cdot}159$. The phase and group velocities for this case have been given by Stoneley and are available in a standard reference (p. 213, Ewing & others 1957). Figures 4 to 7 illustrate the variation of the magnitude of the diffraction coefficients which are *even* functions of the discontinuity angle $\Theta - \pi$. The curves are indexed by four values of the dimensionless parameter $\lambda_1 H$, namely 5, 6, 7, 8; if $\lambda_1 H = 5$, then the second mode is just above cut-off, and if $\lambda_1 H = 8$, the third mode is just below cut-off. It is very interesting to note that the conversion coefficient $T_{12}$ exceeds the reflection coefficient $R_{11}$. That is, there is a tendency for the energy to continue to propagate in the same direction even if it necessitates a transfer of model characteristics.

### (b) *Interpretation*

If we compare any two waves of identical characteristics, then their relative energy is proportional to the absolute square of any corresponding amplitude. On the other hand, before we can compare the energy in the fundamental $\mathscr{L}_1$-wave to that of an $\mathscr{L}_2$-wave, its first harmonic, we need make some further calculations. With no loss in generality, let us specialize our discussion to the horizontal wedge face for which the $\mathscr{L}_i$-waves are given explicitly by (2.5) and (2.6), and evaluate the scalar product along the wavefront $y = 0$. Thus $|A_i|^2 \|\mathscr{L}_i\|^2$ represents the mean square energy flux transported by an $\mathscr{L}_i$-wave of amplitude $A_i$. If we denote the group velocity of an $\mathscr{L}_i$-wave as $\Lambda_i$ it follows that the ratio

$$\frac{|A_1|^2 \Lambda_1 \|\mathscr{L}_1\|^2}{|A_2|^2 \Lambda_2 \|\mathscr{L}_2\|^2} \tag{2.24}$$

compares the power flow of an $A_1\mathscr{L}_1$-wave to that of an $A_2\mathscr{L}_2$-wave. In particular, a mode near cut-off behaves like an unbounded plane wave in the $E_2$-medium; hence such a wave can carry large amounts of power even if its amplitude is deceptively small. As a result, if we are to discuss power transfer, we should renormalize

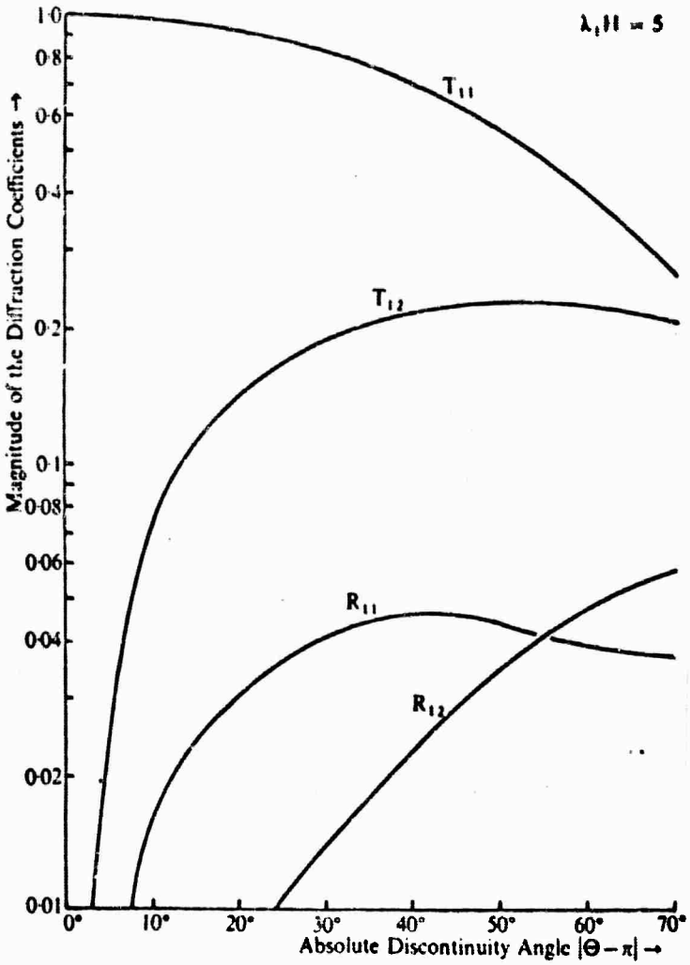


FIG. 4.—The magnitude of the Love wave diffraction coefficients for $\lambda_1 H = 5$; they are even functions of the discontinuity angle $\Theta - \pi$. In this case $k_2/k_1 = 1{\cdot}297$, $\mu_2/\mu_1 = 2{\cdot}159$; the normalization value $N = 2{\cdot}0$.

the amplitude of the conversion coefficients

$$R_{12}^N = NR_{12}, \qquad T_{12}^N = NT_{12} \tag{2.25}$$

where

$$N^2 = \frac{\Lambda_2}{\Lambda_1} \frac{\|\mathscr{L}_2\|}{\|\mathscr{L}_1\|} \tag{2.26}$$

so that $|R_{12}^N|^2$ and $|T_{12}^N|^2$ are proportional to the power transferred by the diffraction of a $\mathscr{L}_1$-wave of unit amplitude at a wedge discontinuity. The appropriate values of $N$ for the previous numerical example are cited in the captions of Figures 4 to 7.

In a fashion similar to the error analysis of Part 1, the function

$$(1 - |R_{11}|^2 - |R_{12}^N|^2 - |T_{11}|^2 - |T_{12}^N|^2)$$

represents the amount of ambiguous energy. These values are much more satisfactory in the present analysis than in Part 1. For example, when $\lambda_1 H = 7$ and

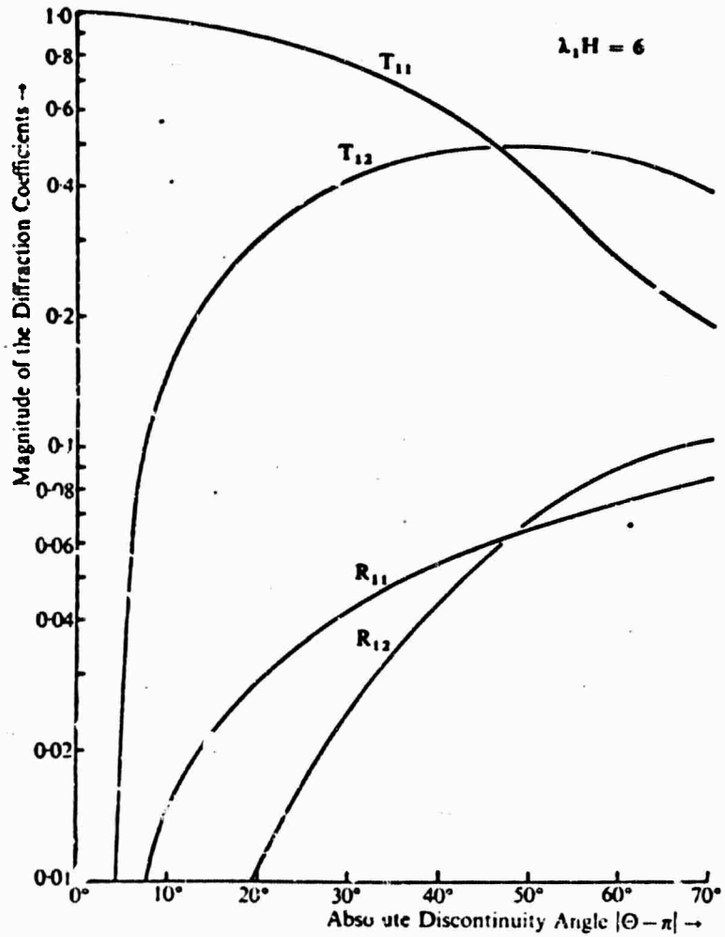


FIG. 5.—The magnitude of the Love wave diffraction coefficients for $\lambda_1 H = 6$; they are even functions of the discontinuity angle $\Theta - \pi$. In this case $k_2/k_1 = 1{\cdot}297$, $\mu_2/\mu_1 = 2{\cdot}159$; the normalization value $N$ [illegible]2.

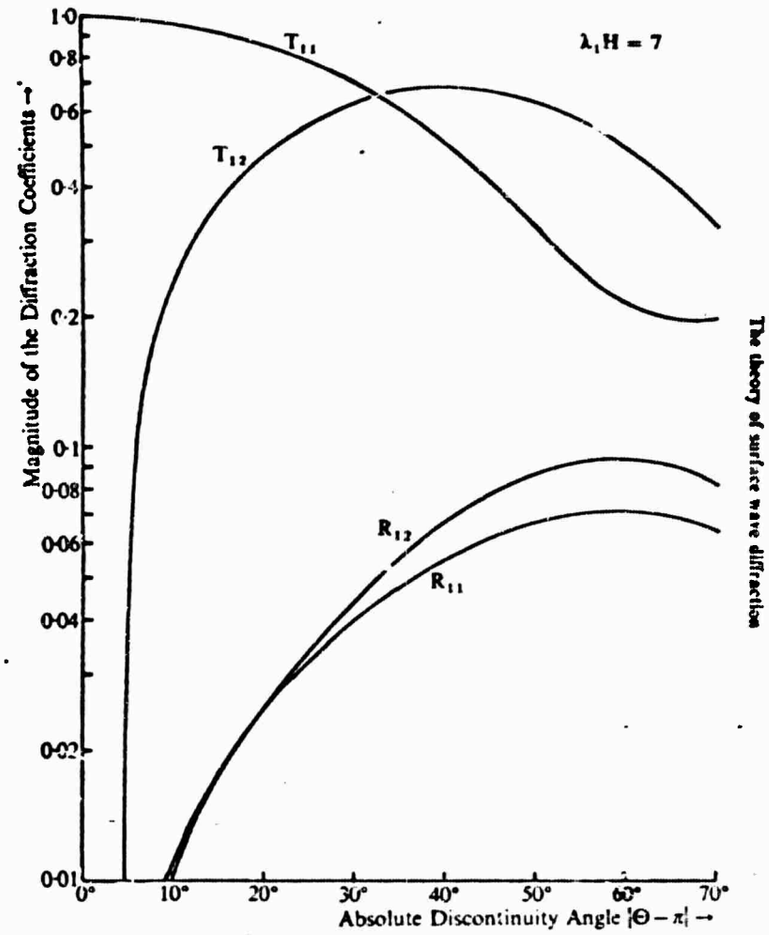


FIG. 6.—The magnitude of the Love wave diffraction coefficients for $\lambda_1 H = 7$; they are even functions of the discontinuity angle $\Theta - \pi$. In this case $k_2/k_1 = 1{\cdot}297$, $\mu_2/\mu_1 = 2{\cdot}150$; the normalization value $N = 1{\cdot}1$.

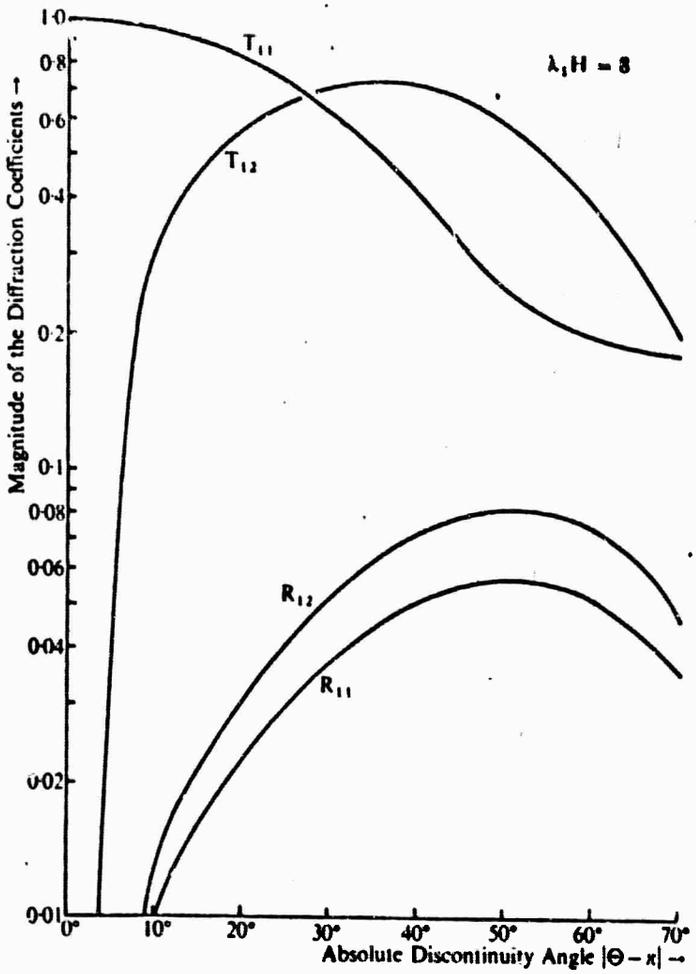


FIG. 7.—The magnitude of the Love wave diffraction coefficients for $\lambda_1 H = 8$; they are even functions of the discontinuity angle $\Theta - \pi$. In this case $k_2/k_1 = 1.297$, $\mu_2/\mu_1 = 2.159$; the normalization value $N = 1.0$.

the discontinuity angle $|\Theta - \pi|$ is as large as 30°, the present analysis accounts for at least 95 per cent of the scattered energy. This improvement is due in large part to a use of a more flexible trial function. In Part 2, two trial coefficients have been available for either symmetry.

**Acknowledgment**

The research described in the present paper has been supported by the Air Force Cambridge Laboratories, Office of Aerospace Research, as part of project *Vela-Uniform*.

*California Institute of Technology,*
*Pasadena,*
*California,*
*U.S.A.*

* *University of Rhode Island,*
*Kingston,*
*Rhode Island,*
*U.S.A.*

1964 *May.*

## References

de Bremaecker, J. Cl., 1958. *Geophysics*, **23**, 253.

Cagniard, L., These, 1939. Translation, 1962. *Reflection and Refraction of Seismic Waves*, McGraw-Hill.

Ewing, M., Jardetsky, W. and Press, F., 1957. *Elastic Waves in Layered Media*, McGraw-Hill.

Friedlander, F. G., 1948. *Quart. J. Mech. Appl. Math.*, **1**, 376.

Hudson, J. A. and Knopoff, L., 1963. Contributions 1177 and 1178, Divisior of Geological Sciences, California Institute of Technology.

Kane, J. and Spence, J., 1963. *Geophysics*, **28**, 715.

Knopoff, L. and Gangi, A. F., 1960. *Geophysics*, **25**, 1203.

Lapwood, E. R., 1958. *Geophys. J.*, **4**, 174.

Viktarov, I. A., 1958. *Soviet Physics—Doklady*, **3**, 304.

## Appendix

Love wave diffraction coefficients would be very difficult to measure in the laboratory, but the techniques of two-dimensional model seismology offer a means of determining Rayleigh wave reflection and transmission coefficients with an accuracy of about 10–20 per cent. The present theory and experiment agree if $\Theta \sim \pi$, but outside this range there are experimental features which are not duplicated by the results of the present elementary variational procedure. The analysis in the harmonic domain could be refined by employing various devices to reduce the amount of unexplained energy. Such calculations would probably require substantial effort, and the idealized formulation of the present problem should be reviewed if the labour is to have relevance to pulse measurements.

There are major distinctions between analysis in the harmonic and time domain. For example, whereas a harmonic Rayleigh wave is a uniquely defined entity, Friedlander (1948) has pointed out that a Rayleigh pulse can assume a variety of waveforms. Furthermore, any Rayleigh pulse cannot have a sharply defined wavefront, and theoretically must give infinite advance notice of its arrival unless it merges continuously with a precursor, typically the shear pseudo-surface wave (Cagniard 1939). Although the amplitude of this shear wave decays with distance, *its integrated flux remains constant*. It is difficult to separate the far-field effects due to the arrival of a Rayleigh pulse and its shear companion at the second wedge face. In other words, in addition to Rayleigh/Rayleigh interactions, there will be some shear/Rayleigh conversions. What contributions might this shear wave introduce? Whereas we cannot give a rigorous answer to this question, we can however make a rough, but simple, estimate.

We first note that if the wedge angle $\Theta$ is $\pi$ or $\pi/2$, then we would expect little or no shear/Rayleigh conversion. In the first case, there is a discontinuity, and the second case corresponds to a geometry for which the shear wave is essentially normal to the second wedge face, and we know that for normal incidence, a shear wave is reflected as a shear wave. Then, from Equation (1.6), we note that we can easily add some additional shear potential to the original excitation by incrementing the Rayleigh wave's shear coefficient $\Gamma$ by an additional contribution $f(\Theta)$ depending on the wedge angle

$$\Gamma' = \Gamma[1 + f(\Theta)].$$

APPENDIX C

*Reprinted from* *Printed in U.S.A.*

JOURNAL OF MATHEMATICAL PHYSICS VOLUME 6, NUMBER 6 JUNE 1965

# Integrals of the Second-Order Linear Differential Equation*

J. KANE
*California Institute of Technology, Pasadena, California*
AND
E. R. SURYNARAYAN
*University of Rhode Island, Kingston, Rhode Island*

(Received 5 October 1964)

In this study we describe procedures for the numerical solution of the second-order linear differential equation which have either continuous or discontinuous coefficients. Our motivation is a well-known technique in the theory of inhomogeneous transmission lines: the treatment of a continuously varying line by considering it to be comprised of various sections of *uniform* lines. Although this procedure is very suggestive physically, there are difficulties with its applications to second-order equations which do not describe wave propagation. First, the language of the circuit engineer is such that a pair of first-order equations describing some analogs of the complex quantities voltage and current seem to be required. Whereas these equations appear naturally in transmission line theory, we show that it is an unnecessary burden to find their counterparts when the problem is but to solve a second-order equation. The second objection to this approach is that it is not apparent that a piecewise constant partition of the coefficients in a differential equation will yield the rigorous solution if the subdivision is carried out to an arbitrary degree. Indeed, we show that the limit of the quantization scheme can *not* yield the rigorous solution. On the other hand, we are led to a well-defined technique which generates the solution by a method suggested by the procedures used in the discrete case. This enables the second-order equation to be solved rigorously by iteration with no complications, and in a form ideally suited for computer programs.

## I. INTRODUCTION

### A. Basic Equations

THE class of problems, mathematical and physical, which require an explicit knowledge of the solutions of the linear second-order differential equation

$$d^2U(t)/dt^2 + A(t)dU(t)/dt + B(t)U(t) = 0 \qquad (1)$$

is legion. Only rarely can exact solutions of this equation be found in closed form. While local approximations are easily constructed, the task of finding global representations offers a major problem. This difficulty is particularly vexing inasmuch as the first-order equation,

$$dV/dt - P(t)V(t) = 0 \qquad (2)$$

possesses an immediate integral

$$V(t) = \exp\left\{\int^t P(\tau)\, d\tau\right\}, \qquad (3)$$

but no similar representation for Eq. (1) has been found. The solution (3) has the interpretation of defining the present value of $V(t)$ in terms of the history of its logarithmic derivative $P(t) = (d/dt)(\ln V)$. If we specify an initial condition on the possible pair of solutions of (1) at say $t = t_0$, then Eq. (1) describes a unique function with that property. From this initial condition and a knowledge of Eq. (1), the behavior of the second-order $U(t)$ should likewise be discernible in terms of the prior trajectory of its logarithmic derivative: the topic of the present analysis.

Following a change of unknown

$$u(t) = U(t) \exp\left\{\frac{1}{2}\int^t A(\tau)\, d\tau\right\} \qquad (4)$$

and an introduction of

$$k^2(t) = B(t) - \tfrac{1}{2}dA(t)/dt - \tfrac{1}{4}A^2(t), \qquad (5)$$

Eq. (1) can be recast into the canonical form

$$d^2u/dx^2 + k^2(x)u(x) = 0 \qquad (6)$$

in which we replace $t$ by $x$ to eliminate confusion between the forms (1) and (6). At some point $x = x_0$, we may suppose that we have a given constraint

$$\frac{d}{dx}\ln u = \frac{du}{dx}/u = g_0 \qquad (x = x_0), \qquad (7)$$

which singles out one solution; another linearly independent solution can be specified by choosing a different value for the parameter $g_0$.

The form of the solution (3) to the first-order equation (2), suggests that it might be more profitable to concentrate our attention on

$$\int_{x_0}^{x} \Gamma(\xi)\, d\xi = \ln u(x), \quad u(x) = \exp\int_{x_0}^{x} \Gamma(\xi)\, d\xi, \qquad (8)$$

* Contribution No. 1344 from the Division of Geological Sciences, California Institute of Technology, Pasadena, California.

that is, the logarithmic derivative

$$\Gamma(x) = \frac{du/dx}{u}, \tag{9}$$

rather than on $u(x)$. Indeed, from the point of view of a mathematical physicist interested in eigenvalue problems, an explicit knowledge of the logarithmic derivative provides more insight than would formulas for two distinct solutions of (1), therefore we shall pay special attention to the logarithmic derivative. The continuity of $\Gamma$ is assured if we restrict our attention to continuous solutions $u(x)$ possessing a continuous first derivative $u'(x)$. If these functions are bounded, then we note that the poles and zeros of $\Gamma(x)$ correspond to the zeros and maxima respectively of $u(x)$. In terms of $\Gamma(x)$, the equations (6) and (7) become

$$d\Gamma/dx = -(k^2 + \Gamma^2), \qquad x_0 \leq x \leq x_m \tag{10}$$

$$\Gamma = g_0, \qquad x = x_0 \tag{11}$$

wherein we have adopted the convention that the initial condition is given at $x = x_0$, and we wish to propagate the solution to the right of $x_0$ up to some arbitrary point $x_m$. Formula (10) describes $\Gamma(x)$ in terms of a Riccati equation, and even though this expression is nonlinear, it can easily be solved by iterative techniques if $k^2(x)$ is negative. On the other hand, if $k^2(x)$ is positive, then $\Gamma(x)$ behaves like an ill-tempered function with numerous singularities. Even high-speed computers have difficulty in coping with such a wildly fluctuating function, and numerical work under such circumstances offers major difficulties. One conclusion of the present work is the need to isolate and describe explicitly the bad manners of $\Gamma(x)$ so that if numerical methods must be used, they should treat slowly-varying functions.

### B. Summary of Results

Equation (6) can be thought of as a reduced wave equation: subject to severe limitations on the behavior of $k^2(x)$, approximate solutions can be found by the phase-integral[1] method. This technique yields reasonably simple solutions of, say, exponential type. However, the character of the solution must change in the vicinity of a turning point of $k^2(x)$: in such a region, the solution must be oscillatory rather than exponential which means that the phase integral needs severe correction. Loosely speaking, the major disadvantage of the phase-integral method is that it involves an argument of the form $\int^x k(\xi)\, d\xi$ in trigonometric or exponential functions. As a result, when $k^2(x)$ changes sign, the argument does not change character correctly because of the integral's inertia in storing the past values of $k(x)$. That is, the phase-integral solution *must* involve complex quantities in the presence of turning points even if the original differential equation's coefficients are real. We know that such equations have real solutions, but the phase integral's hysteresis prevents its providing a valid representation of them. For this reason, we avoid using formulas which depend upon integrals of the form $\int^x k(\xi)\, d\xi$.

One means of avoiding turning-point difficulties is to consider $k^2(x)$ as being piecewise constant $k^2(x) = k_i^2$ over sufficiently small intervals $x_{i-1} \leq x \leq x_i$. Within each quantum cell a pair of trial solutions can be inserted: trigonometric or exponential depending upon the sign of $k_i^2$. By this process, the task becomes an algebraic one of determining the correct coefficients of the trial function in each cell so that it joins smoothly with its neighbors. The difficulties with this procedure are twofold. First, while the procedure appears to converge to a solution of the basis of physical arguments, the mathematical justification for this procedure has neither been simple nor convincing, since the limiting process involves a sequence of step-function approximations. Second, for fine-grained quantization, the large number of algebraic equations to be solved can be overwhelming. In diffraction theory, an approximate means of surmounting this hurdle is the heuristic device of neglecting certain contributions within each cell that can be identified with multiple reflections of a wave at a boundary which has a very small reflection coefficient.[2-4] Indeed, the phase integral is but the leading term in such an expansion.[5] In Sec. II, we consider this discretization process and show how the algebraic difficulties can be sidestepped by introducing the proper variables and format of the trial solution without making any assumption concerning the behavior of the field within each cell. This yields an expression for $\Gamma(x)$ in terms of a product of $n$ $2 \times 2$ unimodular matrices for an $n$th-order quantization. In the limit, as $n \to \infty$, each matrix operator becomes an infinitesimal trans-

[1] We prefer this adjective to any acronym based upon some perturbation of the initials of Liouville, Green, Carlini, Stokes, Horn, Rayleigh, Birkhoff, Jeffreys, Langer, Wentzel, Kramers, Brillouin, *et al.*

[2] L. M. Brekhovskikh, *Waves in Layered Media* (Academic Press Inc., New York, 1960).

[3] K. G. Budden, *The Wave-Guide Mode Theory of Wave Propagation*, (Prentice-Hall, Inc., Englewood Cliffs, New Jersey, 1961).

[4] J. R. Wait, *Electromagnetic Waves in Stratified Media*, (The Macmillan Company, New York, 1962).

[5] H. Bremmer, Comm. Pure Appl. Math. 4, 105 (1951).

formation; we analyze this differential change in $\Gamma$ and find a geometric characterization of the trajectory of the logarithmic derivative. We then find that the quantization scheme cannot yield the rigorous solution if the coefficients in the original differential equation are analytic. Nonetheless, the procedures suggest a transformation which enables the rigorous solution to be found by a related technique. This analysis will be found in Sec. III together with an illustrative numerical example.

## II. DISCRETE FORMALISM AND SOLUTION

### A. Introduction

We assume that $g_0$ and $k^2(x)$ are real [but not $k(x)$] so that we can confine our attention to real solutions of (6). Of course, once the real solutions of (6) are known, complex solutions can easily be constructed by the superposition principle.

Let $[\delta_i]^m$ be any monotone sequence of $(m + 1)$ points which divides any portion of the $x$ axis, say, the interval

$$-\infty \leq x_0 \leq x \leq x_m \leq +\infty \tag{12}$$

into subintervals

$$\Delta x_i = \delta_i - \delta_{i-1}, \quad (\delta_0 = x_0, \delta_{i+1} > \delta_i, \delta_m = x_m). \tag{13}$$

If this quantization is so fine that within the $i$th interval $\Delta x_i$ we can replace $k^2(x)$ by $k_i^2$ to any preassigned degree of accuracy, then the equation

$$d^2u_i/dx^2 + k_i^2 u_i = 0, \quad \delta_{i-1} < x < \delta_i \tag{14}$$

has the general solution

$$u_i = A_i[\Gamma_i k_i^{-1} \sin k_i(x - \delta_{i-1}) + \cos k_i(x - \delta_{i-1})], \tag{15}$$

wherein the discrete parameters $A_i$ and $\Gamma_i$ remain to be specified. From a theoretical point of view, any two-parameter combination of $\sin k_i x$ and $\cos k_i x$ could serve as well as the particular form selected in Eq. (15). However, from a practical viewpoint, major advantages are introduced by the selection (15). First, no assumption has been made concerning the character of $u_i$ in the $i$th interval: oscillatory or damped. For, should $k_i^2$ be negative, or $k_i = i\kappa_i$ be imaginary, then

$$u_i = A_i[-\Gamma_i \kappa_i^{-1} \sinh \kappa_i(x - \delta_{i-1}) + \cosh \kappa_i(x - \delta_{i-1})] \tag{16}$$

will continue to be real provided only that $A_i$ and $\Gamma_i$ are chosen real. Note that at $x = \delta_{i-1}$ we have

$$u_i = A_i, \quad \frac{du_i/dx}{u_i} = \Gamma_i, \quad x = \delta_{i-1}, \tag{17}$$

and so $A_i$ and $\Gamma_i$ can be identified as the amplitude and logarithmic derivative of the solution at the left endpoint. Most important however, is that the form of (15) is such that both the boundary conditions (17) are *decoupled*, and it becomes possible to solve for $A_i$ and $\Gamma_i$ separately: a considerable reduction of computational effort.

### B. Solution

The equations (6) and (7) are homogeneous, and so we can normalize $A_0$ to any convenient value, but we must choose $\Gamma_0 = g_0$ if the boundary condition (11) is to be satisfied. Even though $k_i$ is a jump function, this initial data can be continued as a smooth function for all $x$, provided we choose

$$\Gamma_{i+1} = \frac{\Gamma_i \cos k_i \Delta x_i - k_i \sin k_i \Delta x_i}{\Gamma_i k_i^{-1} \sin k_i \Delta x_i + \cos k_i \Delta x_i} \tag{18}$$

and

$$A_{i+1} = A_i[\Gamma_i k_i^{-1} \sin k_i \Delta x_i + \cos k_i \Delta x_i]. \tag{19}$$

In this manner we obtain a function which satisfies (6) everywhere except that $k^2(x)$ must be replaced by some local average value $k_i^2$. Furthermore, the iterations required to extend $u_i(x)$ are very easily performed since (18) has the form of a Möbius transformation whose coefficient matrix

$$\mathsf{M}_i = \begin{bmatrix} \cos k_i \Delta x_i & -k_i \sin k_i \Delta x_i \\ k_i^{-1} \sin k_i \Delta x_i & \cos k_i \Delta x_i \end{bmatrix} \tag{20}$$

has its determinant equal to unity. As a result, the coefficient matrix $\mathsf{T}_m$ required to transform $\Gamma_0$ into some final value $\Gamma_m$ at the arbitrary point $x = x_m$ is the product of $m$ factors

$$\mathsf{T}_m = \mathsf{M}_m \cdot \mathsf{M}_{m-1} \cdot \ \dots \ \cdot \mathsf{M}_i \cdot \ \dots \ \cdot \mathsf{M}_1, \tag{21}$$

and is likewise unimodular.

### C. Check

It is now but a simple calculation to show that if $m \to \infty$, and $\Delta x_i \to 0$ for any sequence $[\delta_i]^m$, then the process yields a function which converges to the solution of an equation consistent with assumed behavior of $k^2(x)$. Since $\Gamma(x)$ defines $u(x)$ uniquely apart from a multiplicative constant, it will be sufficient to show that the continuous limit of the $\Gamma_i$'s defined (18) satisfies the Ricatti equation (10) on any interval $\Delta x_i$. We calculate that

$$\frac{\Gamma_{i+1} - \Gamma_i}{\Delta x_i} = \frac{-k_i \sin k_i \Delta x_i - (\Gamma_i^2 k_i^{-1}) \sin k_i \Delta x_i}{\Delta x_i[(\Gamma_i k_i^{-1}) \sin k_i \Delta x_i + \cos k_i \Delta x_i]}. \tag{22}$$

and if we pass to the limit $\Delta x_i \to 0$ we obtain

$$\lim_{\Delta x_i \to 0} \frac{\Gamma_{i+1} - \Gamma_i}{\Delta x_i} = \frac{d\Gamma}{dx} = -(k^2 + \Gamma^2), \qquad (23)$$

which is precisely Eq. (10). As a double check, we can repeat the limiting process for Eq. (19),

$$\frac{A_{i+1} - A_i}{\Delta x_i} = \frac{A_i[(\Gamma_i k_i^{-1}) \sin k_i \Delta x_i + \cos k_i \Delta x_i - 1]}{\Delta x_i} \qquad (24)$$

and derive the defining equation for $\Gamma(x)$ in terms of $u(x)$

$$\lim_{\Delta x_i \to 0} \frac{A_{i+1} - A_i}{\Delta x_i} = \frac{du}{dx} = u\Gamma(x). \qquad (25)$$

if we note that in the limit, the amplitude $A_i$ becomes $u(x_i)$.

Since we have always assumed that $dk/dx = 0$ locally, what we have just shown is that *to the extent that the derivative $k'$ can be neglected on any quantum cell the scheme converges to a solution of* (6).

### D. The Infinitesimal Transformation

The preceding analysis furnishes a simple illustration of the algebraic structure of a particular Riccati equation: one example of the general theory of such equations[6] which shows that its solution can be characterized by matrix operators. In the limit, each matrix $M_i$ in the product (21) approaches an infinitesimal transformation, and the total transformation $T_n$ giving $\Gamma(x_n)$ in terms of $\Gamma(x_0)$ can be expressed either as a matrizant[7] or a product integration[8]: the finite result of compounding a sequence of infinitesimal transformations. We can think of this operation as defining a curve traced out by the repeated reaction of the original point $\Gamma(x_0)$ to each infinitesimal product $M_i$. If we can find some analytic means of specifying this trajectory, then we might be spared the need of calculating matrizants, or product integrals to describe the limit of the iterative process. For this purpose, we consider the geometry of the transformation implied by any matrix $M_i$.

No doubt some readers have been struck by the resemblance of $M_i$ to the transmission-line matrices of network theory. However, we caution that this resemblance is deceiving: $M_i$ is a *real* transformation unlike the transmission-line matrix which is a *complex* one. In the context of transmission-line theory, voltage and current, or E and H are out of phase, and the complex entries in the transmission-line matrix emphasize this feature. In our analysis however, we have avoided introducing any analogs of the first-order transmission-line equations since we feel that their use is artificial and contrived for applications other than those described by Maxwell's equations. Furthermore, unlike the $M_i$'s, their geometric interpretation requires a complicated hyperbolic model rather than the more familiar Euclidian plane.

We emphasize that Eq. (20) represents a *real* transformation: in more general terms, it represents a mapping of the complex $\Gamma$ plane upon itself such that the real axis is left invariant. Since Möbius transformations describe elementary geometric deformations of the complex plane, this pro.ides us with a clue to the proper characterization of $M_i$. By direct multiplication, it is easily checked that each $M_i$ can be re-expressed as the product of three terms

$$M_i = C_i^{-1} R_i C_i, \qquad (26a)$$

where

$$C_i = \begin{bmatrix} k_i^{-1} & 0 \\ 0 & k_i^{*1} \end{bmatrix} \qquad (26b)$$

$$R_i = \begin{bmatrix} \cos k_i \Delta x_i & -\sin k_i \Delta x_i \\ \sin k_i \Delta x_i & \cos k_i \Delta x_i \end{bmatrix}. \qquad (26c)$$

Each factor has a simple geometric interpretation. The first, $C_i$ represents a uniform contraction of the $\Gamma'$-plane by a factor $1/k_i$; on the other hand, its inverse $C_i^{-1}$ represents a uniform dilation by the inverse factor $k_i$. Between these two operations, we need perform $R_i$ which represents a rotation of the stereographic projection of the $\Gamma'$-plane on the Riemann sphere.

The sequence of operations is illustrated in Fig. 1 which only shows the plane intersecting the real $\Gamma$-axis and the north pole $N$ of the Riemann sphere. First, we lay off the initial point $\Gamma_i$ on the $\Gamma$-axis

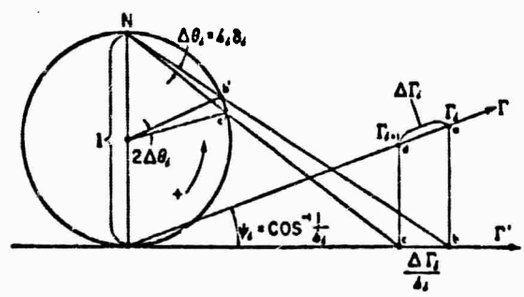


FIG. 1. The geometry of the matrix transformation $M_i$.

[6] R. Redheffer, J. Ratl. Mech. Anal. 5, 835 (1956).
[7] R. A. Frazer, W. J. Duncan, and A. R. Collar, *Elementary Matrices* (Cambridge University Press, New York, 1959).
[8] G. Birkhoff, J. Math & Physics, 16, 104 (1937).

which has been drawn obliquely for convenience. The $\Gamma'$-axis is drawn horizontally and intersects the $\Gamma$-axis at an angle $\psi_i = \cos^{-1}(1/k_i)$. If we project the $\Gamma$-axis onto the $\Gamma'$-axis, then all lengths on this new axis will be uniformly contracted. We continue by finding the sterographic projection of this image point, and then we rotate the Riemann sphere by a *negative* (clockwise) angle $-\theta_i = \tan^{-1}(k_i\Delta x_i)$ if $k_i\Delta x_i$ is positive. We retrace our steps to the original $\Gamma$-axis, and it is a simple matter to show that the aforementioned sequence is mimicked by the matrix product $M_i = C_i^{-1}R_iC_i$. The proof of this assertion is left to the reader, and is easily reproduced once it is recalled that the angle subtended by an arc on a circle from the center is twice the angle subtended by that arc from the north pole.

However, the geometric construction also shows that any transformation $\Delta\Gamma_i$, can be obtained by differentiating the function $\Gamma_i = k_i \tan(-k_ix)$, that is

$$\Delta\Gamma_i = (d/dx)[k_i \tan(-k_ix)]_{x=x_i}\Delta x_i. \tag{27}$$

If we recognize that this transformation must evolve continuously from some initial value $\Gamma_i = g_i$ at $x = x_i$, we thus find the general integral

$$\Gamma(x) = k_i \tan[k_i(\gamma_i - x)] \tag{28}$$

representing the locus of $\Gamma(x)$ on the $i$th interval where the constant $\gamma_i$ is fixed by the initial condition at $x = x_i$.

$$\gamma_i = x_i - k_i^{-1}\tan^{-1}(g_i/k_i). \tag{29}$$

In the limit, as $\Delta x_i \to 0$ it would seem that $k_i$ could be replaced by $k(x)$ and $g_i$ by its initial value $g_0$ since $g_i - g_{i-1} \to 0$. In other words, we expect that the net transformation could be described as

$$\Gamma(x) = k(x)\tan[(\gamma - x)k(x)]$$

$$\gamma = x_0 + [1/k(x_0)]\tan^{-1}[g_0/k(x_0)], \tag{30}$$

where $g_0$ is the initial value of $\Gamma$ at $x = x_0$. However, the promise of this anticipation is broken for if we substitute (30) into the Ricatti equation we find.

$$\frac{d\Gamma}{dx} = -(k^2 + \Gamma^2) + (dk/dx)[\tan[(\gamma - x)k] + k(\gamma - x)\sec^2[(\gamma - x)k]]. \tag{31}$$

In other words, (30) satisfies the Ricatti equation only to the extent that the first derivative of $k(x)$ can be neglected. Where is the fallacy in the preceding argument that can explain our disappointment, and perhaps lead us to a correction?

The resolution of this conundrum depends upon a subtle point in the character of the analysis. The basic assumption was that a continuous $k^2(x)$ could be approximated arbitrarily well by a staircase approximation. Whereas any such approximation is discontinuous, it does approach a continuous limit as the treads and risers get finer and finer. Of the eventual continuity, there is no doubt, but it is a peculiar type of continuity. Think for example of a staircase approximation to $k^2(x) = x$ on the interval $0 \le x \le 1$. Each riser represents the jump from one tread to the next, and the height of any one riser goes to zero as the approximation gets better. However, no matter how fine an approximation we care to make, *the sum of all the risers, or the total jump will always be constant.* In precise terminology, this is the difference between continuity and ***absolute continuity***. The fallacy is now evident: while $\gamma_i - \gamma_{i-1} \to 0$, we can not conclude that $\gamma_0$ will be unchanged as we pass through an unbounded number of quantum cells. That is, as we proceed from the $i$th cell to the $(i + 1)$th one, we can not neglect the differential jump $\gamma_{i+1} - \gamma_i$ at the end of the $i$th interval. In other words, we can think of Eq. (30) as a representation of the continuous or *principal part* of the transformation (21) which overlooks the denumerable collection of minute jumps.

We can now see that the quantization scheme can not yield the rigorous solution even if carried out to the continuous limit, for the result of a staircase approximation to $k^2(x)$ can not be absolutely continuous. From the differential equation (6) it is clear that the ratio $u''/u$ must be equal to $-k^2(x)$, hence in the limit, $u''/u$ can not be absolutely continuous no matter how smooth the original $k^2(x)$ might have been. In general, we know that whenever $k^2(x)$ is analytic, the differential equation (6) must have an analytic solution. As a result, for such equations the fact that the limiting $u''/u$ is not absolutely continuous contradicts the required analyticity of the solution. As a result, we conclude that the limit of the quantization process in general will not converge to the rigorous solution. That the limit of the iterative process might be a weak solution in terms of some norm remains an open question. On physical grounds, there can be no doubt that the discretization approach is a useful procedure when $k^2(x)$ can be considered to be well approximated by a piecewise constant function. Perhaps if we retain information concerning the derivatives of $k^2(x)$, we can construct a rigorous solution? This question is answered affirmatively in the next section.

## III. THE CONTINUOUS TRANSFORMATION

In the preceding paragraphs, we have discussed the hazards that obstruct an extension of the finite quantization theory to the continuous case. In such a situation, it is always well to pause, and reflect upon the possiblity that the infinitesimal case might better be handled by other methods. Basically, we are considering the second-order equation as an initial-value problem. That is, we wish some means of knowing the direction the solution or its logarithmic derivative will take once an initial value is specified. This question is of course immediately answered by the Ricatti equation (10) for it describes the derivative explicity in terms of the function. However, we know that when $k^2(x)$ is positive, $\Gamma(x)$ behaves like the tangent function and has numerous poles and zeros. Any numerical method which attempts to pursue the path of such a spirited function will almost of necessity be doomed from the outset. On the other hand, the poles and zeros of the logarithmic derivative have no more significance than locating the maxima and zeros of the desired solution of the differential equation and should not present any intrinsic hurdle.

In the previous section, we have introduced the notion of the *principal part* of the limit of the quantization process Eq. (30). In the initial stages of our investigation we had had the idea that by considering the constant $\gamma$ to be in fact a slowly varying function of $x$, we could find the actual solution by solving for $\gamma(x)$. This turned out to be a fruitful pursuit and in this fashion we were able to find excellent numerical replicas of the solutions to the differential equation without any trouble except in the neighborhood of a turning point. This difficulty had to do with choosing a trial function for the logarithmic derivative of the particular form (30); the problems vanish by choosing a simpler starting point.

The essential ingredient is to find a slowly varying function which can characterize the solution. One possibility that we have just discussed is to use a component of the argument of the tangent function, that is, some element describing the *phase*. In quantum mechanics, the scattering of a particle by a spherically symmetric potential can be described in terms of phase shifts. By introducing a nonlinear first-order ordinary differential equation, it is possible to find the relevant information without solving the second-order Schrödinger equation. This approach, introduced by Morse and Allis,[9] and more recently discussed by Calogero[10] and Levy and Keller,[11] is a powerful technique for finding the phase shift. However, these authors have been content with specialized information and have overlooked the possibilities inherent in this approach which can lead to solutions of the second-order differential equation.

Consider the function $\Phi(x)$ defined by

$$\Gamma(x) = -k_0 \tan [k_0\Phi(x)], \tag{32}$$

where $k_0$ is some convenient, but arbitrary reference value, for example, the mean value of $k^2(x)$ over some interval. Note that even if $\Gamma(x)$ behaves wildly, the corresponding $\Phi(x)$ will reflect a much calmer character. Since $\Gamma(x)$ is specified once $\Phi(x)$ is known, we can ask what equation must $\Phi(x)$ obey if $\Gamma(x)$ is to be a solution of the Ricatti equation. The answer is found by straightforward substitution into (10), and after simplification we find that $\Phi(x)$ must satisfy

$$d\Phi/dx = [K(x) - 1] \cos^2 (k_0\Phi) + 1, \tag{33}$$

where the function $K(x)$ is

$$K(x) = k^2(x)/k_0^2.$$

The simple formula (33) provides all the information necessary to specify a precise solution of the second-order differential equation with virtually no complication for two important reasons. First, *if $k^2(x)$ is bounded then the derivative $\Phi'$ is always bounded.* Second, *this formula only involves $K(x) = k^2(x)/k_0^2$ so that imaginary quantities will never be introduced if the original differential equation's coefficients are real.* As a result, it is a trivial matter to solve equation (33) by an iterative process. That is, given $\Phi_0 = \Phi(x_0)$ at $x = x_0$, then $\Phi(x)$ is given by the expansion

$$\Phi(x) = \Phi_0 + \Phi_0'\Delta x + \tfrac{1}{2}\Phi_0''(\Delta x)^2 + \cdots + \frac{1}{n!}\Phi_0^{(n)}(\Delta x)^n + \cdots, \tag{34}$$

where the higher-order derivatives are easily calculated from (33),

$$\begin{aligned}
\Phi'' &= -k_0\Phi'(K - 1) \sin (2k_0\Phi) + K' \cos^2 (k_0\Phi) \\
\Phi''' &= -k_0\Phi''(K - 1) \sin (2k_0\Phi) - 2k_0\Phi' \\
&\quad \times [K' \sin (2k_0\Phi) + k_0(K - 1) \\
&\quad \times \cos (2k_0\Phi)] + K'' \cos^2 (k_0\Phi) \\
&\vdots \\
\Phi^{(n)} &= \text{etc.}
\end{aligned} \tag{35}$$

[9] P. Morse and W. P. Allis, Phys. Rev. 44, 269 (1933).

[10] F. Calogero, Nuovo Cimento, 27, 261 (1963).

[11] B. R. Levy and J. B. Keller, J. Math. Phys. 4, 54 (1963).

In other words we have a recurrance relation expressing the higher-order derivatives in terms of *known* lower-order ones. Once we are given $\Phi_0$, it is no problem to determine what $\Phi_1 = \Phi(x_1)$ is at some nearby point $x_1$ to any degree of accuracy by truncating the expansion (34). A repetition of the process allows one to calculate $\Phi_2 = \Phi(x_2)$ and so on. No doubt some purists will argue that this is not a closed form representation of the solution. While this is true, it is in large part a meaningless objection. Any number of closed form expressions, e.g. contour integrals, are very elegant and concise but quite intractable when they are interrogated for numerical data. The important question to be answered is how readily can desired information be obtained. Before we can give any demonstrations of the utility of Eq. (33), we must digress and examine the intractability of a closed form solution, namely Eq. (3).

We have implied that once the logarithmic derivative $\Gamma(x)$ is known, we could reconstruct the solution $u(x)$ from the integral (3). While theoretically this formula should provide the desired answers, the practical situation is otherwise since the integral diverges at the poles of $\Gamma(x)$. If $u'(x)$ is bounded, then any such infinity in $\Gamma(x)$ is just another way of saying that $u(x)$ has a zero at that point, but nonetheless numerical integration of Eq. (3) to obtain $u(x)$ is to a great extent out of the question. In other words, even with an explicit $\Gamma(x)$ at our disposal, we may have all sorts of grief in translating this knowledge into numbers describing $u(x)$ by use of (3)—so much for closed form expressions.

The scheme we prefer to adopt neglects formula (3) and instead interpolates $u(x)$ by a polynomial at each stage of the iterative process. At some $x_i$, suppose we know $\Gamma_i$ and an initial value $u_i$; at $x_{i+1} > x_i$ we are given $\Gamma_{i+1}$. These three pieces of information determine a unique second-order polynomial which must assume the value

$$u_{i+1} = u_i \frac{2 + \Gamma_i(x_{i+1} - x_i)}{2 - \Gamma_{i+1}(x_{i+1} - x_i)} \qquad (36)$$

at $x = x_{i+1}$ (the derivation of this formula is given in the Appendix). The ability of this rational function to predict the future value $u_{i+1}$ in terms $u_i$, $\Gamma_i$, and $\Gamma_{i-1}$ is rather remarkable. For example, with an increment $x_{i+1} - x_i = 0.1$, Eq. (36) reproduces $\sin x$ from its logarithmic derivative $\cot x$ to within four significant figures. In addition, Eq. (36) automatically yields a zero of $u(x)$ should $\Gamma(x)$ have a pole at a point where $u(x)$ is regular, so that the role of the singularities of $\Gamma$ is correctly reproduced.

With these preliminaries, we can find numerical solutions of second-order differential equations to any desired degree of accuracy. The iterative scheme which carries the solution from one point to another is to truncate the Taylor expansion (34) to a polynomial of suitable order for the increment chosen. A numerical example may serve to illustrate the procedure. The differential equation

$$d^2u/dx^2 + (a^2 - 6/x^2)\,u = 0 \qquad (37)$$

is distinguished by having a particularly simple pair of solutions

$$u_1 = (3/ax)\cos ax + [1 - (3/a^2x^2)]\sin ax$$

$$u_2 = \frac{3}{ax}\cos\left(ax + \frac{\pi}{2}\right) + \left(1 - \frac{3}{a^2x^2}\right)\sin\left(ax + \frac{\pi}{2}\right). \qquad (38)$$

Since (37) has a turning point at $x = 6^{\frac{1}{2}}/a$ as well as a singularity at the origin it poses a rather severe computational challenge. We have used this equation as a test of our procedure for various choices of the parameter $a$. The larger this parameter, the more rapid are the oscillations of the solution for $|x| > 6^{\frac{1}{2}}/a$, and the more likely are errors to grow in any computational scheme. By use of a quadratic truncation of (35) we have found that the formulas (35) and (36) reproduce the solution very satisfactorily. As mentioned, the errors get worse with increasing $a$ and Fig. 2, illustrates one of the poorer cases we have considered for which the parameter $a$ had the value 3.5 and $6^{\frac{1}{2}}/a = 0.70$. The increment chosen was $\Delta x = 0.0142$, a rather odd number which resulted from choosing an increment inversely proportional to $a$ and equal to 0.1 if $a = 0.5$. At $x = -10$, the initial logarithmic derivative was adjusted to match $u_2$, the solution with a singularity at the origin. From this initial value a solution was computed in the direction of increasing $x$ using a quadratic formula for $\Phi(x)$ to compute $\Gamma(x)$. This was followed by use of Eq. (36) to determine the solution. The calculation and the actual solution agree so well that it is not worthwhile to draw curves of each. Instead, the absolute error curve is drawn with a *magnified* scale. As might be expected in any initial-value calculation, the errors tend to grow as the computation progresses. However, except in the neighborhood of the singularity we note that the amplitude of the error increases but linearly, and furthermore it oscillates about zero. The divergence at the origin is more apparent than real since the percentage error remains

bounded. By choosing a smaller increment or adding an additional term to the expansion for $\Phi(x)$, the error can be reduced by an additional order of magnitude. We might add that the computations are sufficiently simple and proceed so fast that they can be performed with but the aid of a desk calculator. Even on a relatively slow IBM 1410 computer, the calculations were performed as fast as the machine could print out the answers.

The preceding example illustrates the case with which a second-order equation can be solved without any complications or need of any sophisticated numerical techniques. Of course, certain tricks of the trade can be very beneficial in reducing errors. For example we recommend use of a variable increment which is smaller at the initial stages of the calculation to reduce a buildup of error. In addition the increment $x_{i+1} - x_i$ should be scaled so that $\Phi_{i+1} - \Phi_i$ does not exceed some preassigned bound. In this fashion, a computer program can be both speeded up and made more reliable by using a floating increment whose size varies inversely with the size of the change in $\Phi(x)$ from $x_i$ to $x_{i+1}$. Finally, we note that if the logarithmic derivative $\Gamma_u$ of Eq. (6) is known, then the logarithmic derivative $\Gamma_v$ of equation (1) which inspired the analysis is given by

$$\Gamma_v = \Gamma_u - \tfrac{1}{2}A(x) \tag{39}$$

so that without any further ado, the solution of Eq. (1) can be found.

As a last remark we should like to point out that the results of this section complement rather than supersede the discrete analysis of Sec. II for the case of a differential equation with analytic coefficients. For whereas this section is concerned with accurate representations which need a relatively fine interval for their calculation, the analysis in Sec. II yields good approximation for coarser intervals. While this may be of no matter when an equation is to be solved but once, the distinction becomes important when the differential equation must be solved many times for some set of perturbations in its coefficients. The formulas in Sec. II furnish a quick method of obtaining insight into the effect of a large number of variations and locating regions demanding further investigation. Following this exploration, the formulas of Sec. III can chart these unknown domains. To cite a nautical analogy: it is the difference between using dead reckoning and an inertial guidance system. One is cheap and often adequate, the other is more expensive but arbitrarily accurate.

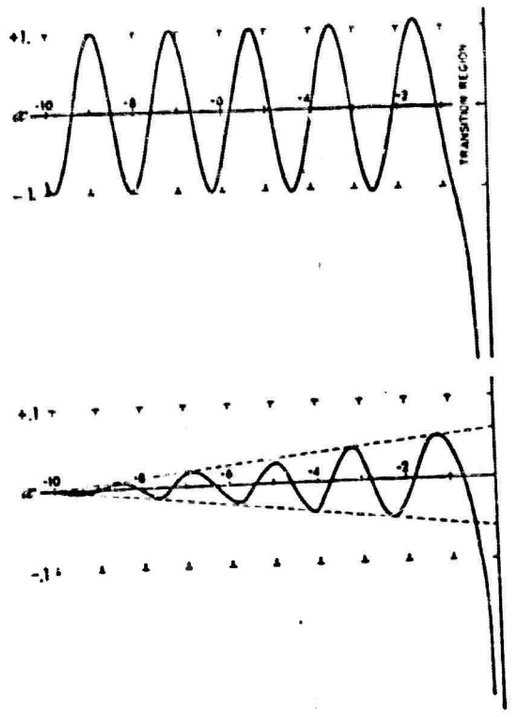


FIG. 2. The upper curve is the solution $u_1(x)$ of Eq. (37), and the lower curve is the computational error of the numerical procedure described in the text. Note that there is a 10:1 ratio between the two scales.

## ACKNOWLEDGMENT

The research described in this report has been sponsored by the Advanced Research Projects Agency, Project Vela-Uniform, under Contract AF 19(628)-319 of the Geophysics Research Directorate, Air Force Cambridge Research Laboratories, Office of Aerospace Research, U. S. Air Force, Bedford, Massachusetts.

## APPENDIX

In this Appendix we shall derive the formula (36) in Sec. III. From the equation (9) we have

$$u\Gamma = u'. \tag{40}$$

With no loss of generality suppose $x_i = 0$. Let us assume that the function $u(x)$ can be approximated by some unknown quadratic expression which can be chosen in the completely general form

$$u(x) = \alpha x(x - \Delta) + \beta(x - \Delta)(x + \Delta) + \gamma x(x + \Delta), \tag{41}$$

where $\alpha$, $\beta$, $\gamma$ are constants to be determined and $\Delta$ is the length of the increment.

Substituting (41) into (40) we find that

$$[x^3(\alpha+\beta+\gamma)+x\Delta(-\alpha+\gamma)-\beta\Delta^2]\Gamma = 2x(\alpha+\beta+\gamma)+\Delta(-\alpha+\gamma). \quad (42)$$

Let $u_+$, $u_0$, $u_-$ and $\Gamma_+$, $\Gamma_0$, $\Gamma_-$ denote the values of $u$ and $\Gamma$ at the points $x=\Delta$, $x=0$, $x=-\Delta$, respectively. Then, from (42) we obtain

$$\begin{aligned} u_+\Gamma_+ &= (\alpha+2\beta+3\gamma)\Delta = 2\gamma\Delta^2\Gamma_+, \\ u_0\Gamma_0 &= (-\alpha+\gamma)\Delta = -\beta\Delta^2\Gamma_0, \\ u_-\Gamma_- &= -(3\alpha+2\beta+\gamma)\Delta = 2\Delta^2\alpha\Gamma_-. \end{aligned} \quad (43)$$

The last two equations imply that

$$\frac{u_-}{u_0} = -\frac{2\alpha}{\beta} = \frac{2-\Delta\Gamma_0}{2+\Delta\Gamma_-} \quad (44)$$

or

$$u_0 = u_-(2+\Delta\Gamma_-)/(2-\Delta\Gamma_0) \quad (45)$$

By similar reasoning more sophisticated formulas can be derived whose accuracy is of arbitrarily high order.

APPENDIX D

JOURNAL OF GEOPHYSICAL RESEARCH VOL. 70, NO. 8 APRIL 15, 1965

# Travel Time and Phase Shift[1]

J. KANE[2]

*California Institute of Technology, Pasadena*

*Abstract.* If any harmonic wave propagates over a path with a nonuniform velocity, then, owing to second-order effects, phase shift data will not be proportional to travel time. The travel time will always seem to be larger than it actually is owing to increased phase shift resulting from diffraction effects. This dilation can be described in a rather elementary manner in terms of a nonlinear first-order differential equation. An integration of this equation gives an explicit formula for the discrepancy between actual travel time and the travel time computed from phase shift data.

*Analysis.* An often drawn conclusion from Fourier analysis is the interchangeability of phase information in the harmonic domain and travel time in the real domain. While this connection can be firmly established for uniform wave propagation, its applicability to propagation in a perturbed continuum is less secure. In this note we will consider this question from a point of view which allows us to derive a formula for the phase shifts of harmonic waves traversing an inhomogeneous velocity profile. This permits us to make an explicit comparison between travel time and phase shift, its presumed harmonic image. The procedure we follow is to introduce a nonlinear first-order equation for the phase variation. In terms of this equation we can compute the phase shift between two points as an integral involving the velocity profile without the need of solving the wave equation. This provides an explicit basis for a comparison between phase shift data and travel time.

For reference, we first cite the formula giving the travel time $T_m$ of a mass particle moving with variable velocity $v(x)$ between the two points $x_1$ and $x_2$, namely

$$T_m = \int_{x_1}^{x_2} \frac{d\xi}{v(\xi)} \qquad (1)$$

From the point of view of causality, we expect that this formula would also express the travel time of a harmonic wave propagating in a perturbed continuum. The question we ask is whether (1) is consistent with phase shift data. This query has significance, for wave motion has features which are foreign to the motion of a mass point—for example, continuous reflection and transmission. For a harmonic wave, we suspect that the cumulative effect of diffraction phenomena will be included in its phase variation. In short, for nonuniform wave propagation we anticipate that the phase shift between two points will have scattering effects corrupting the travel-time information. We want to find a formula that separates these two effects so that phase information can be corrected to yield the travel time.

Uniform steady-state wave motion is described by the wave equation

$$d^2u/dx^2 + k_0^2 u(x) = 0 \qquad (2)$$

where the constant $k_0$ is inversely proportional to the velocity of propagation

$$k_0 = \omega/v_0 \qquad (3)$$

From a knowledge of the plane wave solution $e^{i(k_0x - \omega t)}$, it is possible to measure the travel time $T_w$ between $x_1$ and $x_2$ of a harmonic wave by dividing the phase difference $\Delta\Phi$ by the frequency $\omega$:

$$T_w = \Delta\Phi/\omega = (x_2 - x_1)/v_0 \qquad (4)$$

As long as the velocity is uniform, the solutions of (2) are obtained by inspection, and this technique offers no difficulty. However, complexities arise if the wave traverses an inhomogeneous path along which the velocity is no longer uni-

[1] Contribution 1503, Division of Geological Sciences, California Institute of Technology, Pasadena.

[2] On academic leave from the University of Rhode Island.

form, for then the wave equation is not amenable to direct solution.

Let us write the variable velocity $v(x)$ as

$$v(x) = v_0/[1 + \epsilon(x)] \tag{5}$$

where

$$\epsilon(x) = [v_0/v(x)] - \tag{6}$$

describes the local velocity perturbation. To compute the travel time $T_w$, we need to calculate the phase shift of the traveling wave solution of the perturbed equation

$$d^2u/dx^2 + k_0^2[1 + \epsilon(x)]^2u(x) = 0 \tag{7}$$

between the points $x_1$ and $x_2$ as compared with the phase shift $\Delta\Phi = k_0(x_2 - x_1)$ for the uniform case. For nonuniform wave propagation it is not possible to identify a traveling wave without ambiguity, for there can be no unique distinction between the forward and scattered waves [*Schelkunoff*, 1951]. Hence, the only specification concerning the behavior of $u(x, t)$ that we shall make is that it becomes $\mathrm{Re}\ e^{i(k_0x - \omega t)}$ as $\epsilon \to 0$. For clarity, we shall concentrate on real wave motions; that is, we discuss fields in which

$$u(x, t) \sim \cos(k_0x - \omega t) \tag{8}$$

Note that this forces us to include the effects of time variation in $u(x, t)$.

To obtain the phase we first introduce the logarithmic derivative

$$\Gamma(x, t) = (\partial u/\partial x)/u \tag{9}$$

and in terms of this quantity, (7) becomes the Ricatti equation

$$\partial\Gamma/\partial x + \Gamma^2 + k_0^2(1 + \epsilon)^2 = 0 \tag{10}$$

If $\epsilon(x)$ vanishes, the solution of (10) subject to (8) is

$$\Gamma^f(x, t) = -k_0 \tan[k_0x - \omega t] \tag{11}$$

If $\epsilon(x)$ is nonzero, we seek a solution in the perturbed form:

$$\Gamma(x, t) = -k_0 \tan[k_0[x + \varphi(x)] - \omega t] \tag{12}$$

where $k_0\varphi(x)$ describes the local phase correction owing to a nonuniform velocity. That is, the total phase shift $\Delta\Phi$ will be

$$\Delta\Phi = k_0[\varphi(x_2) - \varphi(x_1) + x_2 - x_1] \tag{13}$$

In terms of $\varphi(x)$ as an unknown, the Ricatti equation becomes

$$\partial\varphi/\partial x = (2\epsilon + \epsilon^2) \cdot \cos^2[k_0[x + \varphi(x)] - \omega t] \tag{14}$$

after substitution of the trial form (12) and some arithmetic. If we integrate this expression, we obtain an integral equation,

$$\varphi(x_2) - \varphi(x_1) = \int_{x_1}^{x_2} [2\epsilon(\xi) + \epsilon^2(\xi)] \cdot \cos^2[k_0[\xi + \varphi(\xi)] - \omega t]\, d\xi \tag{15}$$

for the determination of $\varphi(x)$, since it appears under the integral sign. Note that the net correction to the phase shift $\varphi(x_2) - \varphi(x_1)$ is time-dependent. This situation is forced by our inability to separate the forward wave from the multiply reflected wavelets it excites. Only in uniform wave motion is the phase time-independent, for then the real and imaginary parts of the exponential $e^{i(k_0x - \omega t)}$ are identical apart from a translation. In this special case, the *shape* of the wave does not change as we pass through a period. *For nonuniform wave propagation the shape of the wave changes during one cycle*, and for this reason, we cannot speak in general of a distinct phase shift between two points owing to its time-variation. However, experimentalists often measure phase shift averaged over many cycles. If this is done, the $\cos^2\{\}$ term in the integral equation (13) behaves like a numerical weight factor of $\frac{1}{2}$, and we obtain the explicit relation

$$\langle\varphi(x_2) - \varphi(x_1)\rangle = \int_{x_1}^{x_2} [\epsilon(\xi) + \tfrac{1}{2}\epsilon^2(\xi)]\, d\xi \tag{16}$$

where the angle brackets $\langle\rangle$ indicate an average phase difference. Alternatively, (16) describes what would be measured if $x_2 - x_1$ is large in comparison with a wavelength. Thus, the travel time $T_w$ for harmonic waves in terms of the average phase shift is

$$T_w = (x_2 - x_1) + \langle\varphi(x_2) - \varphi(x_1)\rangle \tag{17}$$

or

$$T_w = \int_{x_1}^{x_2} [1 + \epsilon(\xi) + \tfrac{1}{2}\epsilon^2(\xi)]\, d\xi \tag{18}$$

as compared with (1). This expression can be rewritten as

$$T_a = T_g + A \tag{19}$$

where the anomaly $A$ between $T_a$ and $T_g$ is seen to be

$$A = \frac{1}{2}\int_{x_1}^{x_2}\left(\frac{v_0}{v(\xi)} - 1\right)^2 d\xi \tag{20}$$

and we always have

$$T_a \geq T_g \tag{21}$$

and equality holds if and only if $v(x) \equiv v_0$. We interpret this anomaly $A$ as a result of the increased phase shift due to diffraction.

*Example.* The implication of the preceding remarks is perhaps best illustrated by an example. Consider a surface wave propagating along a path whose layer thickness varies between $h_{min}$ and $h_{max}$, say. For a uniform layer we can find a period equation which relates the phase velocity of any harmonic surface wave and the height $h$. The question we ask is what will the average height $\langle h \rangle$ seem to be if we correlate phase shift data over large distances with phase velocity.

In its rigorous formulation this poses an intractable boundary value problem. But, if the variation of $h$ is small over distances of the order of a wavelength, then, the propogation of the disturbance is described by the one-dimensional equation (7) where $v(x)$ is the local phase velocity. Either the local phase velocity $v(x)$ or the height $h(x)$ determines the other owing to the period equation. For simplicity, let us assume that their interrelationship is a linear one, although the argument we shall present does not depend upon this fact. If linearity holds, the *arithmetic mean* of the velocity $v(x)$ would be proportional the average thickness $\langle h \rangle$. How can we extract the arithmetic mean from measured phase data? We write

$$v(x) = v_0[1 + \delta(x)] \tag{22}$$

where $v_0$ is the arithmetic mean of $v(x)$ and $\delta(x)$ is related to $\epsilon(x)$ by the relation

$$\epsilon(x) = -\delta(x)/[1 + \delta(x)] \tag{23}$$

Since $v_0$ is the arithmetic mean, we have

$$\int_{x_1}^{x_2} \delta(\xi)\, d\xi = 0 \tag{24}$$

but the mean-square value

$$\langle \delta^2(x) \rangle = \frac{1}{x_2 - x_1}\int_{x_1}^{x_2} \delta^2(\xi)\, d\xi \tag{25}$$

is nonzero. For a fixed distance, velocity is inversely proportional to travel time. From (1) we have the second-order equation

$$\langle v \rangle_a = v_0/[1 + \langle \delta^2(x) \rangle] \tag{26}$$

as the effective velocity of a mass point in traversing the distance from $x_1$ to $x_2$. If we interpret $\langle v \rangle_a$ as the velocity we measure, $(1 + \langle \delta^2(x) \rangle)$ is the correction factor we need to renormalize it to the arithmetic mean. However, the inequality (21) indicates that this correction factor is too small for a wave propagating through an inhomogeneous velocity profile owing to scattering effects. In fact, for a wave, we easily find that the effective velocity is related to $v_0$ by the second-order relation

$$\langle v \rangle_g = v_0/[1 + \tfrac{3}{2}\langle \delta^2(x) \rangle] \tag{27}$$

In other words, the effect of scattering is to increase the presumed correction factor by 50%.

*Acknowledgment.* The research described in this report has been sponsored by the Air Force Cambridge Research Laboratories, Office of Aerospace Research, under contract AF 19(628)-319 as part of project Vela Uniform.

## References

Scheikunoff, S. A., Remarks concerning wave propagation in stratified media, *Comm. Pure Appl. Math.*, *4*, 117–128, 1951.

(Manuscript received October 30, 1964; revised December 28, 1964.)

APPENDIX B

# Fiber Optics and Strain Interferometry

JULIUS KANE, SENIOR MEMBER, IEEE

*Abstract*—By use of glass fibers as dielectric waveguides, interferometric measurements of light along the propagation path can be used as a new type of strain gauge. Two novel strain interferometers are proposed: one which uses the phenomenon of crosstalk between adjacent light pipes, and another which is a waveguide version of the Michelson interferometer. Both designs are distinguished by the possibility of digital readout and a basic simplicity. The theory of the instruments is described, and explicit estimates for the strain sensitivity are calculated. The numerical data show that, with digital readout, strains of the order of $10^{-8}$ can be resolved with a basic instrument ten meters long, and strains of the order of $10^{-9}$ can be resolved by a hundred-meter device. With the aid of various refinements, the sensitivity can be enhanced by at least another order of magnitude.

## I. Introduction

GROUND MOTION can be measured with reasonable accuracy by a wide variety of seismometers. However, other than the Benioff strain seismometer or an installation which uses multiple beam interferometry between piers in a seismic vault, there are few instruments that are capable of recording the slow accumulation of tectonic strain. The demands of the projected earthquake prediction program indicate a need for a network of such strain gauges which combine modest cost with adequate performance. In this study, we investigate the possibility that an amalgam of waveguide and optical techniques may be useful in realizing these goals.

Seismologists have long used surface-wave dispersion data to gauge the layering of crustal structures. However, this nonlinear interplay of dispersion and depth is a feature of wave motion, in general, and not confined to the theory of elastic waves. Indeed, optical surface waves have been observed[1,2] and their features studied.[3,4] Owing to the minute character of optical surface waves, interferometric procedures based upon their interaction with matter can supply rather accurate information about small displacements or strains. In this analysis we propose an application of optical surface waves propagating along dielectric fibers as a new type of displacement or strain gauge with digital readout.

The basic instrument can be thought of as a long thin prism with, for example, a square cross section in the quiescent state. Under the action of forces normal to the axis of the prism, the square cross section will be deformed. Depending upon the stress distribution, the strained cross section can assume a variety of forms: compressed square, rhombus, etc. The distorted geometry can be characterized by measuring the perturbed distances between the edges of the prism and comparing them with those of the equilibrium state. At optical frequencies, waveguides can be very small, and we can imagine that the four edges are, in fact, miniature waveguides. If the waveguides are coupled, then, they can interact in such a fashion as to respond to the varying distances between them. We can imagine that these four waveguides are relatively dense dielectric fibers cladded in a transparent matrix to produce a multicomponent glass cable. This configuration would then be imbedded in some elastic medium to couple it to that structure. For example, it could be buried in the earth, or imbedded in a concrete dam or foundation. Once inserted, the *average* distortion of the transverse cross section can be monitored by studying the variation of the propagation characteristics along these coupled microscopic waveguides. The purpose of this paper is to describe how the interaction of coupled waveguides can be used as a metrological tool for the determination of small displacements or strains.

The principle we propose using to achieve our goals is an application of the phenomenon of *crosstalk* which has been observed in the optical range of coupled-mode propagation. This is an exchange of energy between adjacent light pipes which has been analyzed by Snitzer[5] who had in mind the problem of controlling moding in fiber optic lasers.[6] In this regard, crosstalk is a problem and the motivation is to reduce this nuisance. Our interest, however, is to propose its exploitation. For this purpose we review the theory of this effect, obtain estimates for the sensitivity that can be obtained, and propose explicit designs for working instruments.

The basic building blocks of the device are sketched in Fig. 1. Two dielectric waveguides are separated from one another by a distance $d$. Each waveguide is of dimension $h$ and is a dense dielectric of index $n_2$ imbedded between rarer media $n_1$ and $n_3$. The geometry of the device can consist of either a pair of cylindrical fibers, a pair of plane parallel layers, or any other pair of parallel waveguides, provided that the structure has a plane of

Manuscript received July 14, 1965. This research was sponsored in part by the Air Force Cambridge Research Laboratory, Office of Aerospace Research, Cambridge, Mass., as part of Project VELA-UNIFORM.

The author is with the Space Science Center, University of California, Los Angeles, Calif. He is on academic leave from the University of Rhode Island, Kingston, R. I.

[1] H. Osterberg and L. Smith, "Transmission of optical energy along surfaces: Pt. I, Homogeneous media," *J. Opt. Soc. Am.*, vol. 54, pp. 1073–1078, September 1964.

[2] ——, "Transmission of optical energy along surfaces: Pt. II, Inhomogeneous media," *J. Opt. Soc. Am.*, vol. 54, pp. 1078–1084, September 1964.

[3] E. Snitzer, "Optical dielectric waveguides," in *Advances in Quantum Electronics*. New York: Columbia University Press, 1961.

[4] ——, "Proposed fiber cavities for optical masers," *J. Appl. Phys.*, vol. 32, pp. 36–39, January 1961.

symmetry bisecting the distance $d$ separating the component waveguides. Since the operation of the device depends primarily upon symmetry considerations and not especially upon the character of the component waveguides, we shall provide explicit calculations only for plane parallel structures for ease of analysis. However, we stress that the theory is easily generalized to describe other structures. An understanding of the device's function depends upon a knowledge of guided wave propagation in this multilayer system. That is, we seek the dependence of the system's behavior upon the parameter $d$ which is the quantity we should like to measure.

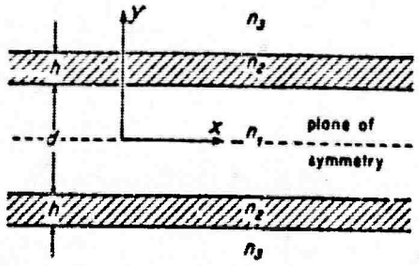


Fig. 1. The geometry of a symmetrical two-fiber system.

## II. Theory

To analyze this multilayer system we need to find those solutions of Maxwell's equations which satisfy the boundary conditions, and which represent propagating modes for our choice of geometry. If we denote the spatial part of the electric vector as $\boldsymbol{E}$ and the spatial part of the magnetic vector as $\boldsymbol{H}$, then in homogeneous, isotropic space, Maxwell's equations assume the form

$$\text{curl } \boldsymbol{E} = ik_0\boldsymbol{H} \tag{1}$$

$$\text{curl } \boldsymbol{H} = -ik_0n_j^2\boldsymbol{E} \tag{2}$$

where a time factor $e^{-i\omega t}$ has been suppressed. The symbol $k_0$ is the propagation constant of free space

$$k_0 = 2\pi/\lambda_0 = \omega/c; \tag{3}$$

and

$$k_j = k_0n_j \tag{4}$$

where we identify $\lambda_0$ and $c$ as the wavelength and speed of light in vacuum, and $n_j$ is the dielectric constant in the $j$th medium. For convenience, the magnetic permeability $\mu$ is assumed to be unity for all media, and we neglect loss terms proportional to conductivity.

If the wave disturbance travels along the $x$-axis in an isotropic medium without dependence on the Cartesian coordinate $z$, then all derivatives with respect to $z$ vanish. One can show from (1) and (2) that only the two transverse components $U(x, y) = E_z$ and $V(x, y) = H_z$ are required to specify all six components of the electromagnetic field. These six components separate into two decoupled groups of three each. Thus,

$$\boldsymbol{TE}: \begin{cases} H_x = \dfrac{+1}{ik_0}\dfrac{\partial U}{\partial y}, \qquad H_y = \dfrac{-1}{ik_0}\dfrac{\partial U}{\partial x} \\ H_z = E_x = E_y = 0, \end{cases} \tag{5}$$

determine $E_x$ and $E_y$ from $U(x, y)$ for $\boldsymbol{TE}$ propagation, and

$$\boldsymbol{TM}: \begin{cases} E_x = \dfrac{-1}{ik_0n_j^2}\dfrac{\partial V}{\partial y}; \qquad E_y = \dfrac{+1}{ik_0n_j^2}\dfrac{\partial V}{\partial x} \\ E_z = H_x = H_y = 0, \end{cases} \tag{6}$$

specify $H_x$ and $H_y$ in terms of $V(x, y)$ for $\boldsymbol{TM}$ excitation. Both $U$ and $V$ satisfy the same reduced wave equation, namely:

$$(\nabla^2 + k_j^2)U, V = 0, \tag{7}$$

in the $j$th medium which has index of refraction $n_j$. The field within the $j$th medium must satisfy this wave equation and the requirement that the tangential components of $\boldsymbol{E}$ and $\boldsymbol{H}$ be continuous across any interface separating two dielectrics. For $\boldsymbol{TE}$ modes, this means that $U$ and $\partial U/\partial y$ must be continuous across any boundary; for $\boldsymbol{TM}$ modes, $V$ and $(1/k_j^2)\partial V/\partial y$ must be continuous.

The nature of the problem to be solved is such that only discrete types of propagation are permissible along the system. For plane layers, the electromagnetic theory is very similar to that of Love wave propagation. Since the $\boldsymbol{TE}$ and $\boldsymbol{TM}$ problems are identical in character, we shall emphasize the analysis for the $\boldsymbol{TE}$ case and just quote the corresponding results for the $\boldsymbol{TM}$ case.

For a traveling mode we must have

$$U(x, y) = u_N(y)e^{(ik_0Nx)}, \tag{8}$$

and then the problem becomes one of determining those values of the dimensionless propagation constant $N$ for which functions $u_N(y)$ can be found which are consistent with Maxwell's equations and the boundary conditions. At each interface, we have two transition conditions to be satisfied. If we take the ratio of these equations, we obtain an equation whose physical significance is independent of considerations of the field amplitude. For this reason we introduce the logarithmic derivative

$$\Gamma(y) = \frac{du}{dy}\Big/u \tag{9}$$

which is essentially an impedance-type function. For the $\boldsymbol{TE}$ case, it is proportional to $H_x/E_z$, which is the normal admittance to any guide wall where it must have the same value on either side of the boundary. For the $\boldsymbol{TM}$ case, the ratio $\Gamma/n_j^2$ is an impedance function and plays an analogous role. In the $j$th region $u_N(y)$ must be of the form

$$u_N(y) = \begin{cases} A_j \cos\left[k_0(n_j^2 - N^2)^{1/2}y\right] \\ \quad + B_j \sin\left[k_0(n_j^2 - N^2)^{1/2}y\right], & N < n_j \\ A_j \exp\left[+k_0(N^2 - n_j^2)^{1/2}y\right] \\ \quad + B_j \exp\left[-k_0(N^2 - n_j^2)^{1/2}y\right], & N > n_j \end{cases} \quad (10)$$

and we must solve an algebraic problem to determine the correct values of $A_j$ and $B_j$ so that the transition conditions across each interface are matched and radiation conditions at infinity are satisfied. Instead of proceeding directly, computational effort can be decreased, and insight enhanced, by considering the operation of the system as a coupling of the characteristics of the individual waveguides. We analyze the behavior of an individual layer first, and then couple two guides together to understand the response of the composite system.

## III. Modal Analysis

### A. The Component Guide: An Isolated Layer

In order to discuss propagation along the structure sketched in Fig. 1, we assume that the $y$-variation behaves like a standing wave within the layer, and an exponentially damped field outside. These fields will match across the interfaces in such a way that the transition conditions are satisfied if the allowable values of the propagation constant $N$ satisfy the characteristic equation.[8]

$$\tan\left[(n_2^2 - N^2)^{1/2}k_0 h\right] = \frac{(n_2^2 - N^2)^{1/2}(\Gamma_1^\infty + \Gamma_2)}{(n_2^2 - N^2) - \Gamma_1^\infty \cdot \Gamma_2} \quad TE \quad (11)$$

for the *TE* case and

$$\tan\left[(n_2^2 - N^2)^{1/2}k_0 h\right] = \frac{(n_2^2 - N^2)^{1/2}\left[(n_2/n_1)^2\Gamma_1^\infty + (n_2/n_2)^2\Gamma_2\right]}{(n_2^2 - N^2) - (n_2^2/n_1 n_2)^2\Gamma_1^\infty\Gamma_2} \quad TM \quad (12)$$

for the *TM* case. In these expressions, the indexed symbols are given explicitly as

$$\Gamma_1^\infty = \sqrt{N^2 - n_1^2}$$
$$\Gamma_2 = \sqrt{N^2 - n_2^2}. \quad (13)$$

For the *TE* case, each $\Gamma_i$ represents the normal wall admittance looking out of the guide at medium $n_i$. For the *TM* polarization, the functions $\Gamma_1^\infty/n_1^2$ and $\Gamma_2/n_2^2$ are the corresponding normal wall impedances. Note that we anticipate the perturbation of $\Gamma_1^\infty$ by affixing the superscript $\infty$. In (13), both $\Gamma_1^\infty$ and $\Gamma_2$ have the values shown because these are the required admittances needed to match a standing wave within the dielectric slab to a decaying exponential field outside. If, however, the field outside is perturbed in such a fashion that the wall admittance is known *exactly*, then (11) and (12) describe *rigorously* the $N$-values for the changed situation as well, provided we use the altered $\Gamma_i$'s.

### B. The Composite Guide: A Multilayer System

For a composite guide, the modes we have just discussed do not satisfy the boundary conditions and cannot propagate. However, they can be combined in such a way to produce modes of the system, and for this reason we shall call them *partial* modes to distinguish them from the true system modes. Imagine that the composite guide is formed by bringing two isolated guides together. If these layers are very far apart, then the modes of the combined system are effectively the partial modes of each element. However, as the separation diminishes, the two guides interact, and the modes of the system are perturbed linear combinations of the partial modes belonging to each layer (cf. Fig. 2). Owing to the symmetry of the system, the multilayer modes must be either *even* or *odd* about the plane of symmetry. For the odd modes $u(y)$ must vanish along the plane of symmetry, and for the even modes the normal derivative $\partial u/\partial y$ must vanish there. If the guides are coupled, the partial modes in either layer interact with one another to meet these conditions. The partial modes on either layer sense the other and respond by warping their characteristics and their $N$-value so as to meet the condition of even or odd symmetry. This can happen in two distinct ways, and since the reaction would be different for either parity, the $N$-value for each symmetry is distinct. This discrepancy vanishes as $k_1 d \to \infty$ and increases as $k_1 d \to 0$. This variation, which depends upon both $n_1$ and $d$, is what we wish to exploit once we have found its explicit behavior.

The two layers sense one another through the exponential term

$$\exp\left[\pm(N^2 - n_1^2)^{1/2}k_0 y\right] \quad (14)$$

in the $n_1$ region. If the guides are infinitely remote, then one can only use that exponential for which the sign is so chosen that the field decays exponentially away from the guide. If, however, the two guides are a finite distance apart, then there will be a reaction term and one must use the exponential with the other sign to describe the coupling. By determining the field that must exist between the guide wall and the plane of symmetry, we can find the eigenvalues for the even and odd modes in the composite structure.

With proper normalization, the expression

$$\exp\left[+(N^2 - n_1^2)^{1/2}k_0 y\right], \quad y < 0 \quad (15)$$

represents the unperturbed decaying field from the lower wall of the upper guide $y = +d/2$. In order for the total field to vanish at the plane of symmetry at $y = 0$,

[8] J. Kane and H. Osterberg, "Optical characteristics of planar guided modes," *J. Opt. Soc. Am.*, vol. 54, pp. 347–352; March 1964.

we need to add the correction term

$$-K \exp\left[-(N^2 - n_1^2)^{1/2} k_0 (y - d)\right] \tag{16}$$

to field (15) where the constant $K$ is

$$K = \exp\left[-(N^2 - n_1^2)^{1/2} k_0 d\right]. \tag{17}$$

This demand of an odd mode at the plane of symmetry $y = 0$ is reflected by requiring an admittance

$$\Gamma_1^o(d) = \Gamma_1^m \frac{1 + K}{1 - K} = \Gamma_1^m \coth\left[\tfrac{1}{2} k_0 d (N^2 - n_1^2)^{1/2}\right] \tag{18}$$

back at the layer boundary $y = d/2$ where $\Gamma_1^m$ is the impedance for $d = \infty$. Likewise, by a similar calculation for even modes, the reflected admittance back at the wall is found to be

$$\Gamma_1^e(d) = \Gamma_1^m \frac{1 - K}{1 + K} = \Gamma_1^m \tanh\left[\tfrac{1}{2} k_0 d (N^2 - n_1^2)^{1/2}\right]. \tag{19}$$

From these expression we note the inequalities

$$\Gamma_1^o(d) > \Gamma_1^m > \Gamma_1^e(d) \tag{20}$$

for any finite value of $d$, and the relation

$$\Gamma_1^e(d) \cdot \Gamma_1^o(d) = (\Gamma_1^m)^2. \tag{21}$$

With a knowledge of $\Gamma_1^e$ and $\Gamma_1^o$, the eigenvalues for the multilayered system are given by (11) and (12) for the even and odd modes provided that expressions (18) and (19), respectively, are substituted for $\Gamma_1^m$. A solution of these equations then yields the corresponding $N$-values for the even and odd modes. The solution of these implicit equations is straightforward, but a computational nuisance. However, it is possible to draw some conclusions without any effort.

An increase in $\Gamma_1^m$ is known to have the effect of lowering the $N$-value of the mode. Likewise, a decrease in $\Gamma_1^m$ increases the $N$-value. From the inequality (20) we infer that the odd mode has a higher $N$-value than the corresponding mode of the isolated guide while the even mode has a lower one. This is to be expected on physical grounds. The parameter $N$ can be thought of as an effective index of refraction for the mode, and described as some weighted average of $n_1$, $n_2$, and $n_3$. The weight factors would be proportional to the relative field concentration in any one region. The odd mode has a node in the $n_1$ region, whereas the even mode has a loop there. As a result, a greater portion of the field of the even mode is in the $n_2$ region which is a relatively rare medium and, thus, its $N$-value is lowered, and *vice versa* for the odd mode.

If changes in the displacement $d$ are being produced by hydrostatic stresses which produce volume deformations, then the dielectric constants $n_i$ will be altered. The perturbed dielectric constants $n_i'$ can be found by use of the Lorentz-Lorenz formula[6] from the expression

$$n_i'^2 = \frac{(n_i^2 + 2) + 2(n_i^2 - 1)V/V'}{(n_i^2 + 2) - (n_i^2 - 1)V/V'} \tag{22}$$

where $V$ and $V'$ are the original and perturbed volumes, respectively. The effect of the altered dielectric constant on $N^e$ and $N^o$ can be included by substituting $n_i'$ for $n_i$ in the characteristic equations. For simplicity we shall neglect the perturbations of the dielectric constant, for this variation affects only the numerical details but not the basic theory, and its influence can be included at a later stage.

## III. The Beat Phenomenon

### A. Theory

In coupled waveguides there are paired modes, one even and the other odd, which are continuous perturbations of the partial modes for variations in $d$. If the separation between the two layers is very large, then the distinction between the $N$-values of the even and odd modes is insignificant owing to the exponential decay of $K$ with increasing $d$ [cf. (17)]. However, as $d$ diminishes, there will be a modest but significant discrepancy between the $N$-values for the modes of either symmetry. We shall call this situation *loose* coupling to distinguish it from *tight* coupling wherein the discrepancy between the $N$-values can be unbounded. For tight coupling, the field variation of the modes of the multilayer will be significantly different from the partial modes of the single layers. On the other hand, when the coupling is loose, the multilayer modes are essentially linear combinations of the partial modes, and this gives rise to some interesting and useful effects.

Let us denote the $N$-value of the even mode as $N^e$ and use $N^o$ for the odd mode. In addition, we set

$$\Delta N = N^o - N^e. \tag{23}$$

In Fig. 2 we have sketched the formation of multilayer modes as a combination of the partial modes. If we designate the $y$-variation of the composite mode in upper case type as $M_N^{e,o}(y)$ and use lower case letters $m(y)$ for the partial modes we have the approximate representation

$$M_N^e(y) = m_N[y - \tfrac{1}{2}(d + h)] + m_N[y + \tfrac{1}{2}(d + h)], \tag{24}$$

$$M_N^o(y) = m_N[y - \tfrac{1}{2}(d + h)] - m_N[y + \tfrac{1}{2}(d + h)]. \tag{25}$$

These equations are valid for loose coupling, for then the partial modes need not be significantly perturbed to form a true system mode. Of course, we can rewrite these equations as

$$m_N[y - \tfrac{1}{2}(d + h)] = \tfrac{1}{2}[M_N^e(y) + M_N^o(y)] \tag{26}$$

$$m_N[y + \tfrac{1}{2}(d + h)] = \tfrac{1}{2}[M_N^e(y) - M_N^o(y)] \tag{27}$$

which might seem to be a peculiar way of doing things, but turns out to be very useful. These last two equations show that we can think of the field on the upper layer as a superposition of $M_N^e$ and $M_N^o$, and a field on the lower layer as their *difference*. For a coupled system

[6] M. Born and E. Wolf, *Principles of Optics*. London: Pergamon, 1959.

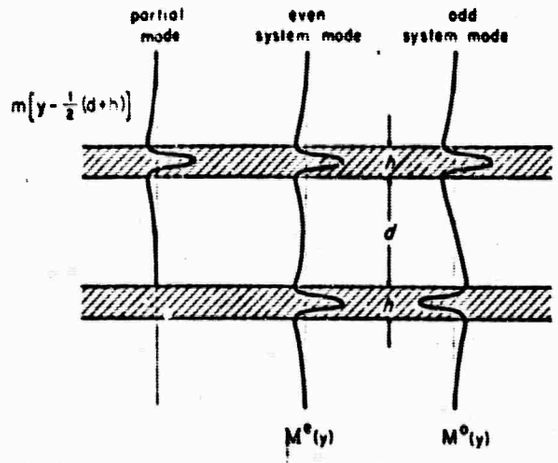


Fig. 2. The formation of the system modes in terms of the partial modes belonging to the individual layers.

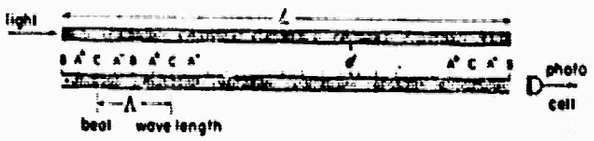


Fig. 3. The beat phenomenon. If light is injected into one of a pair of coupled waveguides, it will oscillate between the two guides with a beat wavelength Λ. As the guides come closer, the beat wavelength decreases and the output state will cycle as $A^+$, $B$, $A^-$, $C$, $A^+$.

only $M_N{}^e$ or $M_N{}^o$ are the possible $y$-variations of propagating modes. Any other field must be represented as a superposition of the allowable $M_N{}^{e,o}$. Suppose we excite the multilayer system as shown in Fig. 3. That is, we illuminate only the upper layer at the aperture plane $x=0$, and suppose that this is done in such a way that $m_N(y-d/2)$ is excited in the vicinity of $x=0$. How does this initial disturbance propagate down the line since $m_N(y-d/2)$ is not the cross section of any mode of the multilayer, but only a piece of one? Equation (26) furnishes the answer; the combination

$$\mathfrak{D}(x, y) = \tfrac{1}{2}[M_N{}^e(y) + e^{ik_0\Delta N x}M_N{}^o(y)]e^{ik_0 N^o x} \quad (28)$$

solves this initial value problem for it is equal to $m_N(y-d/2)$ at $x=0$ and represents the transmission of the disturbance $\mathfrak{D}(x, y)$ for all $x$, since $\mathfrak{D}(x, y)$ is comprised of system modes. That is, we should think of the apparatus as being so arranged that *two* system modes are excited at $y=0$. However, owing to the factor $e^{ik_0\Delta N x}$ in (28), the relative phase between $M_N{}^e$ and $M_N{}^o$ is being shifted as the wave travels down the line. Indeed, at a critical distance $x=\Lambda/2$ such that

$$\Lambda/2 = \frac{\pi}{k_0\Delta N} \quad \text{or} \quad \Lambda = \frac{1}{\Delta N}\lambda_0 \quad (29)$$

there is a change in sign in the coefficient of $M_N{}^o$. From (27) we see that $\frac{1}{2}(M_N{}^o - M_N{}^e)$ represents $m_N(y+d/2)$, a field in but the lower guide. In other words, the energy has been transferred from one layer to the other at $x=\Lambda/2$. A repetition of the argument shows that when $x=\Lambda$, the $y$-variation of the field is restored to its initial state. But then the process repeats itself anew, or the energy oscillates from layer to layer. A cycle is completed when $x=\Lambda$, and for this reason $\Lambda$ is known as the *beat wavelength*. Since $\Lambda$ depends upon $\Delta N$ which in turn depends upon $d$, measurements of $\Lambda$ can be used to determine changes in $d$. Previously, we have introduced the notions of tight and loose coupling in a qualitative manner. In terms of the beat wavelength we say that the coupling is loose, if the beat wavelength is large compared to a wavelength. Before we make some explicit calculations describing the dependence of $\Lambda$ upon $n_1$ and $d$, let us see how we might take advantage of this effect.

### B. Application

Light enters the system as shown in Fig. 3 so that only the upper layer is excited at $x=0$. After a distance $x=L$ equal to an integral number $n$ of beat wavelengths

$$L = n\Lambda, \quad (30)$$

a photocell samples the field in the lower layer. In the quiescent state there is null output from the photocell. Suppose now that $d$ varies in such a manner that $\Delta N$ changes by an amount sufficient to make the new beat wavelength $\Lambda'$ have the value

$$\Lambda' = (L \pm \tfrac{1}{4})/n. \quad (31)$$

If this happens, then the photocell will have maximum reading. Clearly, the photocell output will be a sinusoidal response to fluctuations in $d$, and it is these variations in output that can be used for strain gauge instrumentation. There is a continuous exchange of intensity between the two layers as $d$ varies. Suppose we neglect this smooth variation and classify the output as being in one of three states: $A$, the intensity equally divided between the layers, $B$, all the light in the top layer, and $C$, all the light in the bottom layer. The output will cycle between these three states whenever the relative phase between $M^e$ and $M^o$ changes by $\pi/4$ at the output end. Each change in state can be counted as a unit transition. A count of the cycling between these states would provide a digital readout. What we need is some specific estimate of the sensitivity of the proposed instrument, that is the variation of $\Delta N$ as a function of $d$.

## IV. Solution of the Characteristic Equation

### A. Procedure

The characteristic equation (11) is capable of yielding complete information describing $N^e$ and $N^o$ once the perturbed values $\Gamma_1{}^e(d)$ and $\Gamma_1{}^o(d)$, given by (18) and (19), are substituted for $\Gamma_1{}^{e,o}$. Unfortunately, the resulting equation is an *implicit* transcendental relation for $N^e$ and $N_0^e$ so that it is not possible to display any simple formulas for their determination. However, (11) can

easily be solved by numerical techniques and the results displayed in graphical form.

The procedure used is to rewrite (11) in the form

$$H = k_0 h = \frac{1}{[(N^{e,o})^2 - n_2^2]^{1/2}} \tan^{-1} \cdot \left\{ \frac{[(N^{e,o})^2 - n_2^2]^{1/2}[\Gamma_1^{e,o}(d) + \Gamma_2]}{(N^{e,o})^2 - n_2^2 - \Gamma_1^{e,o}(d) \cdot \Gamma_2} \right\} TE \quad (32)$$

which is an explicit relation for the determination of $H = k_0 h$, the optical thickness of each component guide. No matter how the separation $D = k_0 d$ varies, any thickness $H$ we compute must have this reference value. We can pick some value $N_s$ in the range $n_1 < N_s < n_2$, and solve for that value of $H$ for which an unperturbed layer ($D = \infty$) can support a mode which propagates with this $N_s$ value. If $D$ is finite, this $N_s$ value will split into two values $N^e$ and $N^o$, each of which depends upon $D$. We know that $n_1 < N^o < N_s < N^e < n_2$, so we can guess at upper and lower bounds for $N^{e,o}$ given any value of $D$. If we substitute these bounds for $N^{e,o}$ into (32), we calculate values for $H$ which will be either too large or too small as compared to the reference value previously computed for $D = \infty$. The discrepancy between the calculated $H$ and the reference indicates how poor the assumed upper and lower bounds for $N^{e,o}$ are. By using backward interpolation, these bounds can be refined to yield $N^{e,o}$ to any desired degree of accuracy. In practice, this procedure is easily programmed, takes very little machine time, and has the advantage of yielding $N^{e,o}$ *rigorously* without any assumptions concerning strong or weak coupling; that is, its validity is independent of the distance $D$.

### B. Sample Results

Typical results are illustrated in Fig. 4. In this illustration $n_1 = n_2 = 1.2$ and $n_2 = 2.0$. For convenience, the abscissa is laid off in units of $T = 1/D$, the reciprocal of $D$. The curves show the separation of $N^e$ and $N^o$ from initial values $N_s = 1.3$, 1.5, and 1.7; the corresponding layer thicknesses $H$ are marked on the graphs near the starting points $N_s$. For a given $N_s$, the curves $N^e$ and $N^o$ are almost indistinguishable until $T$ gets sufficiently large. In addition, the separation between $N^e$ and $N^o$ decreases as $N_s$ increases; this is to be expected on physical grounds since an increase in $N_s$ means that a greater fraction of energy propagates in the $n_2$-dielectric; hence, there is less field outside which can sample the presence of the other layer. In other words, for a fixed separation $D$, the coupling will be $_{\text{less}}^{\text{greater}}$ according as $N_s$ or $H$ is $_{\text{greater}}^{\text{less}}$.

### C. Significance

Suppose we consider the variation of $N^e$ and $N^o$ about the value $D = \lambda_0$, as shown in Fig. 4 for $N_s = 1.3$. The values of $N^e$ and $N^o$ are given in Table I to five significant figures. To interpret these numbers, let us suppose that we have two such fibers a wavelength apart; that is, let $D = \lambda_0$ be the quiescent state. If the system is one meter long, and one of the fibers is illuminated by light of wavelength 691.18 mμ, then a beat wavelength $\Lambda$ is 50 micrometers long so that there will be $2 \times 10^4$ beat wavelengths along the axis of this one-meter device. Since the length of the system is an integral number of beat wavelengths, the exit illumination will be in the same layer as the entrance illumination. Suppose now the distance $D$ between the fibers increases from $D = 1.000\lambda_0$ to $D = 1.0526\lambda_0$, a strain of $5.26 \times 10^{-2}$. The fractional change in $\Lambda$ is 8568/7236 so that there are now $1.689 \times 10^4$ beat wavelengths in a meter. This represents a change of $3.111 \times 10^3$ beat wavelengths; this value is the number of times the exit illumination has been transferred from one fiber to the other and back to the original layer. Let us set one bit to be equal to a quarter change of state as the limit of sensitivity. It takes a $5.26 \times 10^{-2}$ strain to produce $1.24 \times 10^4$ transitions; hence, one transition corresponds to a strain of $4.2 \times 10^{-6}$. In other words, for the example cited, a system one meter long should be able to resolve a strain of the order of $10^{-6}$. A system ten meters long would be able to resolve a strain of the order $10^{-7}$, etc.

Several factors control the sensitivity: these include 1) the optical length of the system, 2) the degree of coupling between the two layers, for the closer they are the more sensitive is $\Delta N$ to changes in $d$, and 3) the value of $N_s$ which locates the position on the dispersion curve about which the instrument operates. The sensitivity increases in direct proportion to the length of the instrument. However, the variation of sensitivity with respect to 2) or 3) is more complex and we present sample results in Table II. If $L$ is the length of the instrument in wavelengths, we can specify the smallest strain $\delta$ that it can resolve as

$$\delta = c \frac{\Delta D/D}{\Delta\Lambda/\Lambda} \frac{\Lambda}{L}. \quad (33)$$

The constant $c$ equals $\frac{1}{4}$ if we choose a unit transition as being one quarter of a complete cycle at the exit end as the threshold of observation. Table II illustrates the variation of the sensitivity $\delta$ as the coupling and $N_s$ vary. In Table II we have assumed, for example, that $\lambda_0 = 691.18$ mμ and that the length of the interferometer was ten meters. Note that the strain sensitivity is of the order of $10^{-8}$, if we decrease $D$ from $\lambda_0$ to $\frac{1}{2}\lambda_0$. Of course, an additional order of magnitude or two of strain sensitivity can be gained at the exit end if the luxury of digital readout is sacrificed and fractional phase differentials between the two layers are measured, or if the length $L$ is increased.

One disadvantage is apparent: at the output end there is no simple way of determining whether an *initial* motion which produces a one-bit change corresponds to an increase or decrease in strain. The problem arises from the fact that the output cycles between three states, *A*, *B*, and *C*, by following the sequence

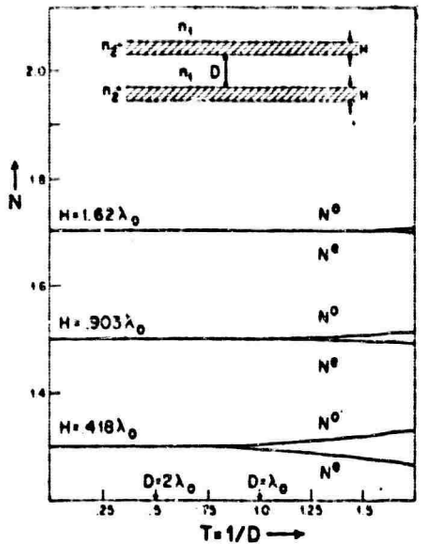


Fig. 4. The variation of $N^e$ and $N^o$ with respect to $T=1/D$. In this illustration $n_1=n_3=1.2$ and $n_2=2.0$.

TABLE I

NUMERICAL VALUES FOR $N^e$, $N^o$, AND THE BEAT WAVELENGTH $\Lambda$ FOR THE CASE $n_1=1.2$, $n_2=2.0$, $N_e=1.3$, and $H=0.4182\lambda_0$

| $D$ | $t$ | $N^e$ | $N^o$ | $\Lambda=\frac{\lambda_0}{N^o-N^e}$ | $\Delta\Lambda$ |
|---|---|---|---|---|---|
| $\lambda_0$ | $1/\lambda_0$ | Dimensionless | | $\lambda_0$ | $\lambda_0$ |
| 1.2500 | 0.8000 | 1.297 | 1.303 | 160.9 | 33.5 |
| 1.1765 | 0.8500 | 1.296 | 1.304 | 127.4 | 24.1 |
| 1.1111 | 0.9000 | 1.295 | 1.304 | 103.3 | 17.62 |
| 1.0526 | 0.9500 | 1.294 | 1.305 | 85.68 | 13.34 |
| 1.0000 | 1.0000 | 1.292 | 1.306 | 72.34 | 10.30 |
| 0.9524 | 1.0500 | 1.291 | 1.307 | 62.04 | 8.13 |
| 0.9091 | 1.1000 | 1.290 | 1.308 | 53.91 | 6.53 |
| 0.8696 | 1.1500 | 1.288 | 1.309 | 47.38 | 5.31 |
| 0.8333 | 1.2000 | 1.286 | 1.310 | 42.07 | |

TABLE II

THE VARIATION OF THE BEAT WAVELENGTH AND STRAIN SENSITIVITY AS A FUNCTION OF THE OPTICAL THICKNESS OF EACH COMPONENT GUIDE AND ITS SPACING. THE FIGURES ASSUME A FIBER LENGTH OF TEN METERS

| $D(\lambda_0)$ | $N_e=1.50$, $H=0.903\lambda_0$ | | $N_e=1.30$, $H=0.418\lambda_0$ | | $N_e=1.40$, $H=0.655\lambda_0$ | |
|---|---|---|---|---|---|---|
| | $\Lambda(\lambda_0)$ | $\delta\times10^{-6}$ | $\Lambda(\lambda_0)$ | $\delta\times10^{-6}$ | $\Lambda(\lambda_0)$ | $\delta\times10^{-6}$ |
| 2.0 | 1704 | 458 | 45400 | 3360 | 145000 | 83000 |
| 1.8 | 909 | 274 | 7270 | 1510 | 50400 | 8290 |
| 1.6 | 485 | 164 | 2930 | 687 | 16390 | 3040 |
| 1.4 | 258 | 99.7 | 1190 | 317 | 5230 | 1120 |
| 1.2 | 137 | 61.4 | 480 | 150 | 1690 | 419 |
| 1.0 | 72.3 | 38.4 | 194 | 72.4 | 544 | 163 |
| 0.9 | 52.3 | 30.5 | 123 | 50.9 | 309 | 163 |
| 0.8 | 37.7 | 24.3 | 77.8 | 36.1 | 175 | 65.5 |
| 0.7 | 27.0 | 19.5 | 49.2 | 25.9 | 100 | 42.4 |
| 0.6 | 19.2 | 15.8 | 30.9 | 18.8 | 56.4 | 27.9 |
| 0.5 | 13.5 | 13.2 | 19.3 | 13.7 | 31.8 | 18.7 |
| 0.4 | 9.51 | 11.9 | 11.9 | 10.2 | 17.8 | 12.9 |
| 0.3 | 6.91 | 8.3 | 7.19 | 8.07 | 9.81 | 9.20 |

$$A, B, A, C, A, B, A, C, \cdots. \tag{34}$$

Given this sequence, we have no way of knowing whether an initial transition from say *A* to *B* corresponds to a positive or negative strain. Note that only the *initial sign* is in doubt if we include a record of the previous transition in the logic of the output circuitry. This problem arises because there are two ways by which the state *A*, equal intensity in both layers, can be reached. There are several ways by which this degeneracy can be eliminated. A calibration strain artificially produced can eliminate subsequent directional ambiguity. Another method is to simultaneously illuminate the system by two distinct monochromatic sources and compare the system response to either color. This also has the potential advantage of increasing sensitivity. Instead of using two different colors an equivalent and simpler procedure would be to excite both *TE* and *TM* modes and analyze the output through polarizers. This would also provide additional resolution, since the *TE* and *TM* modes are uncoupled and propagate with different phase velocities. Assume, for example, that these two velocities differ by ten percent. This difference can be used at the output end to provide a vernier measurement and increase the sensitivity by an order of magnitude. A third alternative is to use a three-layer system (see Appendix) which provides an additional output that can be used for directional calibration.

Perhaps the simplest method is to recognize that a distinction can be made in state *A*, for when the intensity is equally divided between the two layers there is a $\pi/4$ phase difference between the fields in the top and

bottom layers. As a result, $A$ can be divided into two substates: $A^+$, which occurs when the phase in the top layer *leads* the phase in the bottom layer by $\pi/4$, and $A^-$, which arises when the phase in the top layer *lags* the phase in the lower layer by $\pi/4$. Hence, if phase discrimination is included in the sensors, and this can be done easily, then the response would cycle as

$$A^+, B, A^-, C, A^+, B, A^-, C, A^+, \cdots. \quad (35)$$

With any of these refinements, a transition between any two adjacent states would leave no doubt as to the sign of the strain.

## V. Design Notes

### A. Fabrication

Geologists are accustomed to thinking of layered structures as being rather large. For simplicity, we have assumed that the $z$-dimension of our waveguides is infinite. In practice, it is only necessary that this dimension be large compared to a wavelength. At optical frequencies this criterion can be achieved with a depth of but a few millimeters.

On the other hand, the problem of achieving dimensional tolerances may appear to be formidable. This would, of course, be true if the components of the dielectric guides were manufactured separately and then assembled in the microscopic state. However, fiber optic devices are not made this way; they are fashioned from rather large glass samples. All of the components are assembled on a macroscopic scale in a glass matrix with an extreme magnification of scale in the cross-sectional dimensions. Following this, the composite material is heated and drawn into a fine thread which shrinks the cross section by several orders of magnitude. Except for a scale change, the cross-sectional integrity is maintained as the fiber is drawn. In this manner, current technology has no difficulty in producing composite glass fibers with square cores. These have been used in fiber optic lasers to increase their packing density and hence efficiency. Consequently, there should be no problem in fashioning not only a pair of waveguides, but a whole array of them at once by drawing a multicomponent glass matrix. For example, this allows the possibility of drawing many waveguides at once. In the configuration of Fig. 5, pairs of coupled waveguides are at right angles. By mixing the output in appropriate linear combinations it is possible to devise a strain gauge which can discriminate between transverse shear and volume deformations.

A review of the analysis will indicate that tolerances in dimensions are not critical, for what is being measured is the *average* strain in a direction normal to the axis of the dielectric waveguides. In fact, this averaging of strain information should also have the beneficial effect of reducing noise level.

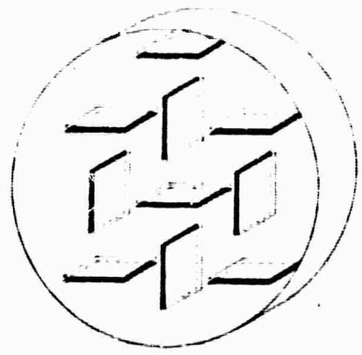

Fig. 5. A diagram of a glass matrix containing an array of waveguides prior to drawing. Following the drawing process the pairs of fibers can yield information on two components of transverse strain.

### B. Directional Response

The proposed device has a directional response for it responds essentially to strains in the $y$-dimension only. It is not hard to see that its polar pattern is basically a $\cos\phi$ pattern in the $x, y$ plane with the major lobe in the direction of the $y$-axis. The strain rejection in other dimensions is due principally to the fact that the only response that can even be elicited occurs when a displacement produces a differential between $N^a$ and $N^b$. That is, even though a strain may change both $N^a$ and $N^b$, the output will respond only to strains which alter $N^a - N^b$ and not to motions which change $N^a + N^b$.

### C. Other Configurations

Although the device we have described is a self-contained transverse strain gauge, the ideas inherent in its operation can be used in other useful ways. Laser interferometry has had high promise in measuring small geological strains, but this anticipation has been largely aborted owing to the unstable character of atmospheric propagation paths when the optical paths are large. The need here is for interferometry along a sheltered optical circuit. Dielectric lines offer one solution to this problem by providing a stable propagation path. Figure 6 illustrates a Michelson interferometer devised on the principles just described to fashion a longitudinal strain gauge. Traditionally, the Michelson interferometer requires a half-silvered mirror and two mirrors to reflect the light at the end of two perpendicular arms. We can achieve these requirements in the following fashion. A pair of coupled fibers at $A$, which is $(n+\frac{1}{4})$ beat wavelengths long, functions as a directional coupler and divides a coherent input into two branches after the fashion of a half-silvered mirror. The fibers then separate into two long paths of lengths $l_1$ and $l_2$ at right angles. Instead of a reflecting surface, the dielectric lines can be bent at $B$ by 180° provided the radius of

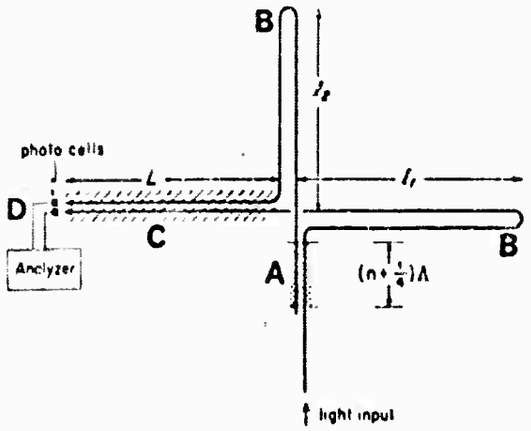


Fig. 6. A Michelson interferometer based on fiber optic waveguide principles. The fiber waveguides are coupled only in the cross-hatched regions *A* and *C*. A beam of light in one fiber will be divided between two waveguides if the coupler *A* is so adjusted that it is $(n+\frac{1}{4})$ beat wavelengths long. After traversing two arms of the interferometer, the light is bent at *B* and brought back to a long coupler *C*. The phase difference between the two beams will be multiplied by a factor depending upon the length of *L* before being analyzed.

curvature $r$ is greater[7] than $r_{min}$

$$r_{min} = 2(h^2/\lambda^2). \tag{35}$$

The two fibers are then coupled together at *C* to provide a comparison of the path lengths $l_1$ and $l_2$. If the length $L$ of the coupled fibers at *C* is long, then amplification of the phase difference produced by variations in $l_1 - l_2$ takes place and, as described previously, digital readout can be achieved at *D*.

### *D. Comparison with Existing Strain Gauges*

The proposed instruments have several unique features which prevent a meaningful comparison with available strain gauges. Existing devices as a rule measure the strain between a pair of points. For example, the Benioff strain seismometer measures the relative motion of two piers, and a crystalline transducer measures the strain of two of its facets. The transverse strain gauge we have described measures the parallel displacement of two *lines* rather than the distance between *points*. For this reason, the two-fiber system is more comparable to an *array* of strain gauges. Therefore, while the theoretical strain sensitivity we have calculated is not competitive with the sensitivity of a first-class Benioff installation, its readings should have a lower noise level, inasmuch as we are reading parallel displacement averaged over a finite distance. To appreciate this point, consider the parallel *displacement* required to yield the figures in Tables I and II for a pair of fibers ten meters long and half a wavelength apart where $\lambda_0 = 400$ m$\mu$. If we assume that the system parameters are such that the second column in Table II is applicable, then we have a strain sensitivity of 13.7 $\times 10^{-2}$. In terms of *displacement*, this means that we should be able to resolve a motion of about 0.003 angstrom, a distance much smaller than the diameter of the hydrogen atom. Clearly any point-to-point displacement of this magnitude would be impossible to measure owing to quantum and thermal effects. However, there is no theoretical reason that limits the resolution of the average displacement of two lines. Indeed, the transverse displacement sensitivity of the fiber pair implies that the device might have other geological uses than a strain gauge. In a conversation, Dr. F. Press has suggested that its most immediate application might be as a digital displacement transducer to monitor the small air gap in a Benioff seismometer.

[7] S. E. Miller, "Directional control in light-wave guidance," *Bell Sys. Tech. J.*, vol. 43, pp. 1727–1739, July 1964.

## VI. Conclusions

In this study we have introduced several novel applications of fiber optics to the problem of optical seismometry. Although the particular configurations described may not prove to be competitive with existing instruments, the ideas incorporated in their operation may prove to have unexpected geophysical applications. Several features stand out and are worthy of emphasis. First is the method of achieving digital readout by using a beat phenomenon. This also has the advantage of operating the device in a balanced state, so that the effect of local perturbations are averaged out in the output stage. As a result, the noise level of the fiber optic strain gauge should be lower than current devices. The basic simplicity is another feature, and this would be reflected in a relatively modest instrument cost. In addition, the design is such that the device could operate in hostile environments owing to the inherent strength and corrosion resistance of glass fibers.

## Appendix
## The Three-Layer System

### *A. Analysis*

The addition of a third layer as indicated in Fig. 7 can provide an unambiguous three-stage output once we understand the characteristics of mode propagation in this system. The simplest way to describe the modes of the three-layer system is to consider them as linear combinations of the modes $M_s^e$, $M_s^o$ of the two-layer system which are *partial* modes of the three-layer configuration. Let us designate the $y$-variation of the system modes as $\mathfrak{M}_s(y)$. The possible system modes $\mathfrak{M}_s(y)$ can be thought of as perturbed linear combinations of the two-layer modes $M_s^e$ and $M_s^o$. The equidistant configuration sketched in Fig. 7 possesses a plane of symmetry about the central layer, hence, the $\mathfrak{M}$-modes will be even and odd combinations of $M_s^e$ and $M_s^o$. The partial mode $M_s^e$ can be combined in two ways to form an $\mathfrak{M}$-mode, one even and the other odd, viz.

$$\begin{cases} \mathfrak{M}_N^{ee}(y) = \frac{1}{2}\{M_N^e[y - \frac{1}{2}(d+h)] \\ \qquad + M_N^e[y + \frac{1}{2}(d+h)]\} \\ \mathfrak{M}_N^{oo}(y) = \frac{1}{2}\{M_N^e[y - \frac{1}{2}(d+h)] \\ \qquad - M_N^e[y + \frac{1}{2}(d+h)]\} \end{cases} \tag{36}$$

and likewise, $M_N^o$ can be arranged in two ways,

$$\begin{cases} \mathfrak{M}_N^{eo} = \frac{1}{2}\{M_N^o[y - \frac{1}{2}(d+h)] \\ \qquad + M_N^o[y - \frac{1}{2}(d+h)] \\ \mathfrak{M}_N^{oe} = \frac{1}{2}\{M_N^o[y - \frac{1}{2}(d+h)] \\ \qquad - M_N^o[y - \frac{1}{2}(d+h)] \end{cases} \tag{37}$$

We can rewrite these expressions in terms of the $y$-variation of the primary modes $m(y)$,

$$\begin{cases} \mathfrak{M}_N^{ee}(y) = \frac{1}{2}\{m_N[y - \frac{1}{2}(d+h)] + 2m_N(y) \\ \qquad + m_N[y + \frac{1}{2}(d+h)]\} \\ \mathfrak{M}_N^{eo}(y) = \mathfrak{M}_N^{oe}(y) = \frac{1}{2}\{m_N[y - \frac{1}{2}(d+h)] \\ \qquad - m_N[y + \frac{1}{2}(d+h)]\} \\ \mathfrak{M}_N^{oo}(y) = \frac{1}{2}\{m_N[y - \frac{1}{2}(d+h)] - 2m_N(y) \\ \qquad + m_N[y + \frac{1}{2}(d+h)]\} \end{cases} \tag{38}$$

Note that $\mathfrak{M}^{eo}$ and $\mathfrak{M}^{oe}$ are degenerate, that is $\mathfrak{M}^{eo} = \mathfrak{M}^{oe}$, or they represent the same state.

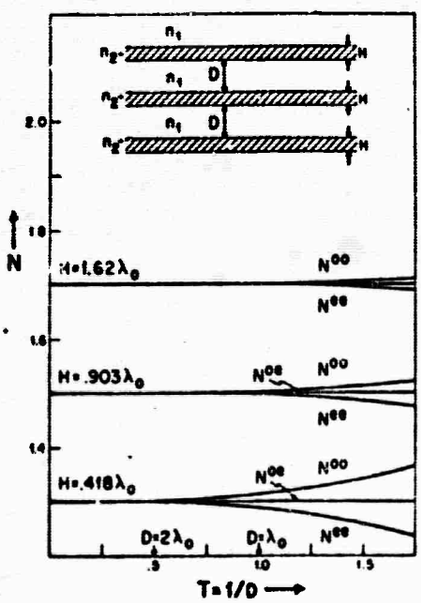


Fig. 7. The geometry of a three-layer device and values of $N^{ee}$, $N^{oo}$, and $N^{oe}$ as a function of $T=1/D$ for the case $n_1=n_3=1.2$, $n_2=2.0$.

### B. The Characteristic Numbers

The eigenvalue $N$ will be different for each of the modes $\mathfrak{M}_N^{ee}$, $\mathfrak{M}_N^{oo}$, $\mathfrak{M}_N^{eo}$, and we can designate these three values as $N^{ee}$, $N^{oo}$, and $N^{eo}$, respectively. Approximate characteristic equations describing these values are readily found by concentrating attention on the central layer. To the first-order, the three numbers $N^{ee}$, $N^{oo}$, and $N^{eo}$ represent the three ways by which the wall admittances $\Gamma_i$ of this layer can be perturbed. We can combine the possible perturbations to find the characteristic equations which describe the three-layer system

$$\tan\{[n_2^2 - (N^{ij})^2]^{1/2}k_0h\} = -\frac{[n_2^2 - (N^{ij})^2]^{1/2}[\Gamma_1^i(d) + \Gamma_1^j(d)]}{n_2^2 - (N^{ij})^2 - \Gamma_1^i(d)\cdot\Gamma_1^j(d)}\,TE. \tag{39}$$

In this expression, the superscripts $i, j$ index the possible states $i=e, o$ and $j=e, o$. It might seem invalid to calculate $N^{eo}$ from an argument involving the field in the central layer which presumably is null. However, we remind the reader that the field there will be relatively small and not null since $\mathfrak{M}^{eo}$ is comprised not of $m_N(y)$ modes, but rather of somewhat perturbed versions so that complete cancellation of field never takes place in the central layer. Even though the resulting field in the layer is very small, (39) can be used to find $N^{eo}$ since (39) depends only upon the logarithmic derivative of the field which is independent of amplitude considerations.

A feature of the point of view just introduced is that it allows us to readily estimate the values $N^{ee}(d)$, $N^{oo}(d)$, and $N^{eo}(d)$ in terms of the preceding analysis. The numbers $N^{ee}(d)$, $N^{oo}(d)$, $N^{eo}(d)$ correspond to a twofold perturbation of the wall admittances of the central layer. To first-order, the two perturbations are independent so that we can combine the $N^e(d)$ and $N^o(d)$ values of the two-layer system to obtain

$$\begin{aligned} N^{ee}(d) &\approx N_e + 2[N_e - N^e(d)] \\ N^{oo}(d) &\approx N_e + N^e(d) - N^o(d) \\ N^{eo}(d) &\approx N_e + 2[N^o(d) - N_e], \end{aligned} \tag{40}$$

which are estimates for $N^{ee}$, $N^{oo}$, and $N^{eo}$. In terms of this simple argument, we can plot the typical behavior of $N^{ee}$, $N^{oo}$, and $N^{eo}$ (cf. Fig. 7) and note that

$$N^{ee}(d) < N^{oo}(d) < N^{eo}(d). \tag{41}$$

### C. The Beat Phenomena

If we invert the set of (38), we find

$$\begin{aligned} m_N[y - \tfrac{1}{2}(d+h)] &= \mathfrak{M}_N^{ee}(y) + 2\mathfrak{M}_N^{eo}(y) + \mathfrak{M}_N^{oo}(y) \\ m_N(y) &= \mathfrak{M}_N^{ee}(y) - \mathfrak{M}_N^{oo}(y) \\ m_N[y + \tfrac{1}{2}(d+h)] &= \mathfrak{M}_N^{ee}(y) - 2\mathfrak{M}_N^{eo}(y) + \mathfrak{M}_N^{oo}(y). \end{aligned} \tag{42}$$

The significance of these equations is that they allow us to express illumination in any one layer as a linear combination of three-system modes. Since the $N$ values of these modes are distinct, the relative phases of the mode that are excited vary as a function of distance along the three-layer combination. Thus, if we illuminate only the top layer at the entrance the light will be transferred between the layers as the disturbance propagates down the line.

As an example, let us choose $n_1 = 1.2$, $n_2 = 2.0$, $H = 0.418\lambda_0$, and $D = \lambda_0$. From Table I and (40), we can use the values

$$N^{ee} = 1.286, \quad N^{eo} = 1.298, \quad N^{oo} = 1.312 \tag{43}$$

for the three-layer system. If we inject illumination only at the top layer at $x = 0$, the expression describing the propagation of the disturbance $\mathfrak{D}(x, y)$ is

$$\mathfrak{D}(x, y) = \mathfrak{M}_N{}^{ee}(y)e^{1.286ik_0x} + 2\mathfrak{M}_N{}^{eo}(y)e^{1.298ik_0x} + \mathfrak{M}_N{}^{oo}(y)e^{1.312ik_0x} \tag{44}$$

or

$$\begin{aligned} 4\mathfrak{D}(x, y) = {} & [e^{1.286ik_0x} + 2e^{1.298ik_0x} \\ & + e^{1.312ik_0x}]m_N(y - d) \\ & + [2e^{1.286ik_0x} - 2e^{1.312ik_0x}]m_N(y) \\ & + [e^{1.286ik_0x} - 2e^{1.298ik_0x} \\ & + e^{1.312ik_0x}]m_N(y + d). \end{aligned} \tag{45}$$

The beat phenomenon that now takes place is a good deal more complex. In Fig. 8 we plot the relative *intensity* of illumination in each layer as a function of distance $k_0x$ from zero to $1000\pi$ or 500 wavelengths. This interval returns the system to its original state apart from a sign change, and the cycling begins anew. Note the basic difficulty of the three-layer system which is the apparent aperiodicity. This results from $N^{ee}$, $N^{eo}$, and $N^{oo}$ having a rather large least-common divisor. For a useful instrument, it would be necessary to devise a three-layer configuration such that $N^{ee}$, $N^{eo}$, and $N^{oo}$ follow some elementary ratio like 4:5:6.

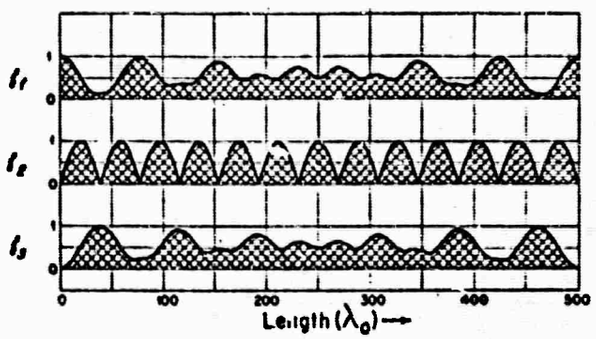


Fig. 8. The beat phenomenon in a system of three waveguides; $f_1$, $f_2$, and $f_3$ are proportional to the *intensity* of light if the excitation is in the top guide at $x = 0$.

*Geophys. J. R. astr. Soc.* (1966) 11, 149–163.

# Vector Wave Diffraction at Crustal Discontinuities I. Basic Theory, Rayleigh Waves at the Continental Margin

**Julius Kane***

*Summary*

In this report, the first of a series on the analytic continuation of wave functions past discontinuities, we introduce an elementary procedure for the solution of problems involving the diffraction of vector fields. In particular, the report discusses the propagation of Rayleigh waves incident obliquely upon the continental margin. The crustal layering on either side of the coastline is modelled mathematically as a two-part boundary layer in such a fashion that the relevant reflection and transmission coefficients emerge as elementary algebraic expressions. The procedure permitting such a solution to be found is to introduce a diffraction analogue of the well-known procedure in electrical engineering: replace a transmission line network by a lumped parameter equivalent in a specified frequency or wave number domain.

## 1. Introduction

From the point of view of a geophysicist, mathematical analysis cannot begin to acquire practical importance unless the solution is in such a form that the answers to his questions can be promptly given. Unfortunately, the class of elastic wave diffraction problems which have tractable solutions usually describes oversimplified geophysical structures. On the other hand, when the theoretician studies complex problems, too often he concentrates on the mathematical details of the solution so that his calculations are often more impressive than useful.

One powerful mathematical technique, the Wiener–Hopf method, has not had the application to geophysics that it should have. The difficulty in the application of this method is that it usually requires an involved transcendental kernel to be 'split' into suitable analytic factors. In my experience with problems of this type, it has been my observation that very often this prolix calculation is of more mathematical than physical interest (1, 2), and that usually the interesting parts of the solution depend in a very minor fashion with respect to this 'split' function. Indeed, the necessity for this function-theoretic decomposition can often be dropped as a requirement from the analysis, and used as the basis of an approximation procedure to solve problems beyond the scope of the Wiener–Hopf theory (3). Other investigators such as Koiter (4) and Carrier (5) have been aware of the relative unimportance of this complex factorization and have suggested the use of simpler substitute

* Present address: Space Science Center, University of California, Los Angeles, California, U.S.A. (on academic leave from the University of Rhode Island, Kingston, Rhode Island, U.S.A.).

kernels which can be factorized by inspection. While there is much merit in this approach, I feel that it is a poor philosophy to take the solution to an idealized problem and then approximate the answer. A preferable procedure is to formulate the problem in such a way that the mathematical difficulties are anticipated and avoided from the start. That is, a certain amount of intuition and insight into the nature of the problem can be used to guarantee that the subsequent analysis will lead to simple representations.

In the sequel, I should like to give an example of this philosophy by considering the propagation of oblique Rayleigh waves past a crustal discontinuity such as the land-sea boundary (Fig. 1). As a side condition, an elementary character for the solution will be required. Of course, there will be a need to make certain assumptions concerning the fields to be calculated. However, we shall be explicit about these modifications and indicate how arbitrary improvements can be made in the analysis if necessary.

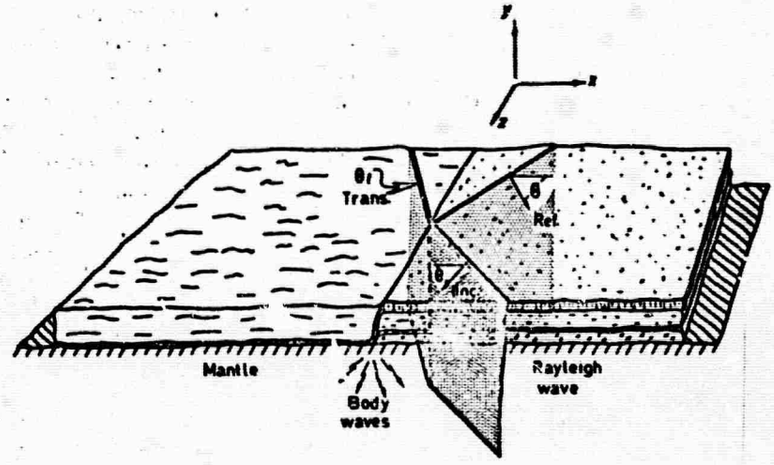


FIG. 1. A Rayleigh wave is incident obliquely upon the land–sea interface at an angle. The transmitted wave is refracted by an angle $t$. For purposes of illustration, the crustal thickness is greatly exaggerated and is considered to be a two-part boundary layer in the analysis.

A crucial phase in this study will be the need to formulate appropriate boundary conditions to characterize the crustal layering of the mantle. In the simpler problem of electromagnetic wave propagation, Leontovich (6) has introduced the notion of an 'impedance boundary condition' to model the physics at an interface. However, this idea while very useful does have its limitations. For one the solution to the associated boundary value problem is still rather complex, second the idea is valid only if the surface impedance is reasonably independent of the nature of the excitation. Although the impedance concept can be generalized to describe interfaces with more general properties (7–9), the intractable nature of the solution remains. A feature of the subsequent analysis will be a derivation of an approximate boundary condition for elastic wave diffraction whose merit is that its accuracy can be arbitrarily great without sacrificing simplicity in the form of the solution.

## 2. Basic equations

In the absence of body forces, small displacements $s(u, v, w)$ of an elastic solid characterized by the Lamé parameters $\lambda$, $\mu$, and density $\rho$ can be derived from a scalar potential $\Phi$ and a vector potential $\Psi(\Psi_1, 0, \Psi_3)$

$$\mathbf{s} = \operatorname{grad}\Phi + \operatorname{curl}\Psi(\Psi_1, 0, \Psi_3) \tag{1}$$

(Three components in the vector potential are redundant for we can express say $\Psi_2 = f(\Psi_1, \Psi_3)$ so that without any loss of generality we can set $\Psi_2 = 0$.) For monochromatic vibrations, we can suppress a time factor $e^{-i\omega t}$ and it can be shown that $\Phi$ and the components $\Psi_i$ satisfy the reduced wave equations

$$\begin{aligned}(\nabla^2 + k_c^2)\Phi &= 0, \qquad k_c^2 = \omega^2\rho/(\lambda+2\mu)\\ (\nabla^2 + k_s^2)\Psi_i &= 0, \qquad k_s^2 = \omega^2\rho/\mu.\end{aligned} \tag{2}$$

Simultaneously we should like a solution for the Rayleigh wave incident from either side of the crustal discontinuity. For this reason let $v_L$ and $v_R$ be the phase velocity of the Rayleigh wave on the left and right sides of the boundary, and let $k_L = \omega/v_L$, and $k_R = \omega/v_R$ designate the corresponding wave numbers. Also, $\Gamma_L$ and $\Gamma_R$ represent the required shear/compressional ratios for either side. In the notation of Fig. 1, the variation of the incident Rayleigh wave in the mantle will have the form (10)

$$\begin{cases}\Phi_{\text{inc}} = e^{-ik_R\xi + a\eta}\\ \Psi_{\text{inc}} = (\sin\Theta, 0, \cos\Theta)i\Gamma_R e^{-ik_R\xi + b\eta}\end{cases} \tag{3}$$

where

$$\xi = x\cos\Theta + z\sin\Theta, \tag{4}$$

$$a = (k_R^2 - k_c^2)^{\frac{1}{2}}, \qquad b = (k_R^2 - k_s^2)^{\frac{1}{2}}, \tag{5}$$

and for the special case of a free elastic half space the coefficient $\Gamma_R$ would be given by

$$\Gamma_R = \frac{[1-(v_R/v_c)^2]^{\frac{1}{2}}}{1-\frac{1}{2}(v_R/v_s)^2} \tag{6}$$

The $z$-variation of all fields will be of the form $e^{+ik_R z\sin\Theta}$, i.e.

$$\begin{aligned}\Phi(x, y, z) &= \varphi(x, y)e^{+ik_R z\sin\Theta}\\ \Psi_i(x, y, z) &= \psi_i(x, y)e^{+ik_R z\sin\Theta}, \qquad i = 1, 3\end{aligned} \tag{7}$$

so that $\varphi(x, y)$ and the $\psi_i(x, y)$ satisfy the reduced two-dimensional wave equations

$$\begin{aligned}\frac{\partial^2\varphi}{\partial x^2} + \frac{\partial^2\varphi}{\partial y^2} + p^2\varphi &= 0, \qquad p^2 = k_c^2 - k_R^2\sin^2\Theta,\\ \frac{\partial^2\psi_i}{\partial x^2} + \frac{\partial^2\psi_i}{\partial y^2} + q^2\psi_i &= 0, \qquad q^2 = k_s^2 - k_R^2\sin^2\Theta.\end{aligned} \tag{8}$$

Note that for angles of incidence such that $\sin\theta > v_R/v_s$ both $p^2$ and $q^2$ will be negative.

A completely general solution of equations (8) can be written down at once by separation of variables as

$$\varphi(x, y) = \frac{1}{2\pi i} \int_{\mathscr{C}} A(\alpha) \exp[i\alpha x - i(p^2 - \alpha^2)^{\frac{1}{2}} y]\, d\alpha$$

$$\psi_i(x, y) = \frac{1}{2\pi i} \int_{\mathscr{C}} B_i(\alpha) \exp[i\alpha x - i(q^2 - \alpha^2)^{\frac{1}{2}} y]\, d\alpha. \qquad i = 1, 3 \tag{9}$$

where $A(\alpha)$ and $B_i(\alpha)$ are kernels to be found, and the contour $\mathscr{C}$ follows the real axis except for the standard pole and branch point deformation (Fig. 2).

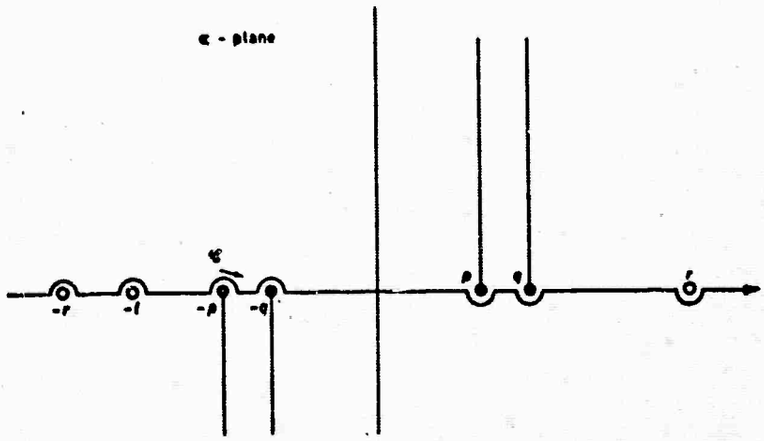


FIG. 2. The complex α-plane. The contour follows the real axis except for the indicated pole and branch point deformations. The pole at $l$ does not play any role in the analysis and is not shown.

## 3. The boundary conditions

Either the oceanic or the continental crustal structure can be considered to be a shallow transition layer that continues the field within the mantle to the free boundary at the Earth's surface. The details of the transition become more important for the shorter period Rayleigh waves. However, the group velocity dispersion curves for Rayleigh waves travelling oceanic or continental paths intersect at about 17 s. This implies that for waves of period greater than 10 s we can treat such a crustal structure as a two-part boundary layer whose coefficients have different values on the land and sea sides of the coastline. For this purpose, we need some way of relating the free surface conditions to the crust–mantle interface.

A. *Exact formulation.* At a free surface, the normal and tangential stresses must vanish or

$$\sigma_{yy} = \lambda\left(\frac{\partial^2 u}{\partial x^2} + \frac{\partial^2 v}{\partial y^2} + \frac{\partial^2 w}{\partial z^2}\right) + 2\mu\frac{\partial v}{\partial y} = 0,$$

$$\sigma_{xy} = \frac{\partial u}{\partial y} + \frac{\partial v}{\partial x} = 0, \tag{10}$$

$$\sigma_{yz} = \frac{\partial w}{\partial y} + \frac{\partial v}{\partial z} = 0,$$

which in terms of $\varphi$ and $\psi_i$ become

$$\sigma_{yy} = -\lambda k_c^2 \varphi + 2\mu\left[\frac{\partial^2\varphi}{\partial y^2} + ik_R \sin\Theta \frac{\partial\psi_1}{\partial y} - \frac{\partial^2\psi_3}{\partial x \partial y}\right] = 0$$

$$\sigma_{xy} = 2\frac{\partial^2\varphi}{\partial x \partial y} + ik_R \sin\Theta \frac{\partial\psi_1}{\partial x} + \frac{\partial^2\psi_3}{\partial y^2} - \frac{\partial^2\psi_3}{\partial x^2} = 0 \tag{11}$$

$$\sigma_{yz} = ik_R \sin\Theta\left[2\frac{\partial\varphi}{\partial y} + ik_R \sin\Theta\psi_1 - \frac{\partial\psi_3}{\partial x}\right] - \frac{\partial^2\psi_1}{\partial y^2} = 0.$$

By means of the Haskell–Thomson (11, 12) matrix method, these equations at the surface can be transformed to an equivalent set which refer the boundary conditions at the free surface to the crust–mantle interface. In this fashion the details of the crustal layering on either side of the boundary will be introduced into the analysis. However, the boundary conditions so obtained will be no simpler than the set (11), and in fact a good deal more complex. Although the programme we have just described would lead to a soluble Wiener–Hopf problem, the complexities of the analysis would render this procedure rather prolix for the information desired.

B. *The simplified formulation.* The important features of the exact formulation described in part A can be incorporated in a much simpler approach. The conditions we need are those that characterize the boundary layer in such a fashion that the geometric acoustics poles mirror the crustal layering correctly. We can assume that we know the dispersion relations for either side of the boundary, this is equivalent to making use of the Haskell–Thomson matrix analysis in an indirect fashion.

The dispersion relations define the $v_{R,L}$ and $\Gamma_{R,L}$ of a Rayleigh wave uniquely. If we refer to the explicit representation (3) we see that at any characteristic depth say $y = 0$ the Rayleigh wave will satisfy the set of equations

$$k_{R,L}\Gamma_{R,L}\Phi - \frac{\partial\Psi_1}{\partial z} - \frac{\partial\Psi_3}{\partial x} = 0$$

$$\frac{\partial\Phi}{\partial z} + \frac{k_{R,L}}{\Gamma_{R,L}}\Psi_1 = 0 \tag{12}$$

$$\frac{\partial\Phi}{\partial x} + \frac{k_{R,L}}{\Gamma_{R,L}}\Psi_3 = 0.$$

These equations are analogues of the telegrapher's equations in electromagnetic theory, and are used to describe the propagation characteristics of Rayleigh waves in a layered half space. They describe the surface loading of the mantle in an exact fashion for Rayleigh wave propagation. That is, they define the correct velocity $v_{R,L}$, and the shear/compressional ratio $\pm\Gamma_{R,L}$ together with its proper change of sign when the direction of propagation is reversed. The surface parameter $\Gamma_{R,L}$ is depth dependent and transforms according to the law

$$\Gamma_{R,L}|_{y=y_0} = \frac{\exp[(k_{R,L}^2 - k_c^2)^{\frac{1}{2}} y_0]}{\exp[(k_{R,L}^2 - k_0^2)^{\frac{1}{2}} y_0]}\Gamma_{R,L}|_{y=0}. \tag{13}$$

With this observation, the propagation of a Rayleigh wave past a step discontinuity can be described as a special case of the subsequent analysis if the step discontinuity is interpreted as a jump in $\Gamma$ according to the law (13), without any discontinuity in velocity (Fig. 3).


FIG. 3. An elastic solid with a small step discontinuity can be thought of as a half space with different values of $\Gamma$ on either side of the transition if the analysis is referred to the reference plane indicated.

Of course there are any number of other simplified boundary conditions equations that the Rayleigh wave will satisfy, but the equations in the set (12) have several important advantages.

(a) They are simple and uncomplicated.

(b) They are isotropic in that they do not depend upon the Rayleigh wave's direction of propagation in the $xz$-plane.

(c) They avoid the use of the transverse operator $\partial/\partial y$ which would have the effect of introducing radicals in the transform plane. This deliberate avoidance of the irrational factors will enormously simplify the subsequent function-theoretical analysis.

(d) They characterize the crustal layering in a direct fashion for they introduce parameters $v_{R,L}$ and $\Gamma_{R,L}$ defined by the relevant period equations.

(e) It can be shown that they imply conservation of energy. That is, the rays which are reflected from a boundary at which these synthetic conditions are imposed will have the same energy as the incident plane wave.

C. *Discussion.* For those familiar with electrical engineering practice, an analogy between formulations A and B may prove to be useful. In simplified terms, the Haskell matrix method is a vector analogue of transforming an impedance through a transmission line network where the details of the crustal structure characterize the network parameters. In symbolic terms, the exact formulation can be considered to be the shunt transmission line networks of Fig. 4a which loads a transmission line representation of the mantle. As is well known, the impedance characteristics of such networks are involved transcendental functions of frequency. Within any significant frequency interval however, a transmission line network can be replaced by an equivalent network consisting of lumped parameter elements. Such networks have much simpler impedance functions which are rational functions of the frequency. In diffraction problems, wave number plays a role analogous to frequency, and the substitute set of equations (12) can be considered to be the mathematical equivalent of a lumped circuit representation of the shunt transmission line networks (11) in a region of the wave number plane centred about the Rayleigh pole.

From a mathematical point of view, the nature of the solution to a Wiener–Hopf problem is that it analytically continues a wave function past a discontinuity. If two distinct but reasonably equivalent sets of boundary conditions are used to characterize each interface then the corresponding fields will also agree rather well.

Koiter's and Carrier's justification of the use of substitute kernels in the transform plane has the immediate corollary of validating the use of simplified boundary conditions to describe the physics, since the kernel is in effect the transform realization of the boundary condition operators. Our use of the set (12) as boundary conditions is however a preferable procedure for it is more direct and we can justify it on physical grounds by using the Haskell method backwards. That is, we can transform the conditions in (12) from the crust–mantle interface to the free surface.

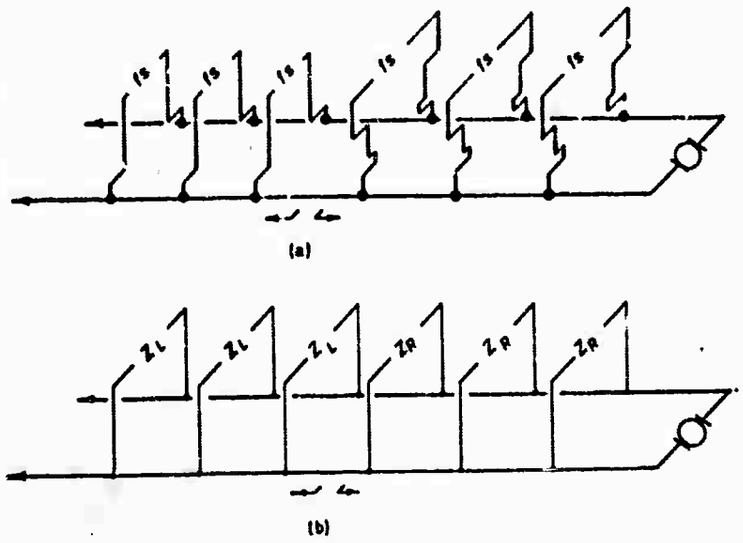


FIG. 4. (a) The crustal layering on either side of the land sea interface can be thought of as a continuous distribution of shunt transmission line networks on either side of the discontinuity if the exact Haskell–Thomson matrix formulation is used. (b) The simplified procedure is analogous to replacing the transmission line shunts by lumped parameter equivalents which have similar characteristics in the relevant region of the wave number plane.

Naturally, they will not imply that the surface stresses vanish except for Rayleigh waves. However, any incident ray whose wave number is close to the Rayleigh wave number will not induce appreciable stresses at the surface. Indeed, for $P$ or $SV$ waves striking the free surface at grazing angles of incidence, the equations in (12) describe the physics exactly. Essentially all the diffracted rays are tangential to the surface discontinuity and for waves of this type the stress mismatch at the surface will be small. In any event, more terms can be added to the simplified boundary conditions after the fashion of the analysis in (7, 8, 9) to get any desired degree of surface matching.

## 4. Solution

In terms of $\varphi(x, y)$ and $\psi_3(x, y)$ the synthetic boundary conditions (12) at the crust–mantle interface can be written

$$k_{R,L}\Gamma_{R,L}\varphi - iS\psi_3 - \frac{\partial\psi_3}{\partial x} = 0, \qquad y = 0 \tag{14}$$

$$iS\varphi + \frac{k_{R,L}}{\Gamma_{R,L}}\psi_1 = 0, \qquad y = 0 \tag{15}$$

$$\frac{\partial\varphi}{\partial x} + \frac{k_{R,L}}{\Gamma_{R,L}}\psi_3 = 0, \qquad y = 0 \tag{16}$$

where

$$S = +k_R \sin\Theta, \tag{17}$$

is a coefficient that always involves $k_R$ owing to the suppressed $z$-variation.

Let $\mathbf{R}(\alpha)$ denote the hermitian matrix $(r_{ij})$ where the coefficients $r_{ij}$ are identified as polynomial components of the realization of the differential operations (14–17) in the transform plane when $x$ is positive, viz.

$$\mathbf{R}(\alpha) = \begin{pmatrix} k_R\Gamma_R & -iS & -i\alpha \\ iS & k_R/\Gamma_R & 0 \\ i\alpha & 0 & k_R/\Gamma_R \end{pmatrix} \tag{18}$$

Likewise, let $\mathbf{L}(\alpha)$ be the matrix counterpart of (19) but with parameters $k_L$ and $\Gamma_L$ appropriate for the left boundary. The right matrix $\mathbf{R}$ is singular when

$$\alpha = \pm r = \pm k_R \cos\Theta, \tag{19}$$

and the left matrix $\mathbf{L}$ is singular when

$$\alpha = \pm l = \pm(k_L^2 - k_R^2 \sin^2\Theta)^{\frac{1}{2}}. \tag{20}$$

These points correspond to the geometric acoustics poles for the right and left boundaries respectively. The relationships (19) and (20) are seen to define the correct angles of refraction at the interface.

We introduce the unknown vector

$$\mathbf{x} = \begin{pmatrix} A(\alpha) \\ B_1(\alpha) \\ B_3(\alpha) \end{pmatrix} \tag{21}$$

and a constant vector $\mathbf{m}$ describing the mismatched components of the incident wave upon the left boundary

$$\mathbf{m} = \begin{pmatrix} m_1 \\ m_2 \\ m_3 \end{pmatrix}, \tag{22}$$

where

$$\begin{aligned} m_1 &= k_L\Gamma_L - k_R\Gamma_R \\ m_2 &= i(k_L\Gamma_R/\Gamma_L - k_R)\sin\Theta \\ m_3 &= i(k_L\Gamma_R/\Gamma_L - k_R)\cos\Theta \end{aligned} \tag{23}$$

A. *Function-theoretic method.* Vajnshtejn (13), Karp (14), and Clemmow (15) have introduced a rather general method for solving dual integral equations. The VKC procedure can be generalized to solve vector problems with either the exact or simplified boundary conditions.

A plus (or minus) superscript on a matrix or vector quantity will indicate that all of its components are analytic in the upper (or lower) $\alpha$-plane above (or below) the contour of integration $\mathcal{C}$. Unless otherwise specified, these quantities vanish uniformly at infinity in their relevant half-plane of regularity. By Jordan's lemma, the boundary condition on the right will be satisfied provided that

$$\mathbf{R}(\alpha)\mathbf{x} = \mathbf{f}^{+}(\alpha) \tag{24}$$

where $\mathbf{f}^{+}(\alpha)$ is unknown as yet. On the left boundary we need satisfy

$$\mathbf{L}(\alpha)\mathbf{x} + \frac{\mathbf{m}}{\alpha + r} = \mathbf{g}^{-}(\alpha). \tag{25}$$

The term $\mathbf{m}/(\alpha + k_R)$ represents a collection of poles whose residues contributions represent the driving effect of the incident Rayleigh wave upon the left boundary. In order to solve these equations, we substitute (24) into (25) and obtain

$$\mathbf{K}(\alpha)\mathbf{f}^{+}(\alpha) + \frac{\mathbf{m}}{\alpha + r} = \mathbf{g}^{-}(\alpha) \tag{26}$$

where the matrix to be 'split' is

$$\mathbf{K}(\alpha) = \mathbf{L}(\alpha)[\mathbf{R}(\alpha)]^{-1}. \tag{27}$$

For the simplified boundary conditions the entries in the matrix kernel $\mathbf{K}(\alpha)$ are seen to be rational functions of the transform variable $\alpha$ so that by elementary means we can split $\mathbf{K}(\alpha)$ as

$$\mathbf{K}(\alpha) = [\mathbf{N}^{-}(\alpha)]^{-1}\mathbf{P}^{+}(\alpha) \tag{28}$$

For the exact formulation, however, contour integration would be required to perform the factorization. In any event, the matrix factors $\mathbf{P}^{+}(\alpha)$ and $\mathbf{N}^{-}(\alpha)$ are regular in their respective half planes, however unlike the vectors $\mathbf{f}^{+}(\alpha)$ or $\mathbf{g}^{-}(\alpha)$ they do not vanish at infinity but approach a constant value.

If we add and subtract the same term, we can rearrange equation (26) into the form

$$\mathbf{P}^{+}(\alpha)\mathbf{f}^{+}(\alpha) + \frac{\mathbf{N}^{-}(-r)}{\alpha + r} = \mathbf{N}^{-}(\alpha)\mathbf{g}^{-}(\alpha) + \frac{1}{\alpha + r}[\mathbf{N}^{-}(-r) - \mathbf{N}^{-}(\alpha)]\mathbf{m}. \tag{29}$$

Each side of this equation is regular in a half plane and defines the analytic continuation of an entire function. Owing to the assumed growths of $\mathbf{f}^{+}(\alpha)$ and $\mathbf{g}^{-}(\alpha)$ this entire function vanishes uniformly at infinity and must thus be the null constant. Hence we can set each side of (29) to zero and obtain

$$\begin{aligned} \mathbf{f}^{+}(\alpha) &= -\frac{[\mathbf{P}^{+}(\alpha)]^{-1}\mathbf{N}^{-}(-r)\mathbf{m}}{\alpha + r} \\ \mathbf{g}^{-}(\alpha) &= -\frac{[\mathbf{N}^{-}(\alpha)]^{-1}}{\alpha + r}[\mathbf{N}^{-}(-r) - \mathbf{N}^{-}(\alpha)]\mathbf{m}. \end{aligned} \tag{30}$$

With the aid of the first of these expressions, the desired solution $\mathbf{x}$ is seen to be

$$\mathbf{x} = -\frac{[\mathbf{R}(\alpha)]^{-1}[\mathbf{P}^{+}(\alpha)]^{-1}\mathbf{N}^{-}(-r)\mathbf{m}}{\alpha + r}. \tag{31}$$

B. *Algebraic method.* For rational kernels the general procedure described in section A is rather abstruse and a more direct approach can yield the solution in a simple algebraic fashion; at the same time the transparency of the analysis will offer an insight into the mathematics that will suggest a generalization that can be used to solve more complex problems.

The matrices **L** and **R** are such that the only singularities we can have in the solution **x** are poles in the complex plane at $\alpha = \pm r, \pm l$. We know that the vector **x** must have entries which are rational functions of $\alpha$. The poles of **x** can only arise at $\alpha = \pm r$ (incident and reflected waves), and at $\alpha = -l$ (transmitted wave) for the residue wave at $\alpha = +l$ is a non-physical contribution. Hence, **x** must be inversely proportional to $(\alpha-r)(\alpha+r)(\alpha+l)$, and we can immediately concentrate attention on the numerators of its components. That is, **x** must be of the form

$$\mathbf{x} = \frac{1}{(\alpha-r)(\alpha+r)(\alpha+l)}\begin{pmatrix} a_1+a_2(\alpha-r) \\ i\Gamma_R \sin\Theta[a_1+a_3(\alpha-r)(\alpha-a_4/a_3)] \\ i\Gamma_R \cos\Theta[a_1+a_5(\alpha-r)] \end{pmatrix} \tag{32}$$

where the $a_i$ are five constants to be determined. The order of the polynomial entries in **x** is easily established if we anticipate that we need use Jordan's lemma after multiplication by either the operator **R** or **L**. The five unknown constants $a_i$ can and must be so chosen that all boundary conditions are obeyed. For $x$ positive, we need satisfy

$$\frac{1}{2\pi i}\int_{\Psi} \mathbf{R}\mathbf{x}e^{i\alpha x}\,d\alpha = 0, \qquad x > 0 \tag{33}$$

and the form of (32) is such that it automatically meets this constraint, since the only residue contribution in the upper half plane is a reflected Rayleigh wave.

For the boundary condition on the left side we need satisfy

$$\frac{1}{2\pi i}\int_{\Psi}\left(\mathbf{L}\mathbf{x}+\frac{\mathbf{m}}{\alpha+r}\right)e^{i\alpha x}\,d\alpha = 0, \qquad x < 0 \tag{34}$$

and by Jordan's lemma this requirement will be met if the residue coefficients at $\alpha = -r, -l$ are null. That is need satisfy

$$(\alpha+r)\mathbf{L}(-r)\mathbf{x}(-r)+\mathbf{m} = 0, \tag{35}$$

and

$$(\alpha+l)\mathbf{L}(-l)\mathbf{x}(-l) = 0. \tag{36}$$

Equation (36) is a homogeneous relation and can be satisfied by specifying two constants to make the residue contribution proportional to a transmitted Rayleigh wave that matches the left-hand conditions, viz.,

$$\begin{aligned} \Gamma_R \sin\Theta[a_1+a_3(l+r)(l+a_4/a_3)] &= -\Gamma_L \sin\Theta_t[a_1-a_2(l+r)] \\ -\Gamma_R \cos\Theta[a_1-a_5(l+r)] &= +\Gamma_L \cos\Theta_t[a_1-a_2(l+r)]. \end{aligned} \tag{37}$$

The three equations in (35) represent the left boundary's reaction that cancels the incident fields and together with the two in (37) we can determine the five constants

$a_i$ uniquely. A simple transformation will have the result of partitioning these equations into easily solvable forms. Let $b_i = \mathbf{T}_{ij}a_j$ where the matrix $\mathbf{T}_{ij}$ is

$$\mathbf{T}_{ij} = \begin{pmatrix} \Gamma_L & -2r\Gamma_L & 0 & 0 & 0 \\ \Gamma_R \sin\Theta & 0 & 2r^2\Gamma_R \sin\Theta & 2r\Gamma_R \sin\Theta & 0 \\ \Gamma_R \cos\Theta & 0 & 0 & 0 & -2r\Gamma_R \cos\Theta \\ \Gamma_L & -(l+r)\Gamma_L & 0 & 0 & 0 \\ \Gamma_R & 0 & i(l+r)\Gamma_R & (l+r)\Gamma_R & 0 \end{pmatrix} \tag{38}$$

In terms of the $b_i$'s, the equations (35) and (36) can be expressed by the matrix relation

$$\begin{pmatrix} k_L & -S & -r & 0 & 0 \\ -S & k_L & 0 & 0 & 0 \\ -r & 0 & k_L & 0 & 0 \\ 0 & 0 & 0 & \sin\Theta_t & -\sin\Theta \\ p_1 & 0 & p_2 & p_3 & 0 \end{pmatrix} \begin{pmatrix} b_1 \\ b_2 \\ b_3 \\ b_4 \\ b_5 \end{pmatrix} = 2r(l-r) \begin{pmatrix} c_1 \\ c_2 \sin\Theta \\ c_2 \cos\Theta \\ 0 \\ 0 \end{pmatrix} \tag{39}$$

where the parameters $p_1$, $p_2$, and $p_3$ are

$$\begin{aligned} p_1 &= -\frac{l+r}{2}\Gamma_R \cos\Theta, \\ p_2 &= -\frac{l+r}{2r}\Gamma_L, \\ p_3 &= \Gamma_L \cos\Theta_t + \Gamma_R \cos\Theta. \end{aligned} \tag{40}$$

The first three unknowns $b_1$, $b_2$, and $b_3$ are easily found to be

$$\begin{aligned} b_1 &= \Gamma_L, \\ b_2 &= 2r(l-r)\Gamma_R \sin\Theta, \\ b_3 &= \Gamma_R \cos\Theta \end{aligned} \tag{41}$$

and then from the last two equations in the matrix relation (39) we can calculate the remaining parameters

$$\begin{aligned} b_4 &= \frac{2\Gamma_R\Gamma_L \cos\Theta(l^2-r^2)}{\Gamma_R \cos\Theta + \Gamma_L \cos\Theta_t} \\ b_5 &= \frac{\sin\Theta_t}{\sin\Theta} b_4. \end{aligned} \tag{42}$$

The inverse transformation, $a_j = \mathbf{T}_{ij}^{-1}b_i$, determines the $a_i$'s. In particular, we shall require expressions for $a_1$ and $a_2$

$$\begin{aligned} a_1 &= 2r(l-r)\left[1 - \frac{2\Gamma_R \cos\Theta}{\Gamma_R \cos\Theta + \Gamma_L \cos\Theta_t}\right] \\ a_2 &= 2r - \frac{2(l+r)\Gamma_R \cos\Theta}{\Gamma_R \cos\Theta + \Gamma_L \cos\Theta_t} \end{aligned} \tag{43}$$

since these numbers are required to evaluate the residue coefficients $-a_1/[2r(l+r)]$, and $[a_1-a_2(l+r)]/[l^2-r^2]$ at the poles $\alpha = r$ and $-l$ respectively.

## 5. Discussion of the solution

The elementary character of the solution (31) or (36) permits a ready evaluation of the scattered fields. For $y = 0$ and $x$ positive the entire field is a collection of residue contributions which can be grouped into an incident Rayleigh wave, and a reflected Rayleigh wave with a relative amplitude

$$\mathscr{R} = \frac{\cos\Theta - (\Gamma_L/\Gamma_R)\sqrt{[1-(v_L/v_R)^2\sin^2\Theta]}}{\cos\Theta + (\Gamma_L/\Gamma_R)\sqrt{[1-(v_L/v_R)^2\sin^2\Theta]}}. \tag{44}$$

Our convention will be to describe the coefficient of the compressional potential of the Rayleigh wave as its amplitude. Although our solution includes scattered body waves, their contribution is null on the reference plane $y = 0$ owing to our formulation.

On the left side of the boundary, the incident Rayleigh wave is cancelled by pole contributions as it should. The remaining residue terms are seen to represent

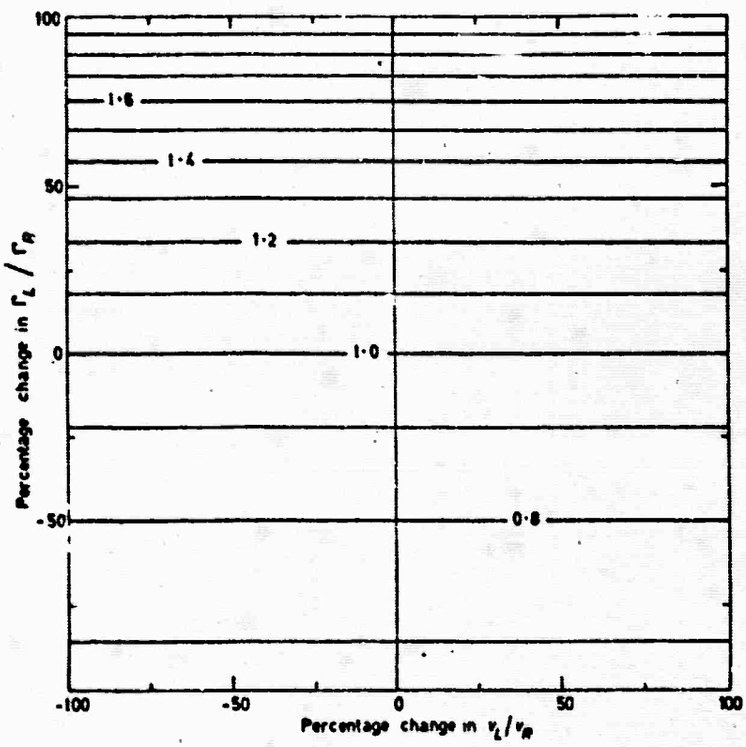


FIG. 5. Contours of constant values of the transmission coefficient $\mathscr{T}$ for an incident Rayleigh wave at normal incidence ($\Theta = 0$) upon crustal discontinuity. For this special case there is no variation of $\mathscr{T}$ with respect to the velocity contrast.

a transmitted Rayleigh wave of amplitude

$$\mathcal{T} = 1 + \mathcal{R} = \frac{2\cos\Theta}{\cos\Theta + (\Gamma_L/\Gamma_R)\sqrt{[1-(v_L/v_R)^2\sin^2\Theta]}}. \tag{45}$$

This wave travels in a direction $\Theta_t$ which is given by

$$\sin\Theta_t = \frac{v_L}{v_R}\sin\Theta, \tag{46}$$

a familiar expression for the refraction of a ray at an interface. In general both phase velocities $v_L$ and $v_R$ depend upon frequency, and as a consequence, the angle $\Theta_t$ is frequency dependent. Thus the diffraction of a Rayleigh pulse incident obliquely upon a crustal interface will sort the transmitted spectral components into different directions after the fashion of an optical prism. In addition, if $\Theta$ exceeds a critical angle $\Theta_c$

$$\Theta_c = \sin^{-1}(v_R/v_L) \tag{47}$$

then total reflection takes place. Just as in optics or acoustics, this can only happen if the wave is incident from a slow to a fast medium. Finally, we note that if

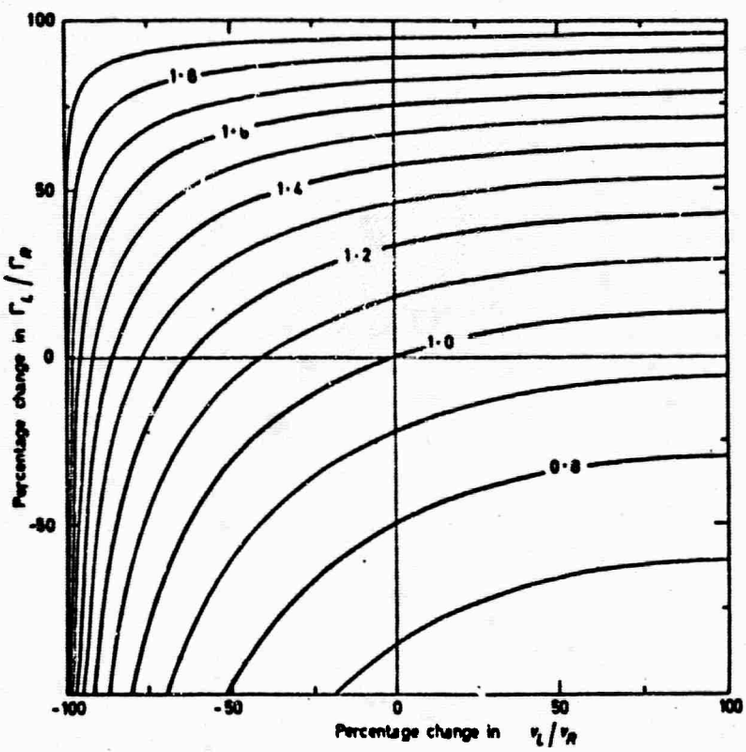


FIG. 6. Contours of constant values of the transmission coefficient $\mathcal{T}$ for an incident Rayleigh wave at oblique incidence ($\Theta = 30°$) upon a crustal discontinuity.

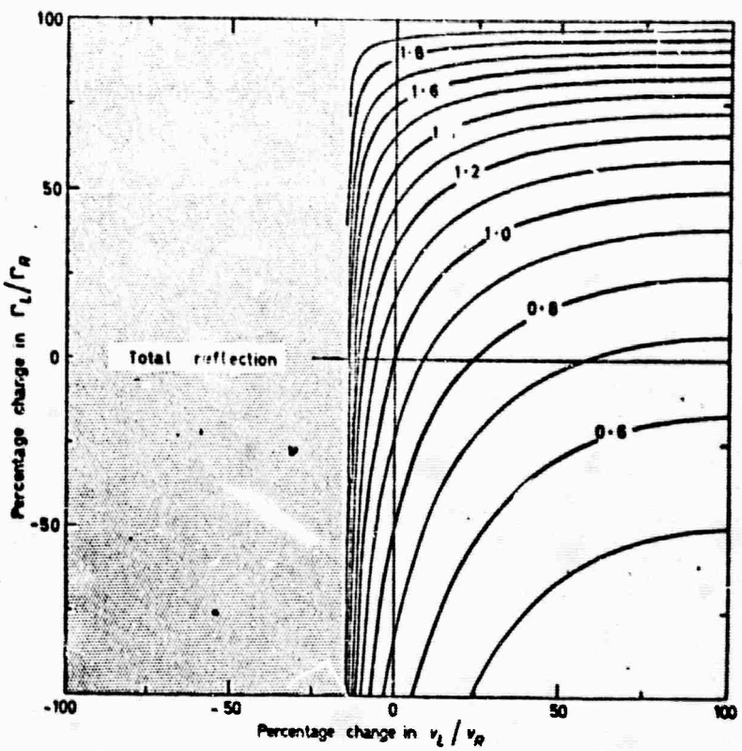


FIG. 7. Contours of constant values of the transmission coefficient $\mathscr{T}$ for an incident Rayleigh wave at oblique incidence ($\Theta = 60°$) upon a crustal discontinuity. Note that total reflection takes place if $v_R/v_L$ exceeds $2/\sqrt{3}$.

$v_L/v_R = 1$, then there is no angular variation in $\mathscr{R}$ and $\mathscr{T}$ for a discontinuity in $\Gamma$. Figs. 5–7 illustrate the variation of the transmission coefficient as a function of the relative discontinuities in the Rayleigh wave parameters for fixed angle of incidence.

*California Institute of Technology,*
*Pasadena, California, U.S.A.*

1965 *June.*

## References

1a. Kane, J., 1960. The efficiency of launching surface waves on a reactive half plane by an arbitrary antenna, *I.R.E. Trans. Antennas Propag.*, Vol. Ap-8, No. 5, pp. 500–507.

1b. Kane, J., 1963. The mathematical theory of a class of surface wave antennas, *Q. appl. Math.*, 21, 199.

2. Kane, J., 1962. The propagation of Rayleigh waves past a fluid-loaded boundary, *J. Math. Phys.*, 41, 179.

3. Kane, J. & Spence, J., 1963. Rayleigh wave transmission on elastic wedges, *Geophysics*, 28, 715.

4. Koiter, W. T., 1954. Approximate solution of Wiener–Hopf type integral equations with applications, *Proc. K. ned. Akad. Wet.*, B, 57, 5.

5. Carrier, G. F., 1965. Analytic approximation techniques in applied mathematics, *J. Soc. ind. appl. Math.*, **13**, 68.
6. Leontovich, M. A., 1944. A method for the solution of the problem of the propagation of electromagnetic waves along the surface of the Earth, *Izv. Akad. Nauk SSSR, Ser. Fiz*, **8**, 16.
7. Kane, J. & Karp, S. N., 1960. An accurate boundary condition to replace transition condition at dielectric-dielectric interfaces, *Res. Rep.*, EM-153. Institute of Mathematical Science, Div. E. M. Research, New York University.
8. Kane, J. & Karp, S. N., 1960. Radio progration past a pair of dielectric interfaces, *Res. Rep.*, EM-154. Institute of Mathematical Science, Div. E. M. Research, New York University.
9. Kane, J. & Karp, S. N., 1964. A simplified theory of diffraction at an interface separating two dielectrics, *J. Res. natn. Bur. Stand.*, D, **68**, 305.
10. Kane, J. & Spence, J., 1965. The theory of surface wave diffraction by symmetrical discontinuities, *Geophys. J. R. astr. Soc.*, **9**, 423.
11. Haskell, N. A., 1953. The dispersion of surface waves on multilayered media, *Bull. seism. Soc. Am.*, **43**, 17.
12. Thomson, W. T., 1950. Transmission of elastic waves through a stratified solid medium, *J. appl. Phys.*, **21**, 89.
13. Vajnshtejn, L. A., 1948. Rigorous solution of the problem of an open-ended parallel-plate waveguide, *Izv. Akad. Nauk. SSSR, Ser. Fiz.*, **12**, 144.
    Vajnshtejn, L. A., 1948. On the theory of diffraction by two parallel half-planes, *Izv. Akad. Nauk. SSSR, Ser. Fiz.*, **12**, 166.
    Vajnshtejn, L. A., 1949. The theory of sound waves in open tubes, *Zh. tech. Fiz.* **18**, 1543.
    Vajnshtejn, L. A., 1950. Radiation of asymmetric electromagnetic waves from the open end of a circular waveguide, *Dokl. Akad. Nauk SSSR*, **74**, 485.
    Vajnshtejn, L. A., 1950. Diffraction at the open end of a circularly cylindrical waveguide whose diameter is much greater than wavelength, *Dokl. Akad. Nauk SSSR*, **74**, 909.
14. Karp, S. N., 1950. Wiener–Hopf techniques and mixed boundary value problems, *Communs pure appl. Math.*, **3**, 411.
15. Clemmow, P. C., 1953. Radio propagation over a flat Earth across a boundary separating two different media, *Phil. Trans. R. Soc.*, A, **246**, 1.

APPENDIX G

Bulletin of the Seismological Society of America. Vol. 56, No. 4, pp. 841–859. August, 1966

# TELESEISMIC RESPONSE OF A UNIFORM DIPPING CRUST

## (PART I OF A SERIES ON CRUSTAL EQUALIZATION OF SEISMIC ARRAYS)

By Julius Kane*

ABSTRACT

Most seismic theory is confined to a consideration of crustal structures that can be abstracted as plane parallel elastic layers. For such configurations, the response of each element of a seismic array will be similar to any other except for a time delay. Signal enhancement of an array located on such an idealized structure can be accomplished by suitable time delays of the individual traces followed by superposition.

On the other hand, if the crustal structure is anything but a plane parallel configuration, the signals received by the individual elements will not be identical to one another, but will include distortion effects characteristic of the local geometry. As a result, the records of seismic arrays located on realistic crustal configurations will have to be equalized to some standard reference if optimum signal processing is to be achieved.

In this paper we introduce a ray procedure for the calculation of theoretical seismograms for the teleseismic response of an array of stations located above a uniform dipping crust (wedge-shaped). In terms of this mathematical model, we demonstrate the signal distortion effects of the geometry and discuss equalization techniques that will permit a superior recovery of the desired signal.

## Introduction

The outcome of any experiment is subject to random errors, and one way of reducing uncertainty is to repeat the measurement many times. Before the results of the individual measurements are averaged there is one *caveat*: one must be sure that the *same* experiment has been performed. In seismology, the need for enhancing low level signals relative to background noise is acute, and for this reason elaborate arrays are being constructed to monitor teleseisms. Owing to various reasons it is not possible to position the site of each station or element in the array on terrain identical to that of its neighbors. As a result, each element will respond to the same signal in a perturbed fashion characteristic of the local crustal structure. This principle is of course well known, and a study of the signal variations across an array of closely spaced stations for ground shots is one way of mapping subterranean strata. In source mechanism studies of seismic sources, the situation is somewhat different from the field mapping environment. The vibrations can be considered to be that of a plane wave, the signal arrives from below rather than above, and the spacing of stations is comparatively wide as compared to those used in field surveys. Nonetheless, for a varying crustal structure, the response of any element will be distorted by terrain effects so that each station's signal should be equalized to some

* Present address: Space Science Center, University of California, Los Angeles, California.

standard reference before processing to reduce noise effects. Several questions are pertinent: how severe might this effect be for realistic crustal configurations, and if the effect is important, how can the signals be processed so as to remove the effects of local geometry? In this paper we consider this first question by determining the

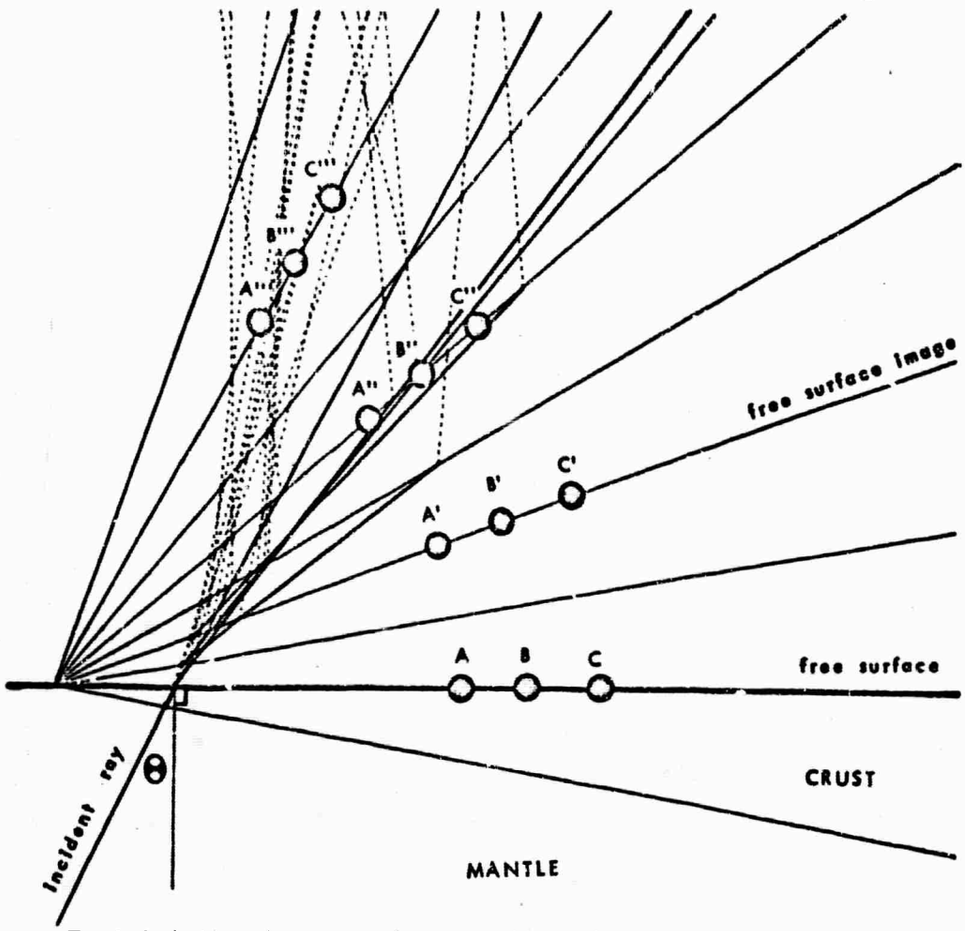


FIG. 1. An incident plane wave arrives at a positive angle Θ measured with respect to the normal to the free surface, and illuminates a crustal wedge. An array of stations $A$, $B$, $C$, are located on the free surface; their images are shown at $A'$, $A''$, $A'''$, etc. The ray paths for the velocity variation given in Table 1 are shown; the $P$-paths are drawn as full lines, and the $S$-paths as dashed lines. Any ray which will fail to intercept another image plane is not drawn.

theoretical seismograms that an array of stations might receive if located on a dipping crustal structure. The advantage of this particular choice of geometry is that it allows a rigorous calculation of the dominant portion of the seismograms for any assumed variation of the incident wave.

In addition to the theoretical significance of the present study, the analysis has practical importance for preliminary analysis at the Caltech Seismological Lab-

oratory (Niazi, 1965) and the U.S. Geological Survey (Roller *et al*, 1964) indicates that the Tonto Forest array is located on a dipping crustal structure with a dip of approximately 8° and an estimated strike of N 17°W.

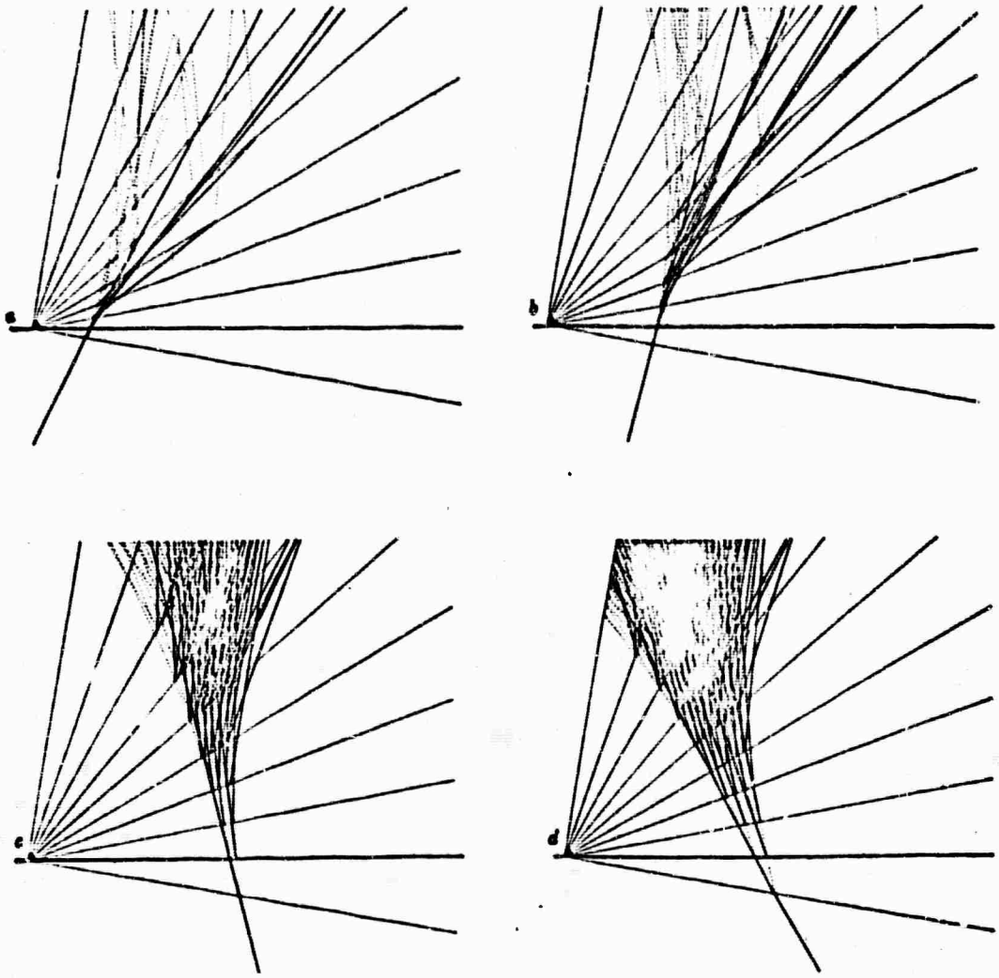


FIG. 2. A sampling of tree diagrams for an incident wave upon a crustal wedge of ten degrees. The angles of incidence are respectively −30°, −10°, +10°, +30° for *a*, *b*, c, and *d*.

## FORMULATION

We consider an array of stations indicated by *A*, *B*, and *C* located on a dipping crustal structure (Figure 1). An incident *P*- or *S*-wave arrives at an arbitrary angle of incidence and illuminates the configuration. Our task is to determine the subsequent ground motion for a given time variation in the incoming wave.

The task posed is an intractable boundary value problem if the entire solution is

to be found. However, the field can be separated into the sum of two components: a multiply reflected field, and an involved cylindrically scattered field re-radiating from a virtual source at the vertex. Fortunately, it can be shown that this complicated diffraction field does not contribute significantly to the ground motion for several reasons. First, the major lobe of this cylindrical field is directed downward away from the stations where it smooths the abrupt transition between the different reflected fields from either boundary. Second, it will be shown that the vertex intercepts only an infinitesimal fraction of the rays that enter the crustal wedge. Indeed, a realistic crustal configuration may not have a vertex since the actual crustal structure may be wedge shaped only in the immediate vicinity of the array. Third, the cylindrical field decays with distance so its amplitude falls off rapidly, and its contribution at the stations will be negligible since we shall assume that they are relatively distant from the discontinuity. For these reasons we shall neglect this cylindrical field, for while its determination would be an interesting (and difficult) mathematical task, this effort would be of limited geophysical interest.

In the time domain, the seismograms can be determined by following the paths of the multiply reflected and refracted rays within the wedge. Unlike the case of a plane parallel layer, the ray tracing procedure can be very tedious unless it is done properly. A very convenient procedure is to reflect the wedge rather than the rays as indicated in Figure 1. In this diagram the stations are multiply imaged at $A'$, $B'$, $C'$, $\cdots$ $A''$, $B''$, $C''$, $\cdots$ $A'''$, $B'''$, $C'''$, $\cdots$ etc. In this diagram the path of a multiply reflected $P$- or $S$-wave is simply drawn as a straight line, since the angle of incidence equals the angle of reflection. However, the paths of rays following $P/S$ or $S/P$ conversions are complex broken lines. To compute the seismogram we consider each station and all its images as one and combine the outputs of each imaged station on one seismogram following the laws of vector addition.

The tree diagram has several advantages. For one thing, it clearly shows that *any ray that enters the crustal wedge other than at the origin will avoid the vertex and eventually migrate to infinity*. Thus the edge intercepts only an infinitesimal fraction of the energy. Another advantage of this presentation is that it shows that the path of any ray has a counterclockwise drift and it will cycle from one layer to the next in a repetitive fashion. This means that all the calculations can easily be done in the computer by reiterating a two-stage computer loop, which describes the two reflecting surfaces. An additional advantage of the tree diagram is that it permits visual interpretation of a vast amount of computer output which greatly assists the computer debugging operation. In Figure 2 we give examples of computer-drawn[1] tree diagrams for a selection of various angles of incidence upon a crustal wedge.

In all our illustrations, we have chosen the parameters in Table 1 for calculation of the reflection coefficients. The values used are proportional to the values shown.

With proper interpretation the program used to generate the tree diagram contains sufficient information to construct a theoretical seismogram for a station *arbitrarily*

[1] Our data is coded on magnetic tape by an IBM 7090, and then transcribed into visual output by the Stromberg Carlson 4020 which automatically drives and photographs the face of a special Charectron® oscilloscope tube.

TABLE 1

ADOPTED VELOCITIES AND DENSITIES

| | $v_p$ | $v_s$ | $\rho$ |
|---|---|---|---|
| Air | 0.335 | 0.000 | 0.001 |
| Crust | 2.826 | 1.632 | 3.000 |
| Mantle | 3.000 | 1.732 | 4.000 |

located on the wedge surface. The diagram is drawn by the computer with the assumption that the incident ray strikes the lower wedge surface at any point say unit distance from the vertex. This point locates the trunk of the tree, and the branches spread out according to the laws of reflection and refraction. Each branch that intersects one of the image planes carries with it nine pieces of data which combine to form a vector $E(e_1, e_2, \cdots e_9)$ called an *event*. Each event represents an incident plane wave striking one of the wedge surfaces together with two reflected rays. The components of this nine-dimensional vector are identified as follows:

(*1*) *Bounce number.* The first coordinate $e_1$ will be referred to as the bounce number. The magnitude of the bounce number $e_1$ locates the image plane, and its parity designates whether the event corresponds to an incident shear (negative), or compressional (positive) ray. The bounce number has any value $\pm\frac{1}{2}n$ where $n$ is any integer other than zero. At the lowest surface, the crust-mantle interface, the bounce number $e_1$ has the value $+\frac{1}{2}$ if the excitation is a compressional wave. An integral bounce number indicates that the ray is incident upon the free surface and the associated event will contribute to the theoretical seismogram; otherwise the ray is incident upon the elastic interface and will not contribute to the response until another reflection takes place.

(*2*) *Travel time.* The second coordinate $e_2$ is the travel time required for the ray to reach the relevant image plane from the root of the tree. At the base of the diagram we set $e_2 = 0$, and the travel time will accumulate arithmetically from this origin as the ray progress from bounce level to bounce level.

(*3*) *Radial distance.* The third coordinate $e_3$ is the radial distance from the wedge vertex to the ray intersection at each bounce level.

(*4*) *Incident magnitude.* The fourth coordinate $e_4$ is the relative magnitude of the incident ray as it strikes the image plane indexed by $e_1$. At the root of the tree we shall normalize $e_4 = 1$, and this coordinate will progress geometrically from level to level in response to a factor proportional to the appropriate reflection coefficient. For convenience, and greater realism, the reflection coefficient used at the earth's surface was not that appropriate to the free surface of an elastic solid, but rather that for a solid-fluid interface wherein the elastic parameters for air are used.

(*5*) *Sine of the angle of incidence.* The fifth coordinate $e_5 = \sin\vartheta$ where $\vartheta$ is the angle of incidence of the incident ray. It is preferable to use the sine of $\vartheta$ rather than $\vartheta$ itself as a variable for the laws of reflection and refraction depend algebraically upon $e_5 = \sin\vartheta$ and in a transcendental fashion upon $\vartheta$. By use of this variable, we obtain the advantage of markedly accelerating the computer program for the time-consuming trigonometric subroutines need never be used in the iterative loops.

(These angles are measured with respect to the vertical erected at the current image level.)

(6) *Reflected P-magnitude.* The sixth coordinate $e_6$ is the magnitude of the reflected compressional ray. In calculating $e_6$ we have to use one of four reflection coefficients depending upon the parity of the incident ray, and whether the reflection takes place at a free or an elastic interface. These four reflection coefficients are designated as

$$RF_{pp}(e_5), \quad RF_{sp}(e_5), \quad RI_{pp}(e_5), \quad RI_{sp}(e_5),$$

wherein the second letter indicates whether the reflection takes place at solid-fluid interface ($RF$), or at a solid-solid interface ($RI$), the subscript $sp$ for example indicates that the reflection is *from* an incident shear wave *to* a reflected compressional wave.

(7) *Sine of the angle of the reflected P-wave.* The coordinate $e_7$ is the sine of the reflected $P$-wave as computed by Snell's law,
and has a sign opposite to the opposite sign to the incident wave.

(8) *Reflected S-magnitude.* The eighth coordinate $e_8$ is the magnitude of the reflected shear ray and requires the proper use of one of four expressions for its calculation; these are written in an obvious notation as

$$RF_{ss}(e_5), \quad RF_{ps}(e_5), \quad RI_{ss}(e_5), \quad RI_{ps}(e_5)$$

(9) *Sine of the angle of the reflected S-wave.* The last coordinate $e_9$ is the sine of the reflected $S$-wave as computed by Snell's law, and has the opposite sign to the incident wave.

The calculation of the tree diagram proceeds in a very simple and straight-forward manner once the geometry, elastic parameters, and excitation are specified. Typically, the excitation will be chosen as a $P$-wave incident from below the wedge, and the time variation of the stress along the incident ray will be assumed to be given. Let $A$ be the relative amplitude of this ray. Upon striking the elastic wedge, two rays will penetrate the crustal structure, and we have the following initial vector $E^0(e_1^0, e_2^0, \cdots e_9^0)$ to start the iteration scheme wherein

$$\begin{aligned}
e_1^0 &= +\tfrac{1}{2}, & e_2^0 &= 0, \\
e_3^0 &= 1, & e_4^0 &= A, \\
e_5^0 &= \sin(\Theta - \alpha), & e_6^0 &= AT_{pp}[\sin(\Theta - \alpha)], \\
e_7^0 &= \frac{v_p}{v_p'} \sin(\Theta - \alpha), & e_8^0 &= AT_{ps}[\sin(\Theta - \alpha)], \\
e_9^0 &= \frac{v_s}{v_p'} \sin(\Theta - \alpha).
\end{aligned} \tag{1}$$

In these expressions, $\Theta$ is the angle of incidence of the wave measured with respect to a vertical on the free surface (Figure 1), and is the wedge angle, and $v_s'$ and $v_p'$

are the velocities of the shear and compressional waves in the mantle. Within the crustal wedge, the excitation is split into two rays with particle amplitudes proportional to $T_{pp}$ and $T_{ps}$, the transmission coefficients for a plane wave incident upon an elastic interface. This initial vector is used to start the iteration scheme. The logic behind the computational process is easily described in two steps.

*Step 1.* At any image level suppose all the events have been calculated. Every event is placed in temporary storage, and in addition if $e_1$ is an integer, then the corresponding event is placed either in permanent storage or written on tape. In particular (1) would be the only event for the lowest level. In general, if $e_1 = \frac{1}{2}n$, then there will be a maximum of $2^{n-1}$ events to be calculated at that level. In practice, this number will be substantially less for we shall discard any incident ray unless its relative magnitude exceeds some threshold value.

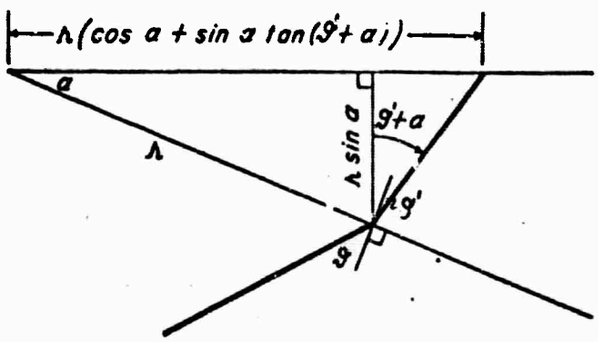


FIG. 3. The geometry behind the iteration scheme.

*Step 2.* Once all the events appropriate to an image level have been calculated and stored, then we use each event in temporary storage to calculate a new pair of events for the next image plane. The calculations at this stage are essentially repetitions of one basic series of algebraic operations. Let $E^i(e_1^i, e_2^i, \cdots e_n^i)$ be a typical event in temporary storage. The two new vectors to be generated can be denoted as $E^p$ and $E^s$ since they correspond to the reflected $P$- and $SV$-waves. The components of these new vectors will be algebraic functions of the preceding coordinates.

Let us introduce the abbreviations for the constants

$$C = \cos\alpha, \qquad S = \sin\alpha, \tag{2}$$

and designate the radial distances $r_p$ and $r_s$ shown in Figure 3 simply as $r$

$$\begin{aligned} r_p &= e_2^i\left[C + S\,\frac{Ce_3^i + S\sqrt{1-(e_3^i)^2}}{C\sqrt{1-(e_3^i)^2} - Se_3^i}\right], \\ r_s &= e_2^i\left[C + S\,\frac{Ce_3^i + S\sqrt{1-(e_3^i)^2}}{C\sqrt{1-(e_3^i)^2} - Se_3^i}\right], \end{aligned} \tag{3}$$

and let

$$d_p^2 = r_p^2 + (e_3')^2 - 2r_p e_3' C,$$
$$d_s^2 = r_s^2 + (e_3')^2 - 2r_s e_3' C, \tag{4}$$

then according to the laws of reflection and refraction we can write

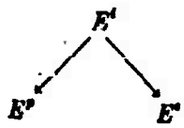


| | |
|---|---|
| $e_1^p = \lvert e_1' \rvert + \frac{1}{2}$ | $e_1^s = -\lvert e_1' \rvert - \frac{1}{2}$ |
| $e_2^p = d_p/v_p + e_2'$ | $e_2^s = d_s/v_s + e_2'$ |
| $e_3^p = r_p$ | $e_3^s = r_s$ |
| $e_4^p = e_3'$ | $e_4^s = e_3'$ |
| $e_5^p = Ce_1' + S\sqrt{1-(e_1')^2}$ | $e_5^s = Ce_1' + S\sqrt{1-(e_1')^2}$ |
| $e_6^p = e_4^p RI_{pp}(e_5^p)$, if $e_1^p$ = positive integer; $e_4^p RF_{pp}(e_5^p)$, if $e_1^p$ = negative integer; | $e_6^s = e_4^s RI_{sp}(e_5^s)$, if $e_1^s$ = positive integer; $e_4^s RF_{sp}(e_5^s)$, if $e_1^s$ = negative integer; |
| $e_7^p = e_6^p$ | $e_7^s = \frac{v_p}{v_s} e_6^s$ |
| $e_8^p = e_4^p RI_{ps}(e_5^p)$, if $e_1^p$ = positive integer; $e_4^p RF_{ps}(e_5^p)$, if $e_1^p$ = negative integer; | $e_8^s = e_4^s RI_{ss}(e_5^s)$, if $e_1^s$ = positive integer; $e_4^s RF_{ss}(e_5^s)$, if $e_1^s$ = negative integer; |
| $e_9^p = \frac{v_s}{v_p} e_8^p$, | $e_9^s = e^s$. |

(5)

Each event from the preceding bounce level is used to generate two vectors in this

fashion until the data is depleted. Once the events in temporary storage are depleted we cycle back to stage 1.

## The Theoretical Seismogram

A. *Preliminaries.* In the fashion just described, we can accumulate a reservoir of events for any desired configuration of system parameters. However, these vectors have little value until they are converted into a theoretical seismogram. In the conversion process a great deal of simplification is introduced if we remind ourselves that *the geometry of the wedge problem is such that it is specified completely by angles, and that it incorporates no fundamental unit of length.* This fortunate circumstance

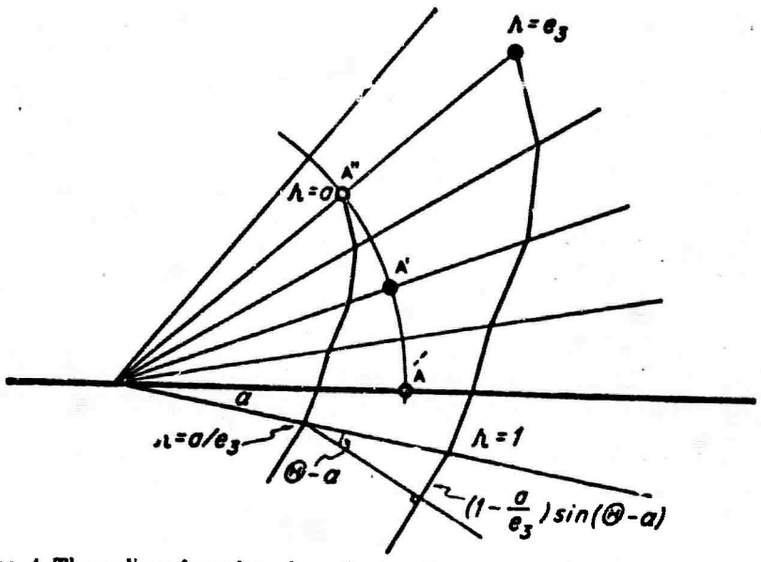


FIG. 4. The scaling of any branch on the tree diagram proceeds by similar triangles, and a causal correction gives the arrival time of any event at any station.

will permit us to use the scaling of similar triangles to normalize each event to the location of any station.

We have calculated the tree diagram with its base at $r = 1$, and let the branches of the tree fall where they may. Suppose we have a station $A$ at $r = a$, then we need to know the travel times when the events reach $r = a$ at the free surface or one of its images. In general, we need alter the travel time $e_2$ and radial distance $e_3$ so that the event is properly normalized to give the correct contribution at any station. By similar triangles (Figure 4), we see that

$$T_a = \frac{a \cdot e_2}{e_3} - \frac{(1 - a/e_3) \sin (\Theta - \alpha)}{v_p'} \qquad (6)$$

is the corrected travel time for the initial occurrence of the event at station $A$. The second term in this expression represents a causal correction for the excitation

wave arrives at different parts of the base of the crustal wedge at different times. We note that the corrected travel time $\tau_n$ depends upon the ratio $a/e_3$ : as a rule, this fraction increases without limit, with increasing bounce number or higher order reverberations. As a result, *the distortions of a station's response relative to another at a different radial distance increase with time.* In other words, one effect of a dipping crustal structure can be given the interpretation that each component of an array of stations will respond to the same signal as though it were written on a rubber sheet. The stretching of the sheet will be proportional to both time and the relative distance of the station from the wedge vertex.

**B.** *The Ground Motion Theory.* If we neglect pure distortions, for two dimensional motion, the displacement $\vec{s} = (u, v)$ of an elastic solid is given by

$$u = \frac{\partial \varphi}{\partial x} + \frac{\partial \psi}{\partial y},$$
$$v = \frac{\partial \varphi}{\partial y} - \frac{\partial \psi}{\partial x}, \tag{7}$$

where $\varphi$ and $\psi$ are solutions of the wave equations

$$\nabla^2 \varphi - \frac{1}{v_p^2} \frac{\partial^2 \varphi}{\partial t^2} = 0,$$
$$\nabla^2 \psi - \frac{1}{v_s^2} \frac{\partial^2 \psi}{\partial t^2} = 0. \tag{8}$$

In our analysis, we have confined our attention to the ray portion of the seismic field so that $\varphi$ and $\psi$ will be plane waves of the particular form

$$\varphi = f\left(t \pm \frac{x}{v_p} \sin \vartheta_p \pm \frac{y}{v_p} \cos \vartheta_p\right)$$
$$\psi = f\left(t \pm \frac{x}{v_s} \sin \vartheta_s \pm \frac{y}{v_s} \cos \vartheta_s\right) \tag{9}$$

where $f(t)$ is an arbitrary function of $t$ and $\vartheta_p$, $\vartheta_s$ are any parameters. An important feature of plane wave reflection and refraction is that the functional form of $f(t)$ is common to both incident and reflected waves so long as the reflection coefficient is real. Should the reflection coefficient be complex as would be the case for total reflection, then the reflected field consists of two parts: the first is proportional to $f(t)$, and the time variation of the second is given by (Friedlander, 1948)

$$\frac{\lambda}{\pi(1 + \lambda^2)} \mathcal{P} \int_{-\infty}^{+\infty} \frac{f(\alpha)}{\alpha - t} d\alpha \tag{10}$$

where $\lambda$ is a parameter related to the complex reflection coefficient. For total re-

flection, the correction (10) represents the signal distortion when the simple geometric ray theory fails to apply. However, this contribution while important for theoretical reasons turns out to be a comparatively minor perturbation. (Arons *et al*, 1950; Cron *et al*, 1965). In our analysis, we shall find that relatively few events correspond to total reflection. In addition, we are less interested in calculating one seismogram exactly than in discerning the operations that carry the response of one station into another, so that small deviations common to all traces will not concern us. Thus, although we could easily correct the response to account for total reflection by including the contributions (10) we have not done so for purposes of simplicity. If an event corresponds to total reflection, then we force the reflection coefficient to be $\pm 1$ depending upon its value at the critical angle.

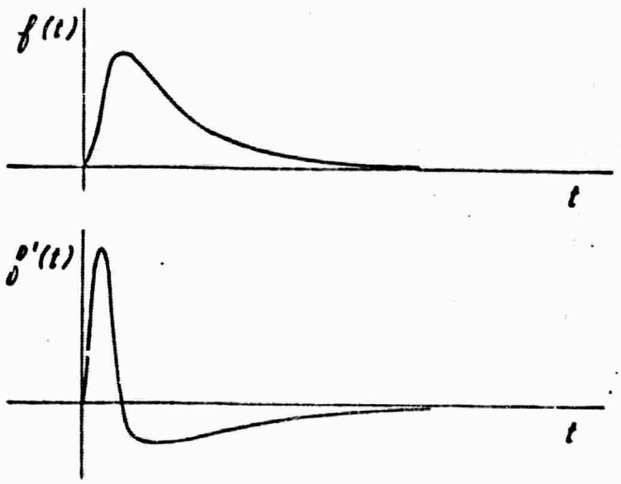


FIG. 5. If the potential variation is given by $f(t)$ then the ground motion is essentially a superposition of delayed responses proportional to $f'(t)$.

*Computation*. Suppose the incident $P$ wave has the *time* variation $f(t)$ at some fixed station on the crust's surface. It is important to note that within the theory of geometric acoustics the *time* variation of $f(t)$ and its derivative $f'(t)$ will be preserved for all the multiple reflected rays except for a translation.

In the sequel, we shall choose $f(t)$ as

$$f(t) = \begin{cases} \left(\frac{t}{t+\beta}\right)^{\gamma} e^{-\alpha t} & t \geq 0 \\ 0 & t < 0. \end{cases} \tag{11}$$

The virtue of this expression is that with a proper choice of the parameters $\alpha$, $\beta$, $\gamma$, just about any realistic pressure variation of the incident wave can be modeled. Typically, $f(t) = 0$ for $t$ negative, thereafter $f(t)$ rises rapidly to some maximum value, and then decays to zero as $t$ becomes more positive (Figure 5). In all our seismograms we have chosen the values $\alpha = .1$, $\beta = 1/4$, and $\gamma = 2$. We shall not need

$f(t)$ explicitly, but rather its derivative $f'(t) = \partial f/\partial t$ which is stored in the computer in digitized form (Figure 6).

From (7) we calculate that the ground motion at a station $A$ corresponding to any event $E'(e_1', e_2', \cdots e_3')$ at station $A$ is proportional to

$$u_a'(t) = \left[e_3'(e_1' + e_3') - \frac{v_p}{v_s} e_3'\sqrt{1-(e_3')^2}\right] f'(t - \tau_a')$$
$$v_a'(t) = \left[\sqrt{1-(e_3')^2}(e_1' - e_3') + \frac{v_p}{v_s} e_3' e_3'\right] f'(t - \tau_a') \qquad (12)$$

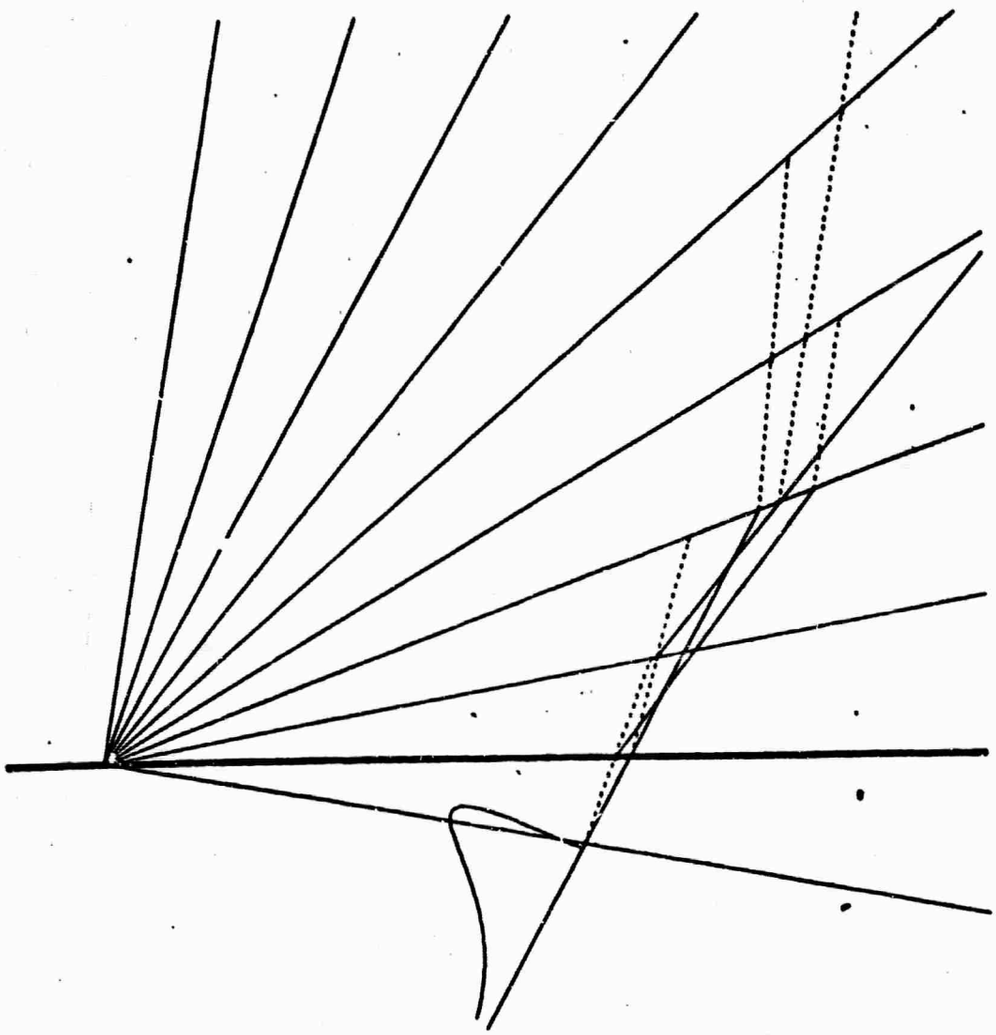

FIG. 6. See opposite page.

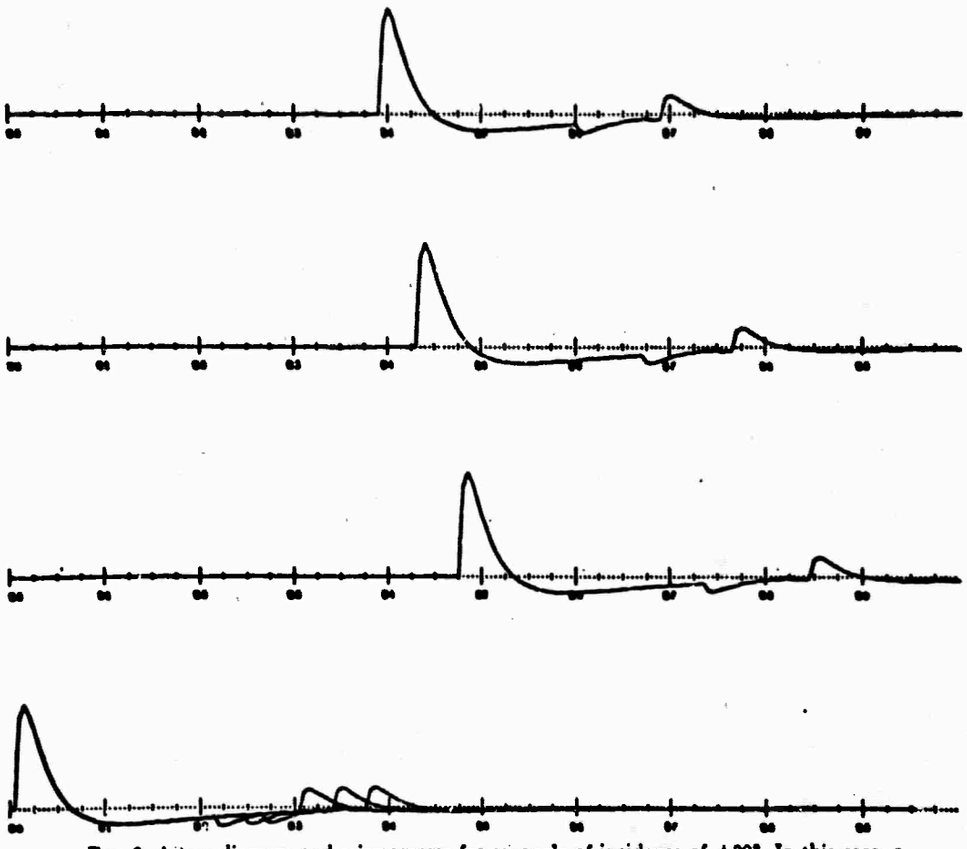

FIG. 6. A tree diagram and seismograms for an angle of incidence of +30°. In this case, a partial tree diagram has been drawn by supressing any ray whose amplitude fails to exceed .005 times that of the largest event amplitude in storage. The pressure variation of the incidental wave front is indicated on the tree diagram. This insert is normalised to a scale appropriate for the central station.

if the incident wave is a $P$ wave ($e_1$ a positive integer), otherwise we have

$$u_0^i(t) = \left[\sqrt{1-(e_0^i)^2}(e_1^i - e_0^i( + \frac{v_0}{v_p} e_0^i e_1^i\right] f^i(t-\tau_0^i)$$
$$v_0^i(t) = -\left[e_0^i(e_1^i + e_0^i) + \frac{v_0}{v_p} e_0^i\sqrt{1-(e_1^i)^2}\right] f^i(t-\tau_0^i) \qquad (13)$$

if an $SV$-wave is incident ($e_1$ a negative integer). We note that the site of any station affects the response only through the term $f^i(t-\tau_0^i)$, that is, a variable translation. The complete seismogram is then found by a superposition of these basic events.

Thus, the left-right motion at station $A$ is given by $\sum_{\substack{\text{all}\\ \text{events}}} u_e^{\,t}(t)$, (14)

and the up-down motion is given by $\sum_{\substack{\text{all}\\ \text{events}}} v_e^{\,t}(t)$. (15)

Likewise, if we substitute $b$ or $c$ for station $B$ or $C$'s coordinate we can compute their seismograms too.

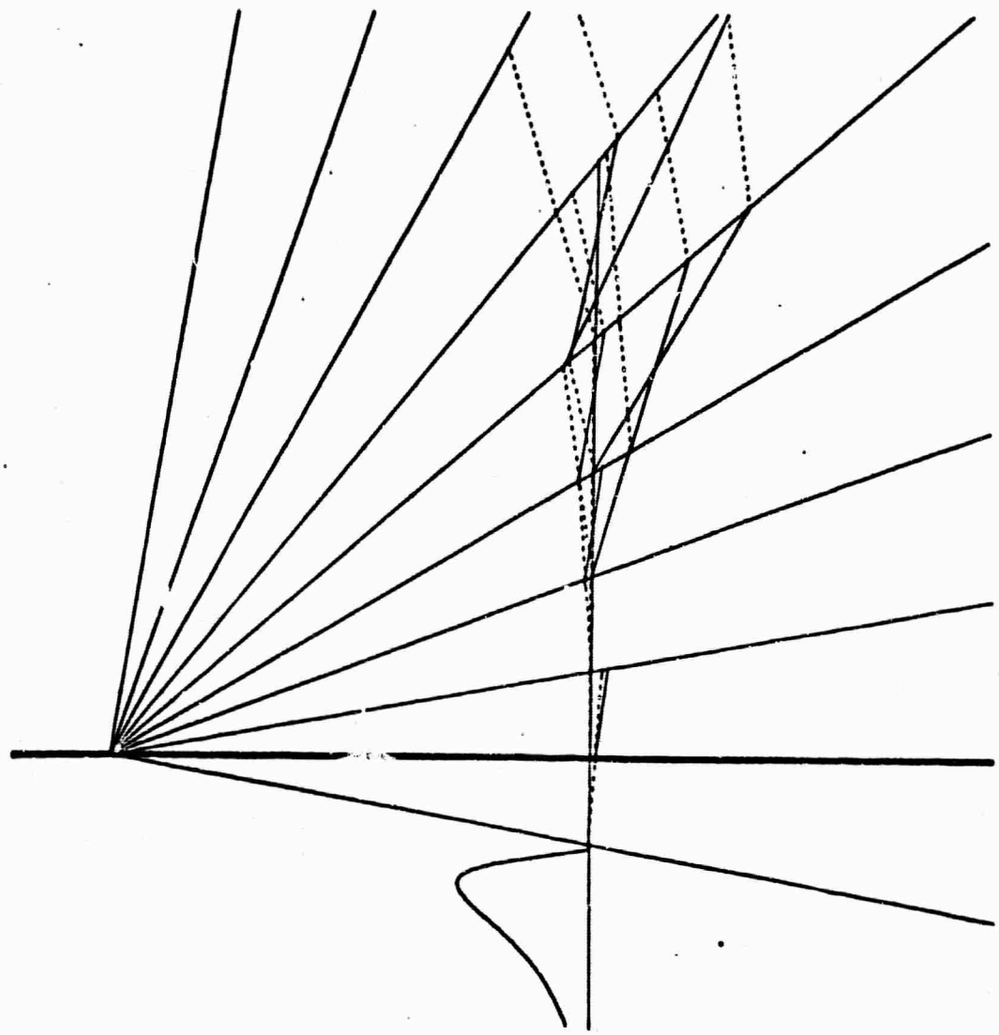

Fig. 7. See opposite page.

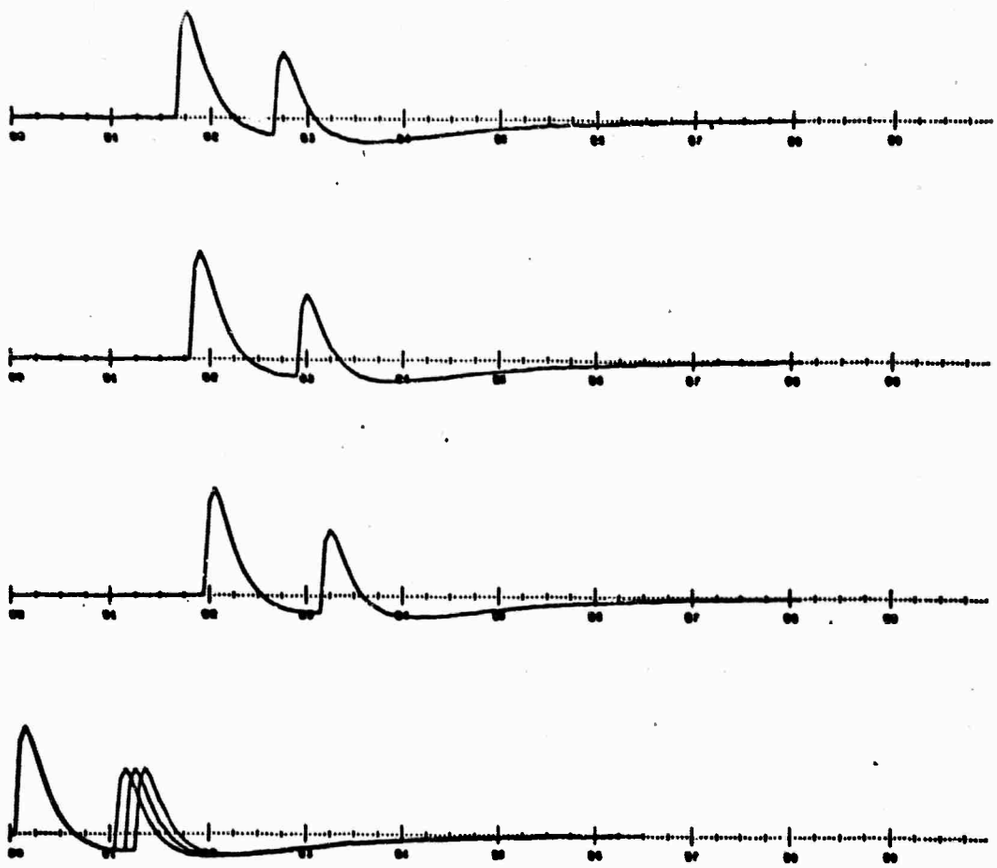

FIG. 7. A tree diagram and seismograms for an angle of incidence of 0°. In this case, a partial tree diagram has been drawn by supressing any ray whose amplitude fails to exceed .005 times that of the largest event amplitude in storage. The pressure variation of the incidental wave front is indicated on the tree diagram. This insert is normalized to a scale appropriate for the central station.

C. *Sample Seismograms.* We have repeatedly emphasized that the geometry of the wedge problem is scale invariant. However, the time variation of the pulse introduces a significant parameter into the analysis. Consider any time variation of the incident wave. Clearly, sufficiently near the vertex it will seem like a pulse of long duration, and far away from the vertex it will have the characteristics of a sharp pulse. Let $t_0$ be the time required for the pulse to build up from its initial value to its maximum. For $f(t)$ given by equation (11) and $\alpha = 1, \beta = \frac{1}{4}$, and $r = 2$, this will set $t_0$ to be 1.2 time units. If we multiply $t_0$ by the $P$ velocity in the mantle we obtain a figure of 3.6 distance units. We can divide this distance unit by the distance of the station from the edge of the vertex. This dimensionless number which we shall write

as $x$ is a unit which indexes the seismograms. In detail, we have

$$x = \frac{t_0 \cdot v_p \text{ mantle}}{\text{station distance}}, \tag{10}$$

There are two extreme cases when intersymbol distortion will not occur: if $f(t)$ is either a delta function ($x = 0$) or a unit step function ($x = \infty$). In these situations the duration of the event is either infinitesimal or unbounded.

In Figures 6 to 8 we present some sample seismograms for a crustal wedge of 10°. The upper three curves are the computations of the vertical motion that three stations located at $A$, $B$, and $C$ would record. Typically, the radial distances of $A$

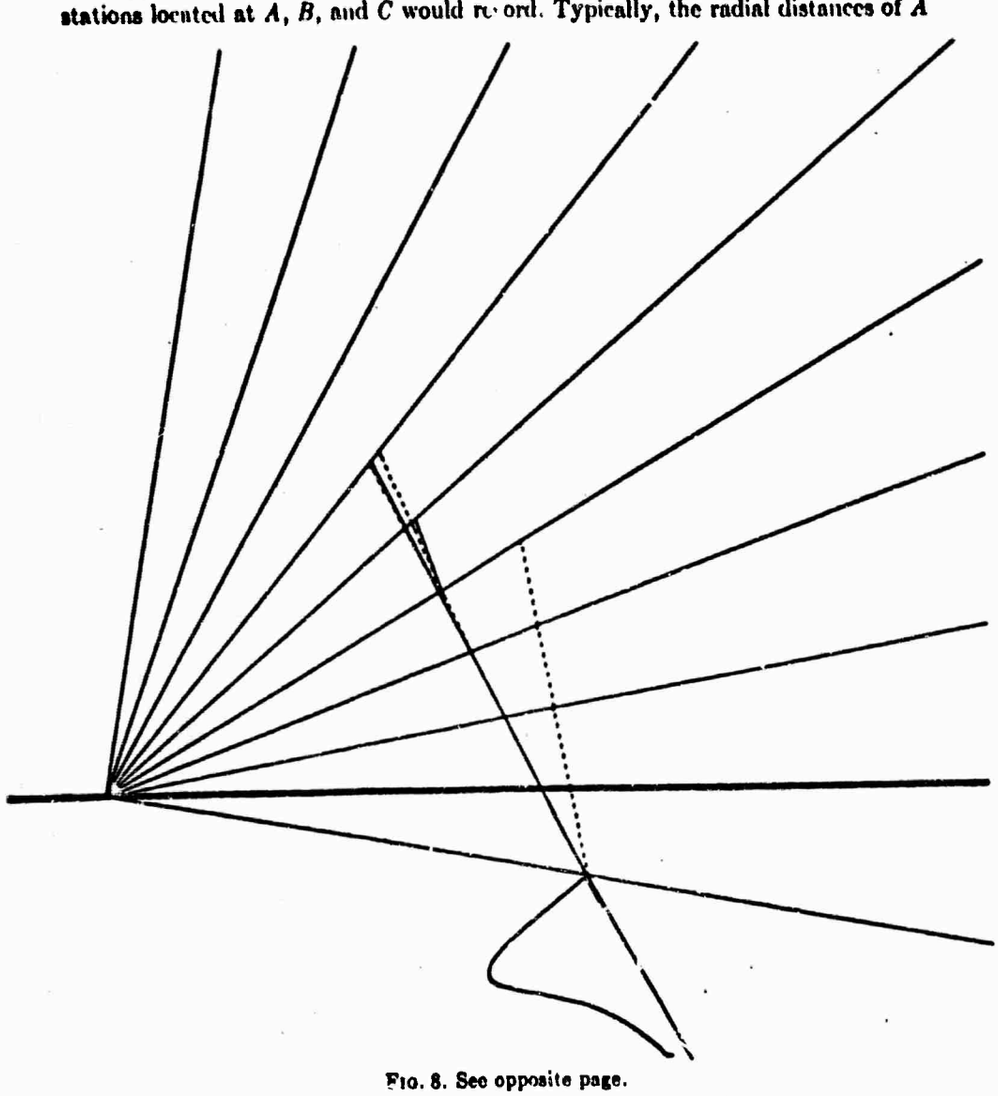

FIG. 8. See opposite page.

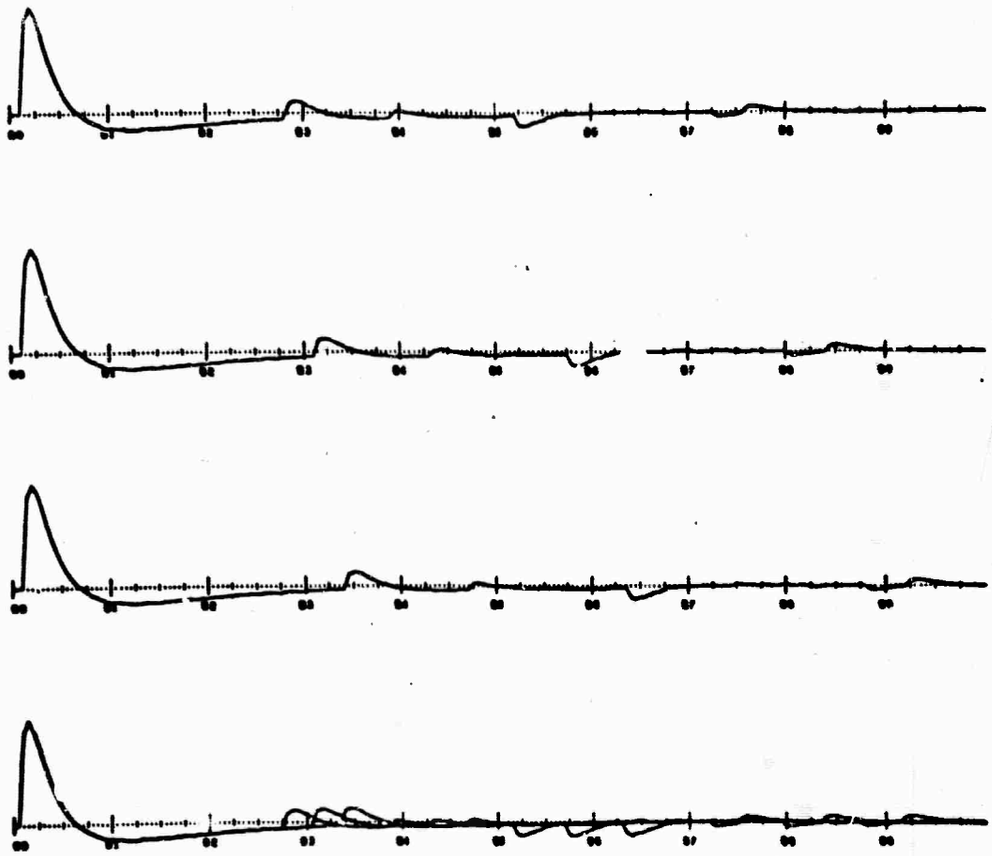

FIG. 8. A tree diagram and seismograms for an angle of incidence of −30°. In this case, a partial tree diagram has been drawn by suppressing any ray whose amplitude fails to exceed .005 times that of the largest event amplitude in storage. The pressure variation of the incidental wave front is indicated on the tree diagram. This insert is normalized to a scale appropriate for the central station.

and $C$ have been chosen to be factors of .9 and 1.1 respectively of that of station $B$ with a radial distance of 25 units. Likewise, the $x$ values are 1.60, 1.44, and 1.31 respectively. The lower trace is a superposition of each of the preceding three translated to a common time origin. It will be noted that except for the first section of the records, the three traces separate and become distinct. As mentioned previously one reason for this "rubber sheet effect" is the effective magnification in the time scale for stations located at increasing distances from the wedge vertex.

It will be noticed that this is but one distortion: another perturbation is the effect of what might be called *intersymbol interference*. The seismogram is constructed by the repeated superposition of a given wave shape $f'(t)$ with various translations of initial time origin. Since $f'(t)$ is not linear, the shape of the combination signal of two contributions will vary as the relative spacing between the events changes. Owing to the rapid decay of field amplitude as the rays are multiply reflected from the

elastic interfaces, the effect of intersymbol distortion is rather difficult to see for relatively few events have significant amplitude. For this reason, we have produced an artificial seismogram shown in Figure 9. In this illustration, the motion was computed by assuming that the rays have rattled between the walls of the wedge with an artificial reflection/conversion coefficient of .9 at each bounce. In this fashion, the

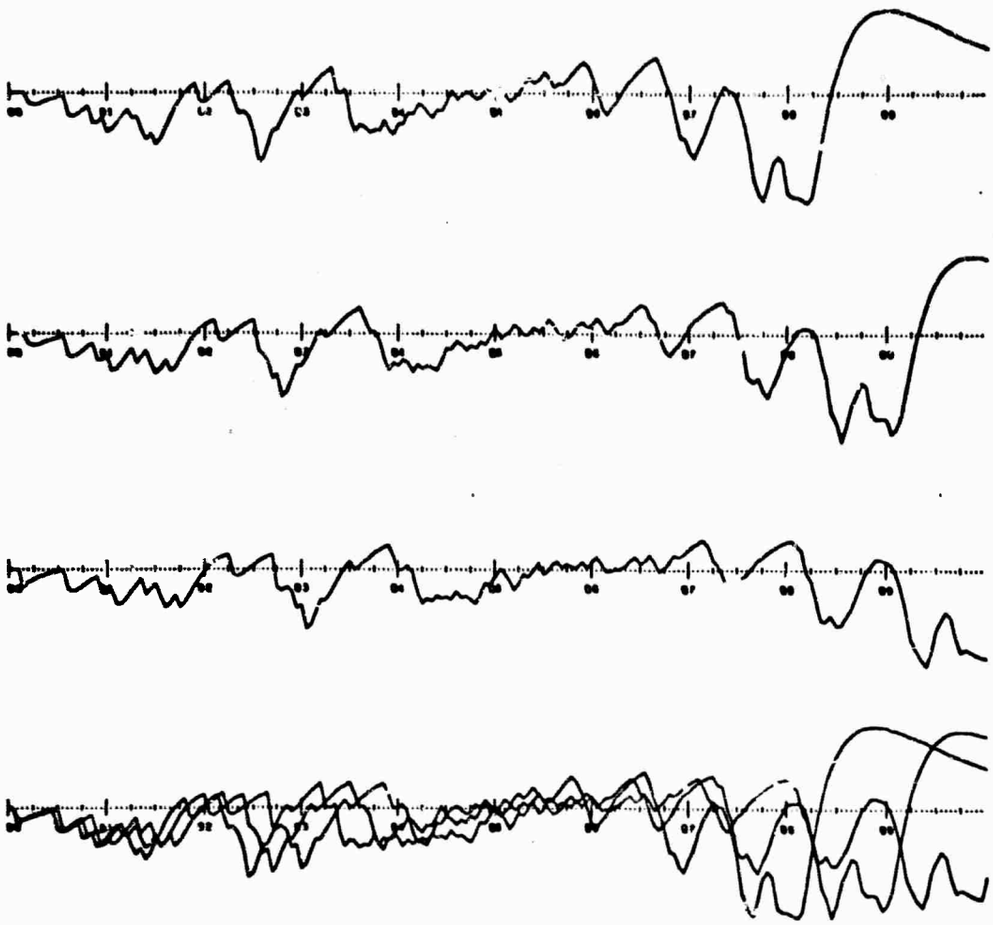

FIG. 9. An artificial seismogram computed by setting all reflection/conversion coefficients to .9. The angle of incidence is −30°. Note the shape distortion owing to intersymbol interference.

time decay on the theoretical seismogram is much less rapid and many more events contribute to the plot so that the effect of intersymbol distortion is emphasized.

For the relatively low order crustal model of a uniform wedge overlying an ideal elastic half-space, "rubber sheet equalization" would be a rather effective technique for adjusting the response of one station relative to another. However, in some extensions of this present work we have considered more realistic crustal configura-

tions, e.g., stacks of skew multi-layers overlying a half space. For these models, *the greater complexity of the crustal structure is reflected by having corresponding seismograms which are much richer in detail.* In these cases, "rubber sheet equalization" is ineffective and more sophisticated techniques are required.

## Conclusions

One aim of the present paper has been to show that theoretical seismograms can easily be constructed for certain problems directly in the time domain when the corresponding situation would be entirely intractable in the harmonic domain. Indeed the problem of diffraction in wedge-shaped elastic regions is one that has yet to yield to the mathematician's touch. In the present case, the analysis is such that seismograms can be computed for angular structures as easily as for plane parallel geometries. Furthermore, the actual vibrations are easily and directly computed without the need to sum and transform slowly converging residue series.

It is also important to note that simple superposition of the response of each element in an array is an inefficient practice and useful only for the first few seconds of the initial motions. Even in the complete absence of noise, there will not be perfect coherence between the elements of an array when recording the same source. However, a "rubber sheet" equalization of the seismic traces will improve the signal enhancement if the array is located over a dipping crustal structure. On the other hand, this rubber sheet equalization will not compensate for the intersymbol distortion. However, neither of these practices are necessary, for if theoretical seismogram can be constructed for a realistic earth model by linear superposition, then it is relatively easy to construct a "matched filter" which can greatly enhance the signal/noise ratio. In subsequent papers we plan to illustrate the computation of theoretical seismograms for skew multilayers, and we shall discuss the construction of matched filters based upon this analysis.

## Acknowledgment

The research described in this report has been sponsored by the Air Force Cambridge Research Laboratories, Office of Aerospace Research, as part of project VELA-UNIFORM under contract number AF 19(628)-319.

## References

Arons, A. B. and D. R. Yennie (1950). Phase distortion of acoustic pulses obliquely reflected from a medium of higher sound velocity, *J. Acoust. Soc. Am.* **22**, 231-237.

Cron, B. F. and A. H. Nuttal (1965). Phase distortion of a pulse caused by bottom reflection, *J. Acoust. Soc. Am.* **37**, 486-492.

Friedlander, F. G. (1948). On the total reflection of plane waves, *Quart. J. Mech.* **1**, 376-384.

Niazi, M. (1965). Private Communication (to be published).

Rotter, J. C. *et al* (1964). *Technical Letter Number* [illegible] written under ARPA Order No. 193-64, Project VELA UNIFORM.

University of Rhode Island
Kingston, R.I.

Manuscript received October 19, 1965.

# TELESEISMIC RESPONSE OF A NON-UNIFORM CRUST*

(part 2 of a series on crustal equalization of seismic arrays)

by Julius Kane and Dror Sadeh

a b s t r a c t

Most seismic theory is confined to crustal structures that can be constructed as plane parallel layers. For such configurations, the response of one element of a seismic array will be similar to any other except for a time delay. Therefore signal enhancement for such an array can be effected quite easily by suitable time delays of the individual records followed by superposition to reduce the effects of random noise.

On the other hand, if the crustal structure is anything but a plane parallel configuration, the signals received by the individual elements will not be translated copies of one another, but will include distortion effects characteristic of the local geometry. As a result, the signals received by seismic arrays located on realistic crustal configurations need to be equalized to some standard reference if optimum signal processing is to be achieved.

In this paper we describe a procedure for the calculation of theoretical seismograms for the teleseismic response of an array of stations located above a non-uniform crust composed of skew-layers. In terms of our mathematical model we demonstrate the distortion effects of such a structure and discuss equalization techniques that will permit a superior recovery of the desired signal.

---

* Presented at the IUGG symposium on geophysics and computers at Cambridge University, Cambridge, England, June 1966.

APPENDIX I

# A COMPUTATIONAL APPROACH TO THE INVERSE STRAIN PROBLEM*

by Julius Kane and Ajit Mal
Space Science Center
University of California
Los Angeles, California 90024

## abstract

In this paper we derive algorithms for the solution of the following problem: An elastic half space is deformed from its rest position by some internal force distribution. The boundary displacement is assumed to be known. The task posed is to find a suitable force distribution in the interior of the solid which can account for the strain of the boundary.

We solve the problem in the following fashion: We introduce a pair of functions which have the property that they are solutions of the relevant partial differential equations and can be used to generate a double sequence of functions which can interpolate the vector data on the boundary. Thus, we show that if an arbitrary point is chosen as the epicenter of the force distribution, then a source field centered at that point can account for any surface displacement, to any desired degree of precision. The ambiguity stems in part from the lack of uniqueness in the geophysical problem, but more from the instability of the solution with respect to the boundary data: That is, a small change in the surface displacement can imply a large change in the source distribution.

---

*Presented at the IUGG Symposium, Cambridge, England, June 1966.

APPENDIX J

# LOVE WAVE DIFFRACTION IN A VARIABLE THICKNESS SURFACE LAYER

by David Joseph Defanti

A Thesis Submitted in Partial Fulfillment
of the Requirements for the Degree of
Master of Science
in
Electrical Engineering

University of Rhode Island
1964

## abstract

Consideration is given to a mathematical analysis of a special case of seismic wave phenomena. In particular, the mixed boundary value problem of Love wave propagation in a solid layer over a solid half-space is investigated where the layer undergoes an abrupt change in thickness. Both the layer and half-space are considered to be homogeneous elastic media. Theoretical background fo the physics of the problem is provided by presenting the fundamentals of elastic wave propagation with specialization to the Love wave case and by a statement of the physical nature and mathematical form of applicable boundary conditions. Interest is focused on the amplitudes of the transmitted and reflected Love waves relative to the magnitude of the excitation, i.e., the transmission and reflection coefficients, for a range of both the "strength" of the discontinuity (magnitude of change

in thickness relative to layer thickness) and the layer thickness. The analysis employs scattered fields in the form of integrals in the complex plane; boundary conditions are applied to the total fields. To satisfy the resulting equations for the boundary conditions, the nature of some of the unknown coefficients in the scattered field integrals is postulated and a function-theoretic argument is employed to determine these coefficients. The transmission and reflection coefficients are then extracted by a standard appeal to the calculus of residues and the energy contained in the diffracted field is evaluated. Both displacement amplitude and energy coefficients are displayed graphically as a function of the parameters h and H. The results presented show that the reflected energy constitudes less than one percent of the incident energy for all crust thicknesses considered here. The amplitude transmission coefficient relating the relative magnitude of the displacements of the transmitted and incident waves is shown to take on values greater than unity for low frequency and an energy analysis shows that this behavior does not violate the principle of energy conservation. A comparison reveals that the results shown here are in close agreement with those given by Knopoff and Hudson (reference 8). However, a discrepancy does exist for intermediate values of crust thickness and is discussed in some detail.

Uncla ..ified

Security Classifi. ion

**DOCUMEN. CONTROL DATA - R&D**

*(Security classification of title, body of abstract and indexing annotation must be entered when the overall report is classified)*

| 1. ORIGINATING ACTIVITY (Corporate author) | 2a. REPORT SECURITY CLASSIFICATION |
|---|---|
| UNIVERSITY OF RHODE ISLAND KINGSTON, R. I. | UNCLASSIFIED |
| | 2b. GROUP |

3. REPORT TITLE

FINAL REPORT -- SEISMIC DIFFRACTION BY CRUSTAL DISCONTINUTIES

4. DESCRIPTIVE NOTES *(Type of report and inclusive dates)*

Final Scientific Report 1 January 1962 - 30 September 1966

5. AUTHOR(S) *(Last name, first name, initial)*

KANE, JULIUS

| 6. REPORT DATE | 7a. TOTAL NO. OF PAGES | 7b. NO. OF REFS |
|---|---|---|
| 15 January 1967 | 99 | 2 |

| 8a. CONTRACT OR GRANT NO. | 9a. ORIGINATOR'S REPORT NUMBER(S) |
|---|---|
| AF19(628)-319 and ARPA Order No.180-62 and 292-12 Project Code No.8100, 4810, | Final Report |
| b. PROJECT NO. 8652,06 | |
| c. DOD Element 62506015 | 9b. OTHER REPORT NO(S) *(Any other numbers that may be assigned this report)* |
| d. no subelement | AFCRL-67 0122 |

10. AVAILABILITY/LIMITATION NOTICES

DISTRIBUTION OF THIS DOCUMENT IS UNLIMITED

| 11. SUPPLEMENTARY NOTES | 12. SPONSORING MILITARY ACTIVITY |
|---|---|
| Hq. AFCRL, OAR (CRJ)<br>United States Air Force<br>L.G. Hanscom Field, Bedford, Mass. 01730 | ADVANCED RESEARCH PROJECTS AGENCY |

13. ABSTRACT

This final report on contract AF19(628)319 describes the research contributions of a group studying theoretical problems of seismic diffraction at the University of Rhode Island. These problems are described in simplified terms and formulations which are mathematically tractable and still relevant to realistic crustal structures. Reprints of papers describing the methods are included as appendices in the report.

DD FORM 1 JAN 64 1473

UNCLASSIFIED

| 14 KEY WORDS | LINK A | | LINK B | | LINK C | |
|---|---|---|---|---|---|---|
| | ROLE | WT | ROLE | WT | ROLE | WT |
| RAYLEIGH WAVES | | | | | | |
| BOUNDARY VALUE PROBLEM | | | | | | |
| ELASTIC WAVE DIFFRACTION | | | | | | |
| REFLECTION AND TRANSMISSION COEFFICIENTS | | | | | | |
| APPROXIMATION TECHNIQUES | | | | | | |
| SIMPLIFIED WIENER HOPF THEORY | | | | | | |
| WIENER HOPF THEORY SIMPLIFIED | | | | | | |
| ANALYTIC CONTINUATION OF WAVE FUNCTIONS | | | | | | |
| DIFFRACTION OF VECTOR WAVES | | | | | | |
| TWO PART CRUSTAL LAYERING | | | | | | |
| CRUSTAL TRANSITIONS | | | | | | |
| DISCONTINUITIES AND DIFFRACTION | | | | | | |

## INSTRUCTIONS

1. ORIGINATING ACTIVITY: Enter the name and address of the contractor, subcontractor, grantee, Department of Defense activity or other organization *(corporate author)* issuing the report.

2a. REPORT SECURITY CLASSIFICATION: Enter the overall security classification of the report. Indicate whether "Restricted Data" is included. Marking is to be in accordance with appropriate security regulations.

2b. GROUP: Automatic downgrading is specified in DoD Directive 5200.10 and Armed Forces Industrial Manual. Enter the group number. Also, when applicable, show that optional markings have been used for Group 3 and Group 4 as authorized.

3. REPORT TITLE: Enter the complete report title in all capital letters. Titles in all cases should be unclassified. If a meaningful title cannot be selected without classification, show title classification in all capitals in parenthesis immediately following the title.

4. DESCRIPTIVE NOTES: If appropriate, enter the type of report, e.g., interim, progress, summary, annual, or final. Give the inclusive dates when a specific reporting period is covered.

5. AUTHOR(S): Enter the name(s) of author(s) as shown on or in the report. Enter last name, first name, middle initial. If military, show rank and branch of service. The name of the principal author is an absolute minimum requirement.

6. REPORT DATE: Enter the date of the report as day, month, year; or month, year. If more than one date appears on the report, use date of publication.

7a. TOTAL NUMBER OF PAGES: The total page count should follow normal pagination procedures, i.e., enter the number of pages containing information.

7b. NUMBER OF REFERENCES: Enter the total number of references cited in the report.

8a. CONTRACT OR GRANT NUMBER: If appropriate, enter the applicable number of the contract or grant under which the report was written.

8b, 8c, & 8d. PROJECT NUMBER: Enter the appropriate military department identification, such as project number, subproject number, system numbers, task number, etc.

9a. ORIGINATOR'S REPORT NUMBER(S): Enter the official report number by which the document will be identified and controlled by the originating activity. This number must be unique to this report.

9b. OTHER REPORT NUMBER(S): If the report has been assigned any other report numbers *(either by the originator or by the sponsor)*, also enter this number(s).

10. AVAILABILITY/LIMITATION NOTICES: Enter any limitations on further dissemination of the report, other than those imposed by security classification, using standard statements such as:

(1) "Qualified requesters may obtain copies of this report from DDC."

(2) "Foreign announcement and dissemination of this report by DDC is not authorized."

(3) "U. S. Government agencies may obtain copies of this report directly from DDC. Other qualified DDC users shall request through _____."

(4) "U. S. military agencies may obtain copies of this report directly from DDC. Other qualified users shall request through _____."

(5) "All distribution of this report is controlled. Qualified DDC users shall request through _____."

If the report has been furnished to the Office of Technical Services, Department of Commerce, for sale to the public, indicate this fact and enter the price, if known.

11. SUPPLEMENTARY NOTES: Use for additional explanatory notes.

12. SPONSORING MILITARY ACTIVITY: Enter the name of the departmental project office or laboratory sponsoring *(paying for)* the research and development. Include address.

13. ABSTRACT: Enter an abstract giving a brief and factual summary of the document indicative of the report, even though it may also appear elsewhere in the body of the technical report. If additional space is required, a continuation sheet shall be attached.

It is highly desirable that the abstract of classified reports be unclassified. Each paragraph of the abstract shall end with an indication of the military security classification of the information in the paragraph, represented as *(TS)*, *(S)*, *(C)*, or *(U)*.

There is no limitation on the length of the abstract. However, the suggested length is from 150 to 225 words.

14. KEY WORDS: Key words are technically meaningful terms or short phrases that characterize a report and may be used as index entries for cataloging the report. Key words must be selected so that no security classification is required. Identifiers, such as equipment model designation, trade name, military project code name, geographic location, may be used as key words but will be followed by an indication of technical context. The assignment of links, roles, and weights is optional.